Spring 2021

In-Situ Process Monitoring for Metal Additive Manufacturing (AM) Through Acoustic Technique

Md Shahjahan Hossain

IN-SITU PROCESS MONITORING FOR METAL ADDITIVE MANUFACTURING (AM) THROUGH ACOUSTIC TECHNIQUE

by

MD SHAHJAHAN HOSSAIN

(Under the Direction of Hossein Taheri)

ABSTRACT

Additive Manufacturing (AM) is currently a widely used technology in different industries such as aerospace, medical, and consumer products. Previously it was mainly used for prototyping of the products, but now it is equally valuable for commercial product manufacturing. More profound understanding is still needed to track and identify defects during the AM process to ensure higher quality products with less material waste. Nondestructive testing becomes an essential form of testing for AM parts, where AE is one of the most used methods for in situ process monitoring. The Acoustic Emission (AE) approach has gained a reputation in nondestructive testing (NDT) as one of the most influential and proven techniques in numerous engineering fields. Material testing through Acoustic Emission (AE) has become one of the most popular techniques in AM because of its capability to detect defects and anomalies and monitor the progress of flaws. Various AE technique approaches have been under investigation for in-situ monitoring of AM products. The preliminary results from AE exploration show promising results which need further investigation on data analysis and signal processing. AE monitoring technique allows finding the defects during the fabrication process, so that failure of the AM can be prevented, or the process condition can be finely tuned to avoid significant damages or waste of materials. In this work, recorded AE data over the Direct Energy Deposition (DED) additive manufacturing process was analyzed by the Machine Learning (ML) algorithm to classify different build conditions. The feature extraction method is used to obtain the required data for further processing. Wavelet transformation of signals has been used to acquire the time-frequency spectrum of the AE signals for different process conditions, and image processing by Convolutional Neural Network (CNN) is used to identify the transformed spectrum of different build conditions. The identifiers in AE signals are correlated to the part quality by statistical methods. The results

show a promising approach for quality evaluation and process monitoring in AM. In this work, the assessment of deposition properties at different process conditions is also done by optical microscope, Scanning Electron Microscope (SEM), Energy-Dispersive X-ray Spectroscopy (EDS), and nanoindentation technique.

INDEX WORDS: Additive manufacturing, Nondestructive testing, Acoustic emission, Process monitoring, Wavelet transformation, Convolutional neural network, Machine learning, Image processing

IN-SITU PROCESS MONITORING FOR METAL ADDITIVE MANUFACTURING (AM) THROUGH ACOUSTIC TECHNIQUE

by

MD SHAHJAHAN HOSSAIN

Bachelor of Science, Chittagong University of Engineering & Technology, Bangladesh, 2014

A Thesis Submitted to the Graduate Faculty of the Georgia Southern University in Partial

Fulfillment of the Requirements for the Degree

MASTER OF SCIENCE

IN-SITU PROCESS MONITORING FOR METAL ADDITIVE MANUFACTURING (AM) THROUGH ACOUSTIC TECHNIQUE

by

MD SHAHJAHAN HOSSAIN

Major Professor:	Hossein Taheri
Committee:	Daniel Cox
	Drew Snelling

Electronic Version Approved:

May 2021

DEDICATION

I would like to dedicate this work to my parents, my wife, and my family member. Had it not been for my parent's support, I would not be able to pursue my MS at Georgia Southern University. I also dedicate this work to my advisor, friends, and professors for their support and inspiration in my study.

ACKNOWLEDGMENTS

I want to thank the Almighty for all the blessings to complete this thesis. I am extremely grateful to the Georgia Southern University for the facilities by which they support me throughout my study.

I would like to express my gratitude to my academic advisor *Dr. Hossein Taheri* for his inspiration, support, and guidance regarding my graduate studies at Georgia Southern University. His effort to provide information from his prudential knowledge to guide me during my completion of study which is highly appreciable. He also encouraged me to work on various projects during my masters.

I also would like to assert my appreciation to the research committee *Dr. Drew Snelling* and *Dr. Daniel Cox,* for their support in completing my thesis. I am also thankful to my fellow researcher who supported me mentally and helped me with their ideas during the study period. I would like to thank *Dr. Mahmoud Baniasadi* for his support in working with Nanoindentation. I am thankful to Mr. *Andrew Michaud* for his support for any machining and other work during my study. I am also very thankful for the support during working with the SEM and EDS machine to Mr. *Andrew Diamanduros* and *Dr. Nathan Takas* of the Chemistry department. I would like to acknowledge all the people in the Manufacturing Engineering department to support my research activities. I also like to thank everyone who actively or passively helped me during my study.

TABLE OF CONTENTS

LIST OF TABLES

LIST OF FIGURES

NOMENCLATURE

AM - Additive Manufacturing

AE – Acoustic Emission

ANN – Artificial Neural Network

CAD – Computer-Aided Design

CNN – Convolutional Neural Network

DED – Direct Energy Deposition

EDS – Energy Dispersive Spectroscopy

EMI – Electromagnetic Interference

FFT – Fast Fourier Transformation

FMD – Fused Deposition Modeling

IIT – Instrument Indentation Testing

LAM – Laser Additive Manufacturing

LMD – Laser Metal Deposition

LPBF – Laser Powder Bed Fusion

LU – Laser Ultrasonic

NDT – Nondestructive Testing

PCA – Principal Component Analysis

SEM – Scanning Electron Microscopy

UT – Ultrasonic Testing

WT – Wavelet Transformation

YAG – Yttrium-Aluminum Garnet

CHAPTER 1

INTRODUCTION

With the advancement in Additive Manufacturing (AM) technologies, the use of AM has increased for commercial functional parts as well as for prototyping. Complex geometries can be manufactured via AM technologies from computer-generated 3D models. Using AM techniques, minimum or no material removal is needed, which is not currently possible through traditional manufacturing techniques (Taheri, Shoaib, et al. 2017). AM is spreading in many industries during the last few years, such as the medical equipment industry (Kruth, P.d.i.J.P., B. Vandenbroucke, I.J. Vaerenbergh van 2005) and the aerospace industry (Bontha et al. 2006). The key point in using AM for part production is that the parts fabricated by the additive manufacturing process must have at least similar mechanical characteristics compared to conventionally manufactured parts (Berumen et al. 2010).

Because of the complex geometries involved and complicated processing parameters, there is a high probability of AM manufacturing defects due to variations in process parameters or quality of feedstocks. If these anomalies can be found during the manufacturing process, manufacturing costs can be reduced rather than after completion. Nowadays, there is industrial demand to have a high-quality automated manufacturing product line. The need is to have real-time fault detection to ensure that higher quality parts are being produced (Ge, Song, and Gao 2013)(Kano and Nakagawa 2008)(Qin 2012)(Yin et al. 2014). Offline quality control, such as part sampling during production for inspection, can be expensive and time-consuming, sometimes resulting in rejection of the full lot (Milo, Roan, and Harris 2015).

Specific to AM, the layer-by-layer nature of fabricating parts elicits the opportunity for better monitoring of the manufacturing process (Frazier 2014). Various techniques are currently being used to control AM parts, such as optical camera and image processing, thermography, radiography, and acoustic

Emission (AE) (Hossain and Taheri 2020; Hossain, Taheri, et al. 2020). However, the in-situ characterization of failures is not sufficient by the previous study such as using optical and thermal-based systems, because they provide (a) difficulty of crack localization and further propagation, (b) limited penetration capability, (c) limitation of finding internal defects, and (d) detailed accurate thermographic measurement, (Lu and Wong 2017)(Strantza et al. 2015). Acoustic methods have provided promising results for defects identification in AM parts, where the results and methodologies are depicted in several articles (Taheri 2018). Acoustic sensor data can be acquired and analyzed by signal processing techniques to detect defects (Plotnikov et al. 2019). Acoustic Emission (AE) is among the most used acoustic methods for quality evaluation in various applications. Acoustic emission is being used to detect defects in vessels, bridges, and other structures as a potential solution (Angulo et al. 2019). Based on the long history of promising capabilities, AE can measure ultrasonic guided waves and compare different data in various ranges for the assessment of defects in AM components during the parts fabrication.

Despite previous efforts using optical and thermal methods, the in-situ characterization of failures in AM is not adequate because these techniques have (a) restricted penetration, (b) complex thermographic calculation, (c) restriction of the identification of internal faults, and (d) difficulty in detecting cracks and further dissemination (Lu and Wong 2017)(Strantza et al. 2015). On the other hand, promising results for defect detection were achieved by acoustic techniques when testing AM parts (Taheri 2018). Acoustic data are acquired and analyzed using acoustic sensors through signal processing to detect defects. (Plotnikov et al. 2019).

These flaws need to be identified for taking corrective actions during the manufacturing process to save the time and cost of fabrication (Lu and Wong 2017)(Strantza et al. 2015). On the other hand, for detailed analysis of the parts' defects and microstructure, other surface crack detection techniques such as microscopy methods are also used for AM evaluation, which cannot detect internal defects (D'Accardi et al. 2019)(Everton et al. 2016). These techniques can be used for the validation of the AE technique during the development of the method. Optical microscopy, SEM, EDS, and nanoindentation can be used for

quality inspection and characterization of AM parts after the building process has been completed (Zhang et al. 2019).

Scanning Electron Microscope (SEM) uses a focused beam of high-energy electrons to create various signals at the samples' surface. The EDS is mainly used for qualitative material study, but it can produce semi-quantitative results. SEM scanners are often quipped with an EDS system, which allows the chemical composition of features observed on the scanner to be carried out. The electron-sample interaction signals reveal sample properties, chemical composition, crystalline structure, crystalline orientation, and including external morphology (texture) of the target materials (Swapp n.d.)(Nasrazadani and Hassani 2016)(Rahman 2020). A relatively new type of mechanical testing, instrumented indentation testing (IIT), also known as nanoindentation, greatly extends conventional hardness testing capabilities. Mechanical characteristics are extracted from the load-displacement indentation data gathered in simple experiments. IIT has numerous advantages, as indentation load-displacement data contains knowledge and techniques for characterizing several mechanical properties that have been established. The most frequently used method measures the hardness, and from the same data, it also measures the elastic Modulus (Young's Modulus) (Hay and Pharr 2000)(Doerner and Nix 1986)(Newey, Wilkins, and Pollock 1982).

Various experiments based on acoustic emissions for AM process control have been undertaken in recent years to enhance signal processing and characterization (Hossain and Taheri 2020). The studies implemented different experimental setups to acquire data, and different statistical methods, feature extraction techniques, and machine learning algorithms have been used for characterization and defect detection (Taheri, Shoaib, et al. 2017; Lu and Wong 2017). However, the commercial application of acoustic emission in the additive manufacturing process needs further advanced analysis. For example, a study by Gaja et al. (2016) on laser metal deposition (LMD) showed that AE gives critical information during the formation of cracks, propagation, grain nucleation, and pores (Gaja and Liou 2016). Another study by Taheri et al. (2019) has used K-means clustering to classify the different AM process conditions based on acoustic signatures recorded over the AM manufacturing process (Taheri et al. 2019). In AE, a

fault in the process or part extends the signal through sensors in the form of high-frequency sound waves. In Figure 1, a diagram of the acoustic emission system used for data collection is shown (Hossain and Taheri 2020).

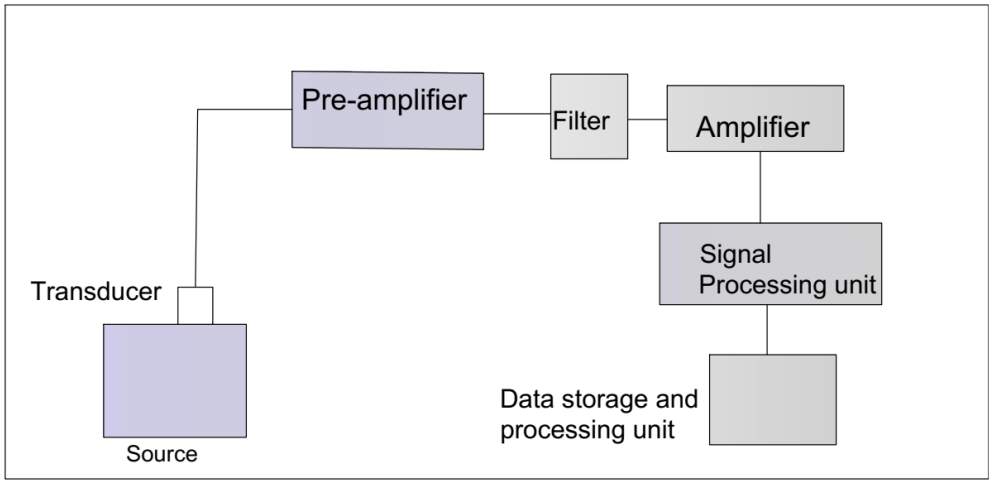

Figure 1: Schematic setup for acoustic emission testing (Hossain and Taheri 2020)

In recent years, there have been a number of studies of acoustic emission systems for AM process monitoring to improve signal acquisition and characterization (Taheri, Shoaib, et al. 2017; Lu and Wong 2017; D'Accardi et al. 2019; Everton et al. 2016). However, more advanced research is required for implementing acoustic emission in the additive manufacturing process. In a study on defect monitoring of laser metal deposition, Gaja et al. (2016) found that AE provides critical information during the formation of cracks, pores, grain nucleation, and propagation (Gaja and Liou 2016). In spite of the fact that monitoring of AM by acoustic emission (AE) is still in the development stage and there is inadequate information available in this field, previous reviews were done by authors such as Tapia and Elway (Tapia and Elwany 2014). In Everton et al. (2016), the authors provide broad information on AM process monitoring. Besides, this paper provides a detailed review of acoustic techniques with an emphasis on AE in the field of AM monitoring, including the basics of AE and relevant data processing techniques (Everton et al. 2016).

Although the Acoustic Emission (AE) testing of AM is still in the implementation process, there is insufficient information available. In this study, the collected AE signals from the AM process in different

build conditions from the authors' former publications (Taheri et al. 2019)(Koester, Taheri, Bigelow, Bond, et al. 2018)(Koester, Taheri, Bigelow, Collins, et al. 2018) have been further analyzed in details using wavelet and CNN techniques for improving the accuracy and consistency of the results of acoustic in-situ monitoring methodology. The data is analyzed statistically, then feature extraction through wavelet transformation, which is finally analyzed by image processing through a Convolutional Neural Network (CNN). SEM, EDS, nanoindentation, and microscopic data are also collected over a different region between the substrate material and the additive deposited layer (Ti-6Al-4V) 2-dimensional images are created that show spatial variations in these properties. The comparison between three different process conditions has been made to evaluate the research done by classification of process conditions using Acoustic Emission (AE) data in another study.

1.1 Hypothesis

The acoustic signatures of the additive manufacturing processes contain rich information about both process and part conditions. The Additive Manufacturing (AM) process's acoustic signatures are recorded and analyzed for finding significant features such as central frequency and amplitude, and this data can be used for AM process quality monitoring and evaluation. This quality monitoring needs to be done by a proper classification of five different process conditions. If the classification of the process building conditions can be done with statistical analysis with more than 90% accuracy, then the results of the classification can be used for process condition monitoring, and evaluation of metal AM systems. In addition, the classification results can be correlated to the properties of the manufactured parts.

1.2 Objectives

Main objectives of this study include:

- Analyzing the recorded preliminary data to find out the characteristic of the data.
- Clustering of the data for different build conditions to separate the different process conditions.

- Wavelet transformation of the data for showing the variation of the signal of each condition.
- Image processing of the transformed data to show how effective the classification is for classification.
- Evaluation of this technique is analyzed with other material characterization techniques.

CHAPTER 2

LITERATURE REVIEW

2.1 Challenges with NDT of AM

Nondestructive Testing (NDT) is an analysis technique used to evaluate a material's properties without causing any effects on materials for the assurance and inspection of product quality. NDT has become increasingly popular in various types of material manufactured by different methods (Hossain, Krenek, et al. 2020). However, the technology development in implementing NDT to AM has grown rapidly throughout the last few years. There are still challenges in applying these techniques for online monitoring of defects due to the complexity of additively manufactured parts and AM processes. Unlike the conventional subtractive manufacturing systems, AM fabricates parts in a layer-by-layer procedure which requires alternate material characterization techniques. More specifically, powder bed fusion parts have more porosity due to lack of fusion and flaws such as keyhole, laser timing, and toolpath generation (Lu and Wong 2017). This porosity is the challenge for understanding the associated flaws (Waller et al. 2014). In-situ process monitoring is more important than offline techniques for AM because it can monitor the entire fabrication process, which is beneficial for subsurface defect detection. As AM can create complex parts, conventional NDT techniques such as ultrasonic and eddy current techniques are less applicable (Waller et al. 2014). Because of complex geometry, the AM parts are not a good case for less geometry responsive NDT techniques, for example, magnetic particle testing. Though there are some imperfections, one of the most prominent techniques for finding defects is based on the x-ray computed tomography technique (Du Plessis et al. 2015). Testing of AM parts becomes even more complex when multiple materials are used in the fabrication process. High-speed x-ray imaging can validate the various models for characterizing of Direct Energy Deposition (DED) process by finding the laser-matter interactions (Wolff

et al. 2019). During Laser Additive Manufacturing (LAM) x-ray imaging can detect the pore migration, dissolution, dispersion, and bursting (Leung et al. 2018). Many researchers have currently used the acoustic technique as a potential solution for identifying different defects. Though signal acquisition and analysis still have some challenges, the acoustic technique is one of the promising areas where subsurface defects can be identified. The main obstacle for such a study is to identify data with proper filtering and thresholding to give more precise output for fault finding. More research is necessary for developing the acoustic NDT techniques for additive manufacturing. This chapter is a survey of different acoustic methodologies for AM in-situ monitoring. First, a brief overview of different in-situ monitoring techniques for AM will be presented, and then, the focus of the survey will be on acoustic in-situ monitoring techniques.

2.2 Importance of AM and in-situ monitoring in AM

Industrial metal components have historically been made using different types of forming, casting, and molding. For creating complex geometries in these processes, parts are made by assembling different components. Recently, Additive Manufacturing (AM) has been used to create an intricate part in one single step. AM is increasing in various manufacturing industries, which can create complex parts through Computer-Aided Design (CAD) with a low waste of material, which is quite tricky in other forms of manufacturing (Taheri, Shoaib, et al. 2017). AM processes' versatility offers the possibility of designing innovative product designs that are not feasible with casting or subtractive methods (Gaynor et al. 2014). For example, AM often incorporates polymers and nanocomposites to develop biocompatible, strong, and lightweight materials. Biocompatible and biodegradable polymers such as PVA and PHA could find their applications in wearable devices. Composites are useful in terms of energy saving for space applications (Rahman and Bhoi 2021). Besides, AM also facilitated the chemical industry by producing numerous ceramic-based catalysts (Rahman et al. 2021). Therefore, in recent years, AM has expanded to many markets, such as medical devices (Kruth, P.d.i.J.P., B. Vandenbroucke, I.J. Vaerenbergh van 2005), chemical industry (Dutta and Sam Froes 2015), and the aircraft industry (Bontha et al. 2006).

For maintaining the current industrial demand, high-quality automated manufacturing is required, so that manufacturing costs can be reduced by saving time and material waste. Therefore, the demand is increasing gradually in the field of real-time fault detection to ensure higher quality parts being produced (Ge, Song, and Gao 2013)(Kano and Nakagawa 2008)(Qin 2012)(Yin et al. 2014). Offline quality control can be costly and time-consuming, such as product sampling during manufacturing for testing, often resulting in the rejection of the entire lot (Milo, Roan, and Harris 2015). Unique to AM, the layer-by-layer fabrication of the components offers the potential for better control of the production process. (Frazier 2014). For the quality inspection of AM pieces, various techniques are currently being used, such as radiography, optical camera and image processing, thermography, and acoustic emission. (Hossain and Taheri 2020).

2.3 Types of Monitoring Systems for AM

There are a variety of systems used for process monitoring in AM. Some of the most common techniques are reviewed in this section to overview all potential techniques for in-situ monitoring for AM.

2.3.1 Optical camera and image processing

Optical methods are one of the most used monitoring systems for AM. In optical methods, the process images are captured at a high-speed rate using appropriate types of detectors. These images will be processed to detect any anomalies or unwanted features as an indication of process flaws. The advantages of optical inspection systems are that they do not require direct contact to the parts, a large amount of information can be taken as well as the versatility of the data can be found (Purtonen, Kalliosaari, and Salminen 2014). Optical methods can only visualize the surface features; therefore, other integrated methods are required to detect the defects in the material structure's subsurface. Figure 2 shows a typical optical monitoring system that utilizes a semi-transparent mirror to transfer images into a high-speed camera and a photodiode. The light emitted corresponded to definite temperatures displayed in different

grayscale values. Another study by Berumen et al. (2010) showed simple errors during the building process identified by a single photodiode sensor, which required high temporal and local resolution of the melt pool (Berumen et al. 2010). For collecting better data, algorithms and tools still need to be upgraded to allow the automatic receiving of the information (Craeghs et al. 2012). In a further study, Clijsters et al. (2014) created a position-based algorithm to find defects during process failure by monitoring the whole powder bed. In this study, the defects were indicated successfully, and the optical microscopy verified the results after cutting and polishing the material in the defective location (Clijsters et al. 2014).

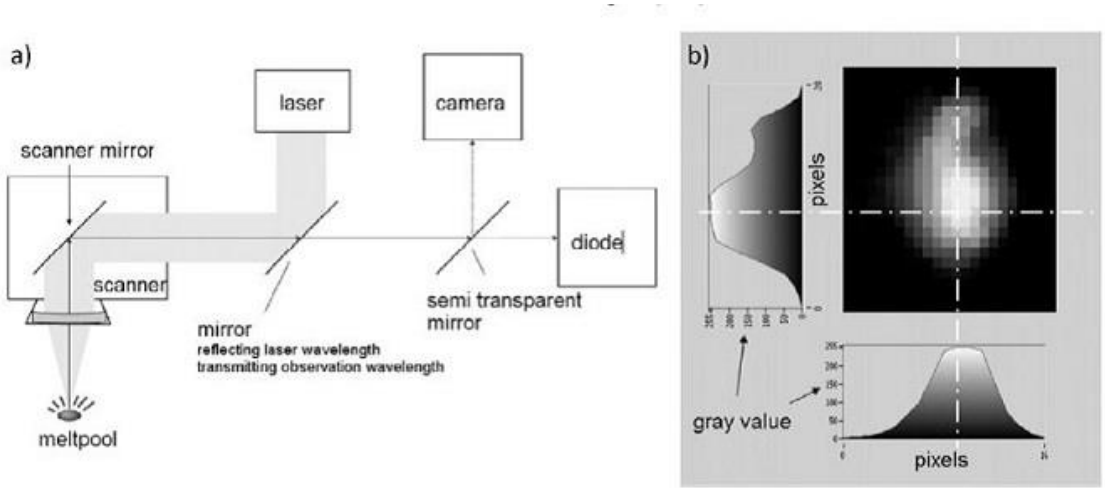

Figure 2: (a) Schematic showing arrangement of photodiode and camera and (b) an example output from the camera system showing varying intensity values for laser- and powder-bed AM achieved (Berumen et al. 2010).

2.3.2 Thermography and thermal camera

Thermography is based on the electromagnetic radiation spectrum's infrared band. The infrared band has four categories which are near-infrared (0.8–1.7 μm), short-wavelength infrared (1–2.5 μm), mid-wavelength infrared (2–5 μm), and long-wavelength infrared (8–14 μm) (Usamentiaga et al. 2014). Infrared radiation is a straight line ray and propagates in a vacuum, and the intensity of the spectral emission from the body depends on the absolute temperature. Three factors that affect thermal inspection include emissivity, surroundings, and atmosphere. Thermography works with the variance in thermal behavior

between the defects and its actual body (Lu and Wong 2017). Monitoring with this process has some advantages: it can work with a certain distance and gives fast results to correct the defects (Mireles et al. 2015).

For detecting defects and process instabilities, heat dissipation is mainly monitored by their cooling rate and thermal gradients using a thermal camera (Bontha et al. 2006). In the experiment by Krauss et al. (2015) for powder bed additive manufacturing of nickel-base super-alloy (Inconel 718), the data was collected in every layer and then composed into a 3D quality report shown in Figure 3**.** For monitoring each layer, the temperature between the powder on the build platform and pantry was used to find localized defects based on heat dissipation. Post-processing of data is still required for correlating measurement values with material properties and optimization of image processing to increase the possibility of defect characterization (Krauss, Zeugner, and Zaeh 2015).

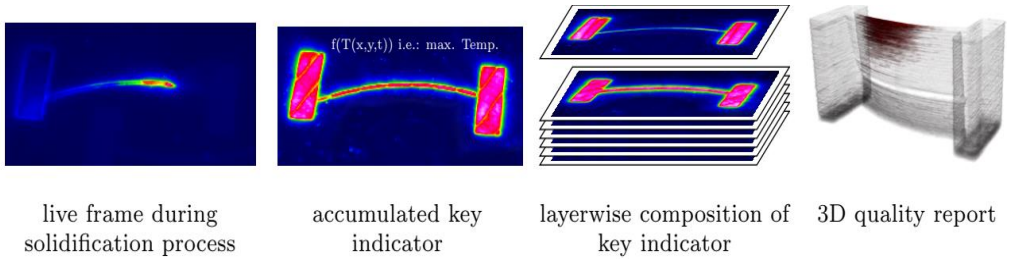

Figure 3: Data processing steps in thermography for AM process monitoring (Krauss, Zeugner, and Zaeh 2015).

2.3.3 Radiography

Passing radiation energy into a material, which creates a homogeneous image except in the region where deformation occurs due to defects and density differences, provides an understanding of possible defects in the material. Parameters such as voltage, current, and time of exposure need to be adjusted for different thicknesses and materials to acquire adequate resolution in radiography images (Lopez et al. 2018). Figure 4 shows that different types of defects such as porosity, inclusions, and lack of fusion can be detected by radiographic testing. This study has found that 2D defects and minor defects are challenging to

identify by this technique and the locations where cracks occur. Lopez et al. (2018) compared the dye penetrant inspection results with the X-ray technique to detect defects in two different samples, as shown in Figure 5, and the results were satisfactory (Lopez et al. 2018). The Aspect of physics was being clarified using LAM for finding defects and molten pool dynamics, and it could be utilized where porosity and spatter are common issues (Leung et al. 2018; Wolff et al. 2019). A study by Wolff et al. (2019) in-situ monitoring of complex 3D process was done to find the 'overhang condition' phenomenon in the LAM process on the top of loose powder instead of a solid substrate (Leung et al. 2018). Imaging of the melt pool and the material's internal structure was done using a high-resolution X-ray where cavity porosity formation could be identified. This study was done during the phase transformation and rapid cooling though it was only for qualitative measurement. Further study is required to achieve higher accuracy in the results (Wolff et al. 2019).

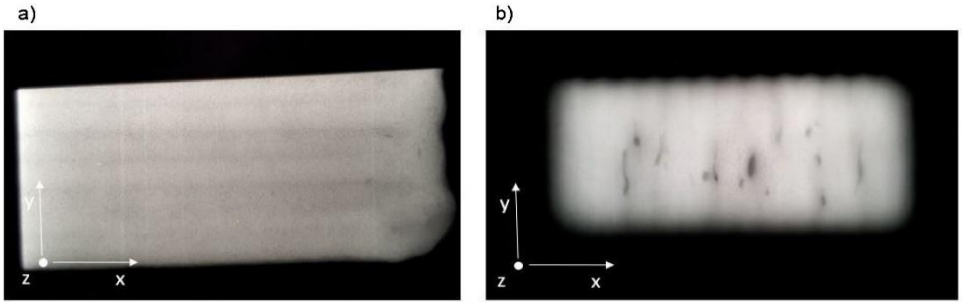

Figure 4: Examples of X-ray results in material inspection. (a) Aluminum and (b) Mild-steel (Lopez et al. 2018).

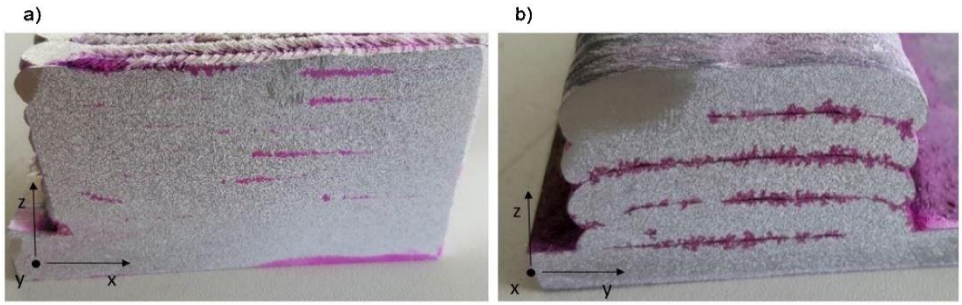

Figure 5: Cutting sections to confirm the X-ray NDT test results with dye penetrant to make defects more evident. (a) Aluminum and (b) Mild-steel (Lopez et al. 2018).

The radiography technique can detect embedded defects, but the X-ray's sensitivity across the perpendicular direction is inferior. Due to the requirement of a long time to inspect the material, radiography is not suitable for online monitoring (Lopez et al. 2018).

2.3.4 Acoustic and Ultrasound

Acoustic and ultrasound techniques convert acoustic energy into electrical signals measured by sensors (Shao and Yan 2005). During Laser Metal Deposition (LMD), the defect sources can be identified by the acoustic emission technique to detect defects such as cracks and pores through their nucleation and propagation. Additional defect information such as vaporization, plasma generation, and keyhole formation (L. Li 2002) can be obtained with AE time-space waveforms feature analysis, such as amplitude, energy, rise time, count, and frequency (Gaja and Liou 2016). Ultrasonic Testing (UT) uses high-frequency sound, which comes from the material and defects inside the material. These sounds are used for analyzing material characteristics for finding flaws. A combination of AE and UT can provide higher quality assurance in the monitoring of AM parts. Laser Ultrasonic (LU) is another promising non-destructive ultrasonic technique in additive manufacturing that uses laser irradiation for the generation of ultrasound waves in either ablation or thermoelastic regime (Taheri, Koester, et al. 2017) (C. Scruby and Drain 1990)(Koester, Taheri, Bigelow, Bond, et al. 2018)(Taheri 2018)(Taheri, Shoaib, et al. 2017). In LU, a pulsed laser illuminates the surface of the structure. Depending on the laser energy level, different wave modes can be generated through thermally induced displacement in part. LU has the advantages of being non-contact and not being influenced by environmental conditions such as high temperature, making it an ideal solution for in-situ monitoring of manufacturing processes such as AM (Taheri, Koester, et al. 2017). Acoustic monitoring has been extensively used for online and offline monitoring systems. Strantza et al. (2015) studied Ti6Al4V samples produced by SLM (Selective Laser Melting) and AISI 316L samples produced by LMD in an offline monitoring procedure. It was found that SLM samples had more fracture than the LMD samples after applying the external step-by-step static load. The results showed that when the load increased to the

maximum value, the number of AE high magnitude events rapidly increased, indicating possible crack propagation during the higher load levels. The number of AE events (counts) was higher when parts had more fractures (Strantza et al. 2015).

Gaja and Liou's (2016) purpose was to collect data, make a dependable analysis method, and classify them based on the type of defects and experimental setup, as shown in Figure 6. It was found that the AE signal's energy is a critical component for detecting the defect source. Validation of AE defect identification was done by optical microscopy, which shows a correlation between the signal events and the defects (Gaja and Liou 2016). However, additional research is still required for AE monitoring in the additive manufacturing process.

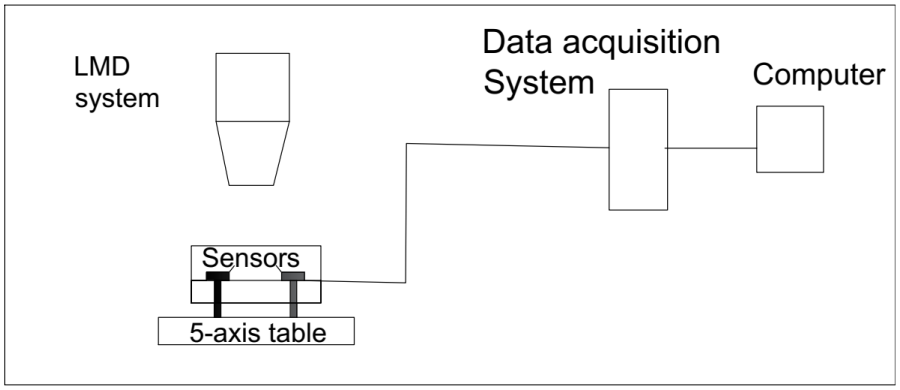

Figure 6: Experimental setup showing the LMD system and AE data acquisition system (Gaja and Liou 2016)

The formation of porosity and cracks generates an acoustic emission signal, an elastic wave that travels from the source toward a sensor, moving through the substrate until it arrives at the acoustic emission sensor. The sensor produces an electrical signal passed to electronic equipment for further processing and detecting a defect in response. Since the LMD is an additive process and deposits metals in a layer-by-layer process, the AE signal was recorded for each layer and analyzed to extract any useful information from the AE events (Lu and Wong 2017).

2.4 Methodology of AE

2.4.1 What is AE?

Many Nondestructive Evaluation (NDE) approaches to gain industrial traction thus far generate optical datasets that can be used to identify surface-breaking mechanical defects (Grasso and Colosimo 2017) but fail to capture information in the subsurface, where porosity is known to form through different conditions such as keyhole mechanism (Zhao et al. 2017). Acoustic Emission (AE) is formed from the phenomenon of the material where transient elastic waves are generated by the continuous release of energy during the fabrication (ASTM E1316-07b 2007). Acoustic Emission (AE) can be used for finding internal structural defects using the acoustic signals generated by internal defects. An AE testing can be done mainly by two integrated components; a defect, such as the source of energy release in the material, and transducers that collect the information from the generated source (Nair and Cai 2010). Thus, the technique is mainly based on generating a signal, data acquisition, data comparison, and finally, making the decision. The schematic shown in Figure 7 represents the general working principle of an acoustic emission system, and Figure 8a shows a typical characteristic of AE signals where defects' limits and threshold limit are shown. A fault spread its signal in the form of high-frequency sound waves that are received by sensors.

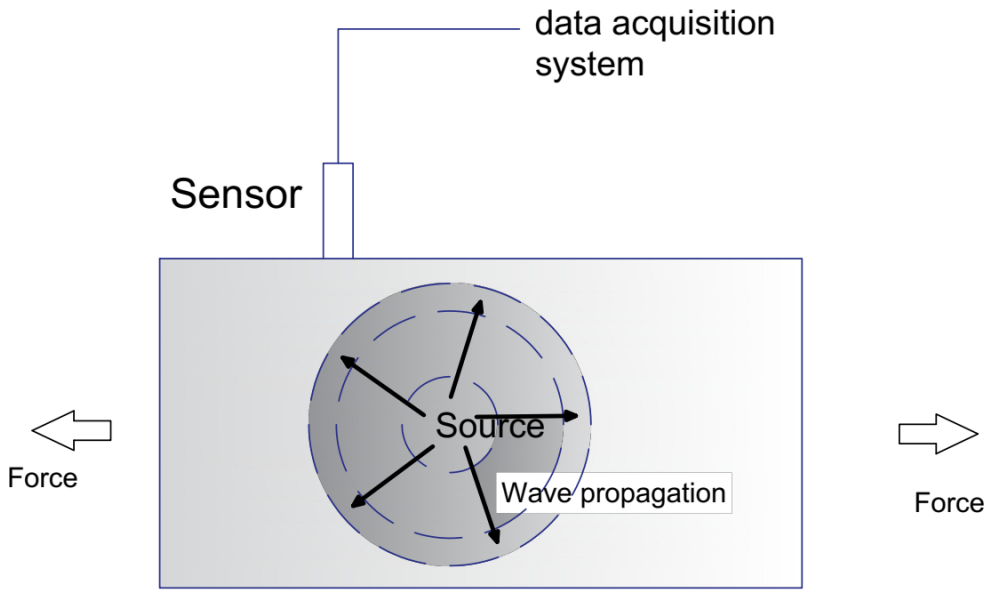

Figure 7: Principle of acoustic emission

Amplitude, rising time, energy, duration, and count are the main characteristic features of the emitted AE waves (Figure 8(a)), which can be used to evaluate and characterize the AE signals. Depending on the defects, the values and intensity for each of these features might be different, which should be processed precisely. However, the longtime history of research on AE testing shows that the range of the AE frequency spectrum provides essential information regarding the category of defect types, as shown in Figure 8(b).

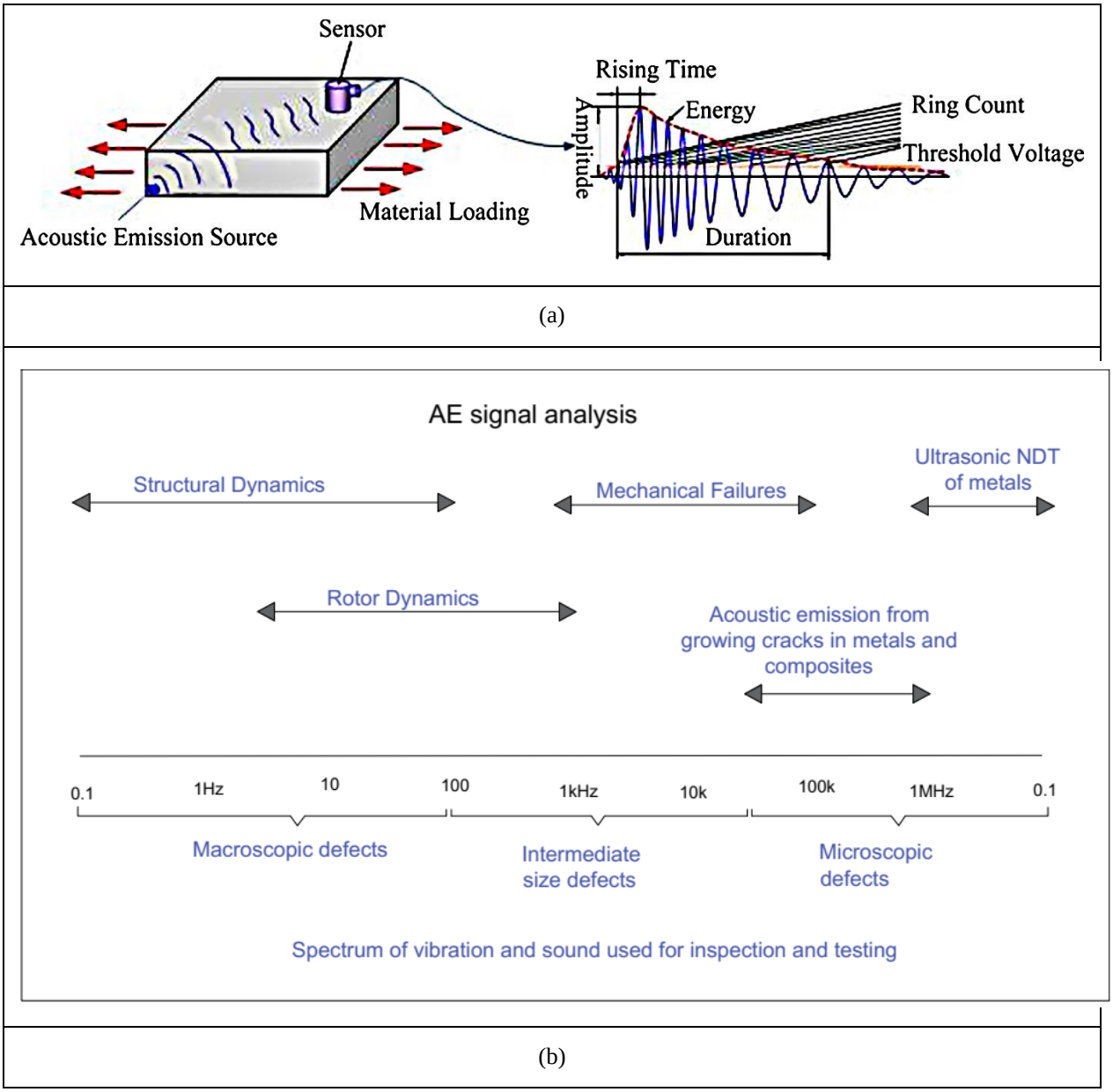

Figure 8: a) Typical AE signal and relevant major features, (b) range of AE frequency for different types of defects

Damage detection using AE testing is based on the recording and analysis of the AE signals. Recording AE signals is accomplished by direct coupling of piezoelectric transducers with the part under test. Piezoelectric transducers work based on the piezoelectric effect, which is the electric charge that accumulates in lead zirconate titanate (PZT) materials in response to applied mechanical stress. The

piezoelectric sensors' output will be amplified through a low-noise preamplifier, and further will be sent to the processing unit for analysis (Figure 9).

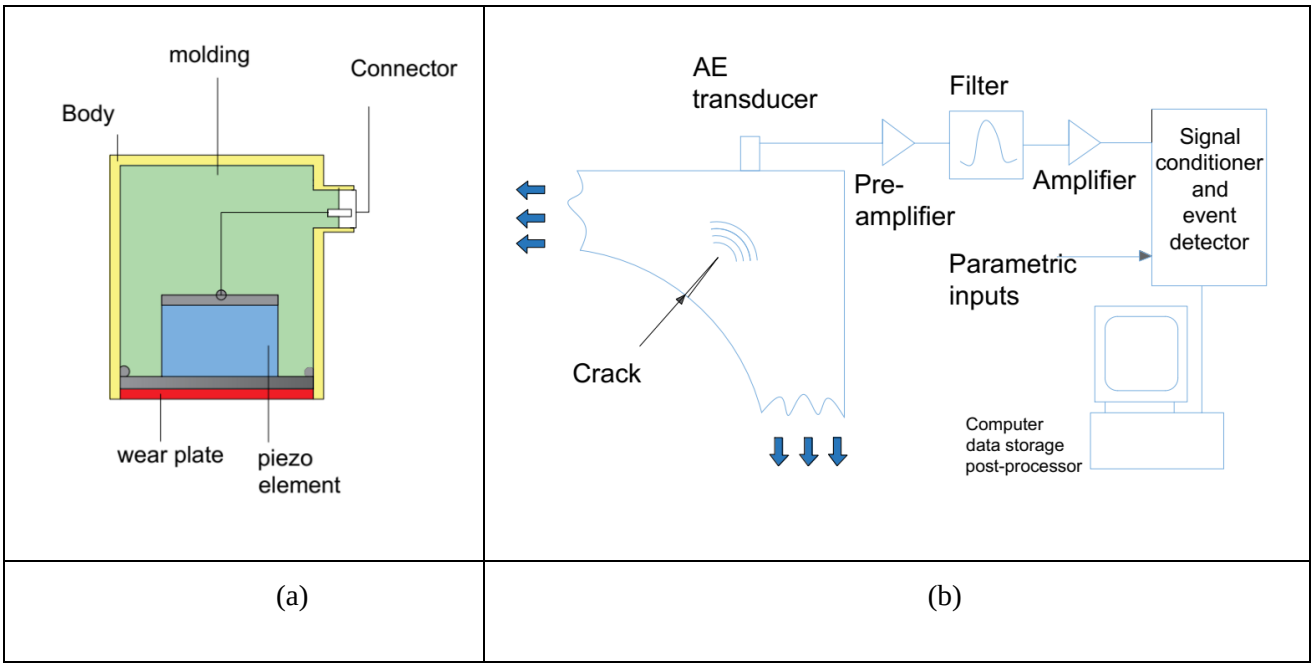

Figure 9: Working principle and structure of (a) AE sensors and (b) defect detection and signal recording

Because of AE testing characteristics and its related instrumentation, many external phenomena can create noise on the AE signal. Examples include Electromagnetic Interference (EMI), rubbing of the crack nose, fretting in weak joints, turbulent flow of fluids, environmental conditions, frictional noise, and impact sources. Also, at lower frequencies, background noise from the environment can considerably disturb the measurement. Techniques to remove the noise consist of three significant steps: (i) defining the active sources of noise; (ii) characterizing the signals generated by the sources of noise; and (iii) designing a method to remove the noise signals (Wevers and Surgeon 2000). Some potential strategies include manufacturing special sensors with electronic gates for noise prevention, taking measurements to position sensors from noise sources as far as possible, and electronic filtering to remove noise.

2.4.2 Mechanism of acoustic emission in materials

Acoustic waves are a kind of stress wave generated when stress conditions happen in the materials. The change in the material's stress condition can be generated due to deformation, crack initiation and growth, crack opening and closure, dislocation movement, twining and phase transformation, and delamination. These damage-related causes of stress are the primary sources of AE. These potential stresses generate some stress waves that can be detected using AE sensors to contact the material under stress and be used for defect detection and material characterization.

Both acoustic signal characteristics and the metallurgical properties of the material can influence the AE results. At higher frequencies, the acoustic emission is not intense enough in most cases, and the material absorbs large parts of the signal. The sensitivity and frequency range of the piezoelectric transducers are limited such that not all of the defect generating during the metallurgical processes in the material can be detected via AE. These influences show the strong dependence of AE testing on acoustic signal characteristics (frequency, threshold, bandwidth) and metallurgical variables (crystal structure, composition, grain size, precipitate structures). The importance of having a good understanding of the effects of metallurgical variables is prominent when AE is used to detect growing flaws, and it is essential to know the origins of the detectable AE. Several detailed metallurgical studies have discussed acoustic emission sources during plastic deformation, dislocations, brittle fracture, and other metallurgical phenomena (C. B. Scruby et al. 1981).

2.4.3 Background of AE as a monitoring technique

AE has been used in various manufacturing processes for quality control. It has recently become more popular for structural health monitoring, process monitoring, and quality assurance for online or offline monitoring in different fields such as tool wear monitoring, monitoring of civil structures,

mechanical or electrical devices monitoring, and the field of additive manufacturing. In this section, the application of the acoustic emission technique in some different types of engineering fields is discussed.

Timely damage detection is necessary for bridge monitoring for estimating the entire life of the structure. AE is the most helpful technique for this continuous monitoring, and nowadays, it is the most widely used technique for highway structural assessment (Rens, Wipf, and Klaiber 1997; Nair and Cai 2010). AE monitoring of bridges is divided into two types of long-term and short-term monitoring, where long-term is applied to new bridges, and short-term monitors the structural integrity of existing structures. Though it is one of the most effective monitoring types, quantitative monitoring of bridges is still challenging (Nair and Cai 2010). Similar to other monitoring types, noise cancelation and filtration needs to be done for accurate data analysis. The Kaiser effect and Felicity effect analysis have been done to find defects in the bridge structure, where the Kaiser effect is shown to exist at 70-85% of ultimate strength and the Felicity effect shows damage progression in the same material (Ziehl and Lamana 2003) (Gostautas et al. 2005). In a case study by Nair et al. (2010), a large amount of information was found from the applied live load to a concrete bridge, and a steel bridge was analyzed via quantitative and qualitative analysis. The information found was valuable for characterizing defects, which show a promising implementation of the acoustic technique in continuous bridge monitoring (Nair and Cai 2010).

As another field of application, various works have been done to monitor tool wear in machinery turning operations. The work has been done with AE signals generation, acquisition, and different types of signal analysis techniques from this complex metal cutting process. Tool wear has an adverse effect on the product's final quality, which makes monitoring a compulsory operation so that undesirable consequences can be avoidable. For tool wear monitoring, the tool's AE signal is different from the machine vibration and other noises. AE is also used to refer to stress waves generated by the sudden change in energy generated from the defects in parts, and it has been successfully used in laboratory tests to detect tool wear and fractures in single-point turning operations. Dornfeld (1989) (Liang and Dornfeld 1989) explain the various

sources of AE signal in turning operations such as plastic deformation, frictional contact, breakage, and tool fracture, which is shown in Figure 10 (X. Li 2002).

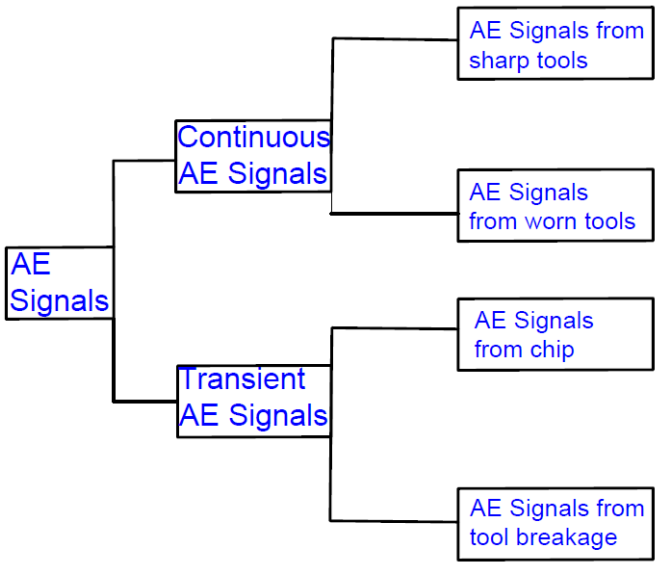

Figure 10: AE signal types in cutting operation (X. Li 2002)

The most important sources of AE signals are friction between the workpiece and tool fracture. As a result, the amplitude of AE signals can be used for tool fracture monitoring. Figure 11 shows a step-by-step procedure for a specific tool wear monitoring system. Signals were corrected using amplifier and bandpass filter, and signal processing is also done by using temporal and different transformation techniques, neural networks, and sensor and data fusion. It is found that the different techniques of data analysis can be effective for monitoring tool wear with the integration of other types of sensors (X. Li 2002).

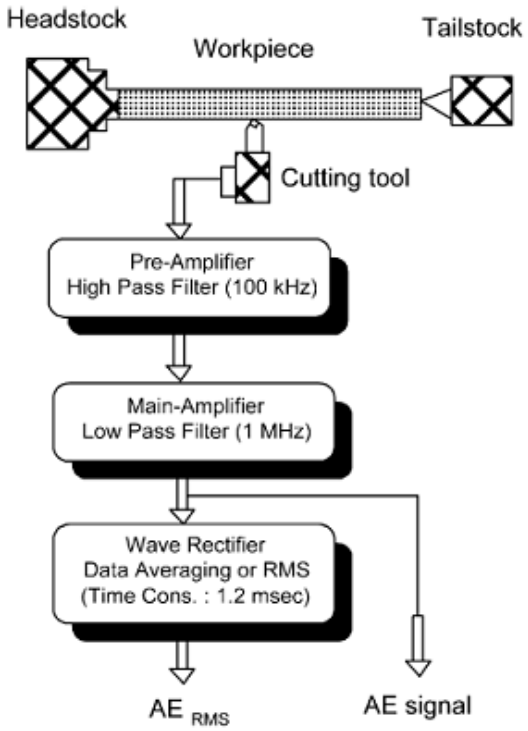

Figure 11: AE signal correction and processing (X. Li 2002)

Rotating machinery is another type of mechanical system where AE can be effectively used for operational health monitoring. Because the problem mainly occurs in a rotating device due to faulty bearing, online monitoring of bearing becomes an important issue. During the operation, AE signals come from the defects caused by roller and raceway contact with different frequencies, identifying the location of defects (James Li and Li 1995) (Choudhury and Tandon 2000). A sketch of the test rig on which the experiments were conducted by Choudhury et al. (2000) for detecting defects in the bearing is shown in Figure 12. In this study, the motor is used with other equipment and the AE sensor to identify the effects of applied load on the bearing (Choudhury and Tandon 2000). With the understanding of the statistical distribution of events and peak amplitude, the inter-relationship of defects under various loads and speeds and location of defects could be identified for the monitoring of bearing in rotational parts (Choudhury and Tandon 2000; James Li and Li 1995) (Yadavar Nikravesh et al. 2019).

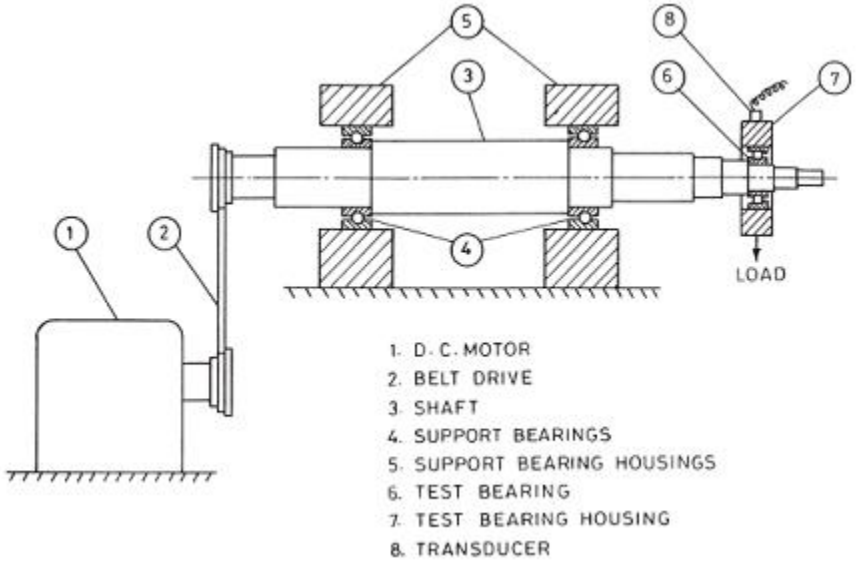

Figure 12: The experimental test ring for the detection of defects in bearing (Choudhury and Tandon 2000)

2.5 Survey on AE applications for the process and part quality monitoring in AM

Acoustic signals provide much information about the process condition, part quality, and structural integrity. Based on these capabilities, acoustic signals and sensing equipment have been studied in different research works for process and part monitoring in AM (Fisher et al. 2016). However, the base of all these works is to use acoustic signals for in-situ monitoring, but the AM technique, type of AM machine, the feed materials, and the data processing methodologies are very different in the studies that used in-situ acoustic monitoring. To have an overall picture of the diversity of AM techniques used for in-situ acoustic monitoring, a summary of the type of AM process, type and number of acoustic sensors, process signatures or data processing technique, and research literature for in-situ acoustic monitoring of AM is presented in Table 1.

Table 1: Type of AM process, type and number of acoustic sensor(s), process signature(s) or data processing technique, and research literature for in-situ acoustic monitoring of AM

Type of AM process	Type and number of the acoustic sensor(s)	Process signature(s) or data processing technique	Literature(s)
Laser Powder Bed Fusion (LPBF)	Piezo acoustic sensor - 1	RMS value of acoustic emission signals	(Ludwig 2020)
Laser Powder Bed Fusion (LPBF)	Piezo acoustic sensor - 4	Hsu-Neilsen technique was used to locate the defect signal on the build plate	(Ball 2018)
Laser Powder Bed Fusion (LPBF)	Fiber Bragg Grating (FBG)	Relative energies of the frequency bands obtained using Wavelet Packet Transform (WPT) and classified based on spectral Convolutional Neural Network (CNN)	(Shevchik et al. 2018)
Laser Powder Bed Fusion (LPBF)	Piezo acoustic sensor - 1	Fast Fourier Transform (FFT) of acoustic signals fed to an Artificial Neural Network (ANN)	(Eschner et al. 2020)
Laser Powder Bed Fusion (LPBF)	ICP microphone - 1	Short-Time Fourier Transform (STFT) of acoustic signals	(Kouprianoff et al. 2020)
Laser Powder Bed Fusion (LPBF)	Piezo acoustic sensor - 3	RMS value of acoustic emission signals	(Plotnikov et al. 2019)
Direct Energy Deposition (DED)	Piezo acoustic sensor - 1	RMS of the AE signal used for monitoring the mass flow rate of powder feedstock	(Whiting, Springer, and Sciammarella 2018)

Direct Energy Deposition (DED)	Piezo acoustic sensor - 1	Time-domain and frequency-domain features of AE signals are used as the indicators and analyzed using unsupervised pattern recognition analysis (K-means clustering) in conjunction with a Principal Component Analysis (PCA)	(Gaja and Liou 2016; 2018)
Direct Energy Deposition (DED)	Piezo acoustic sensor - 5	— Peak amplitudes of the frequency spectrum — The difference in peak amplitudes of frequency spectrum compared to the baseline condition — The peak frequency of the spectrum — Centroid amplitude of the frequency spectrum — Centroid frequency of the spectrum	(Taheri et al. 2019; Bond, Koester, and Taheri 2019; Taheri 2018)
Fused Deposition Modeling (FDM)	Piezo acoustic sensor - 1	Time-domain features of AE signals are used as the indicators and analyzed using Support Vector Machines (SVM)	(Wu, Wang, and Yu 2016; Wu, Yu, and Wang 2016)
Fused Deposition Modeling (FDM)	Piezo acoustic sensor - 1	RMS of the AE signal used for monitoring the distortion defects	(F. Li et al. 2019)
Fused Deposition Modeling (FDM)	Piezo acoustic sensor - 1	Instantaneous skewness and relative similarity of the AE raw waveform used for filament breakage monitoring	(Yang et al. 2018)

2.5.1 AE equipment and sensors

Various experimental setup types have been used for collecting the data without losing any critical information during the AM processes. The basic setup includes AE sensors, amplifiers, data filtering

devices, data acquisition systems, and data storage devices. Data needs to be collected by the sensors directly connecting them to the build plate to lose no or fewer data. In some configurations, sensors are connected at the bottom of the build plate or the build plate's upper side in other cases. During the monitoring of the Fused Deposition Modeling (FMD) machine (with ABS material), Wu et al. (2015) used the AE sensor which could eliminate background noise and was attached to the side surface of the extruder and connected to a preamplifier, and data acquisition device (Wu, Wang, and Yu 2016).

In a study by Koester et al. (2018) where titanium alloy (Ti-6Al-4V) was deposited by a Direct Energy Deposition (DED) system, an array of acoustic sensors (commercial sensors; digital wave, B1025-MAE) was installed below the baseplate with a customized arrangement. A high-temperature ultrasonic couplant was used to keep the transducers in an acceptable temperature range, and the data were collected in five different building conditions (Koester, Taheri, Bigelow, Bond, et al. 2018). The setup is shown in Figure 13.

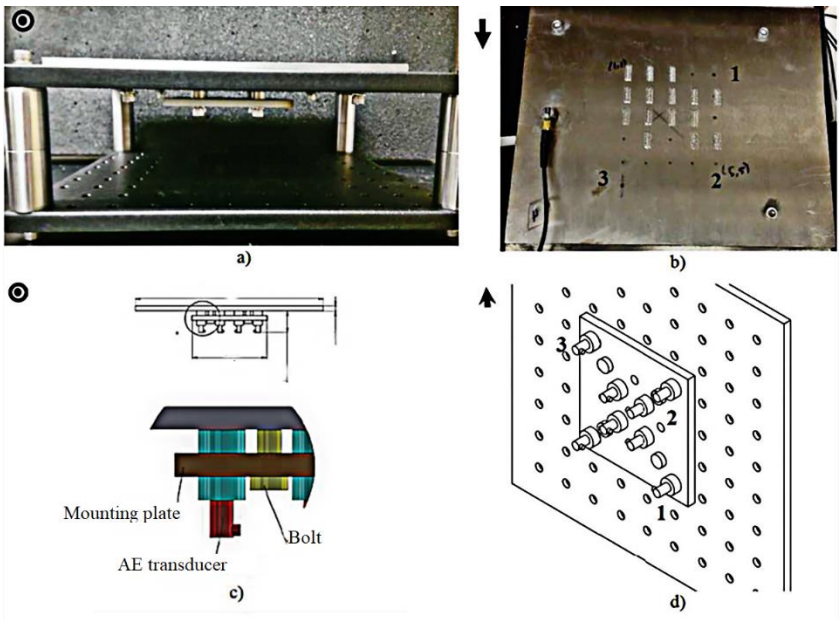

Figure 13: Acoustic monitoring array design including a) posts for clearance to allow for sensor array (FRONT view), b) transducer arrangement including transducer 4 attached directly to the build plate (TOP view), c) detail drawing showing the transducer mounting plate, transducers, and posts for temperature mitigation, and d) the array attached to the underside of the build plate. Arrows indicate the direction of the front of the assembly in all plots (Koester, Taheri, Bigelow, Bond, et al. 2018)

During defect monitoring of LMD by Gaja and Liou (2017), distinguishing the type of defects in the LMD process has been done by clustering AE signals. Corrective action could be done, such as machining and remitting, based on the results. Also, a classification method for analyzing AE was used to identify defects based on types of defects. AE sensors were connected to a substrate for recording the signals. These sensors were used for capturing AE signals and then transferring them to the computer. The YAG laser was connected to a numerical control system after LMD for postprocessing machining, and then the data was taken from the processed material for defect identification. Figure 14 shows the step-by-step method used for the analysis of acoustic techniques (Gaja and Liou 2016).

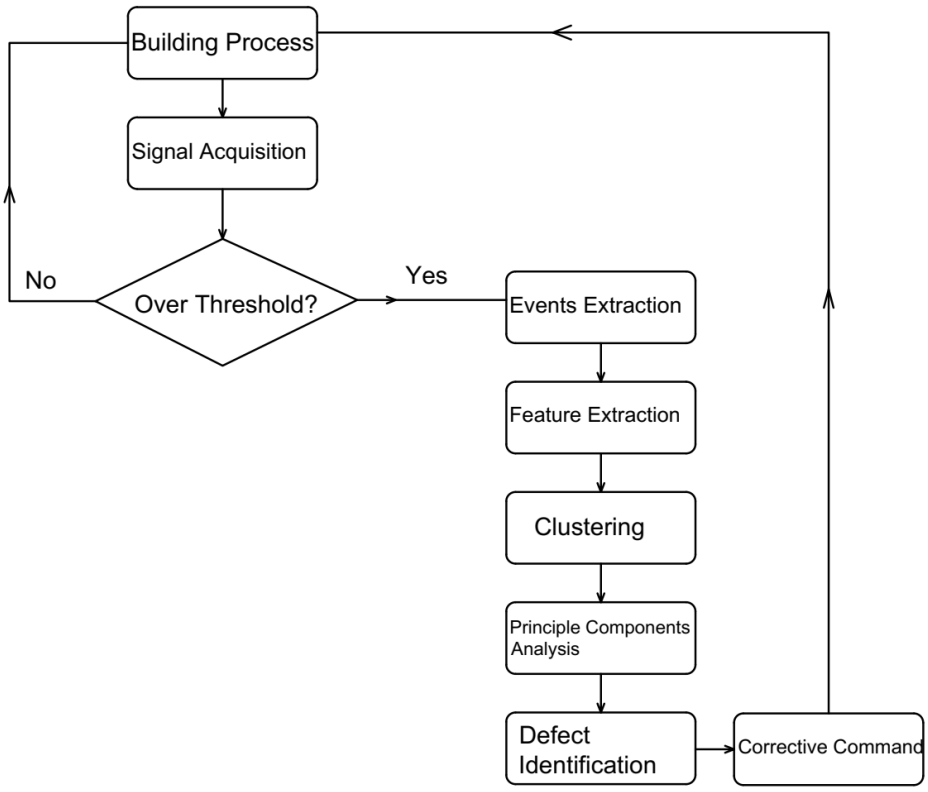

Figure 14: Traditional step-by-step operations used to perform the acoustic emission analyses (Gaja and Liou 2016).

A study was done by Shevchik et al. (2018) for AM process monitoring, which used an industrial machine concept M2 with one Fiber Bragg Grating (FBG) sensor to detect the airborne AE, which is

imprinted into the core of the optical fiber, as shown in Figure 15. It was installed on a unique plastic holder and mounted in the lateral wall (Shevchik et al. 2018).

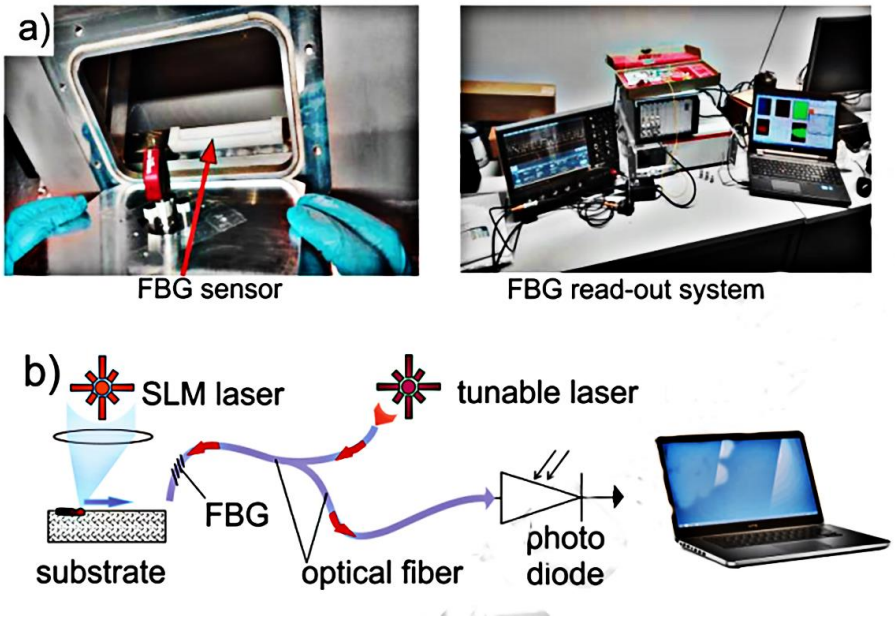

Figure 15: a) (left) view of the FBG location inside the AM chamber with the optical feedthrough on the chamber panel and (right) the FBG read out system and (b) scheme of the FBG read out system (Shevchik et al. 2018)

A different approach was taken by Purtonen, Kalliosaari, and Salminen (2014), where acoustic emission sensors were used without directly connecting to the build plate but combining it with optical methods. During the monitoring of direct energy-driven additive manufacturing, the acoustic emission is generated by the weld pool. Gold et al. (2018) worked with two samples: the baseline acoustic profile from a known suitable workpiece and another acoustic profile with significant defects. The leading equipment used in this process was an acoustic sensor mounted in the location within the product building apparatus, contact microphones mounted to the outside of the build platform, and free air microphones installed above the table, a rigid structure for making the planer work surface. During the process, the system incorporated defects for creating acoustic events to monitor the build process for identifying those defects (Gold and Spears 2018). In another study by Redding et al. (2018), presented in US patent “US 10073060 B2,” a non-

contact acoustic inspection system was connected into the powder bed additive manufacturing process, which was referred to as “laser ultrasonic inspection.” The system measures the displacement of the sample’s surface due to the ultrasound wave propagation. The sources' return signal is captured from acoustic waves for further analysis by non-contact acoustic sensors (interferometer) (Redding, Gold, and Spears 2018).

2.5.2 AE data and signals

2.5.2.1 Mechanisms of AE signal acquisition

Proper online acquisition of AE signal from the additive manufacturing process and parts is significant for making consequent analysis easier. The data acquisition can be made considering the storage limit by selecting a proper sampling rate and threshold limit. The acoustic waves move through the parts to the sensor, where it produces an electrical signal and then passes to the central unit for further processing. In the study by Wu et al. (2015), the sampling rate was set to 5 M samples per second to avoid external noise. The data recorded when only the extruder operated for one of the experiments. In the next experiment, the AE signals were taken during the transition of regular operation and no material operation. The experiments were also conducted in three different states to measure the feasibility of the study. AE hits were recorded with ABS- Energy (absolute energy), counts (number of pulses that cross-defined threshold), Freq-C (frequency centroid), and P-Freq (peak frequency). The AE from the material loading state and the normal extruding state were recorded avoiding mechanical noise, which was first amplified by a PAC 2/4/6 preamplifier and then calculated by the PAC PCI-2 (PAC PCI-2 is a fast data acquisition system) system in real-time, which acquires data with a sampling rate of 40 M samples per second. Then the data was analyzed to identify the defects (Wu, Wang, and Yu 2016). In the study by Koester et al. (2018), a signal conditioning unit (digital wave FM-1,8 channel) was used for signal acquisition intermittently at 300 Hz with a duration of ~800 microseconds (4096 points at 5 MHz) till a small period after finished building. From LMD additive manufacturing process, the AE signal was recorded from the different layers (Koester,

Taheri, Bigelow, Bond, et al. 2018). In the study of in-situ monitoring by the convolution neural network by Shevchik et al. (2017), the acoustic emission signals were taken from the periodic extension/compression of the fiber core. The sample rate was downsampled from 10 MHz (initial setting) to 1 MHz, and it was taken from each layer of the entire workpiece. Layer-by-layer data acquisition helps to avoid any noise during the transition/intermediate period. Data was taken in three different states: low energy density (porosity defects found), optimal process (lowest porosity and most minor defects), and high energy density (tubular defects), so that different types of defects can be identified after further data analysis which is shown in Figure 16 (Shevchik et al. 2018).

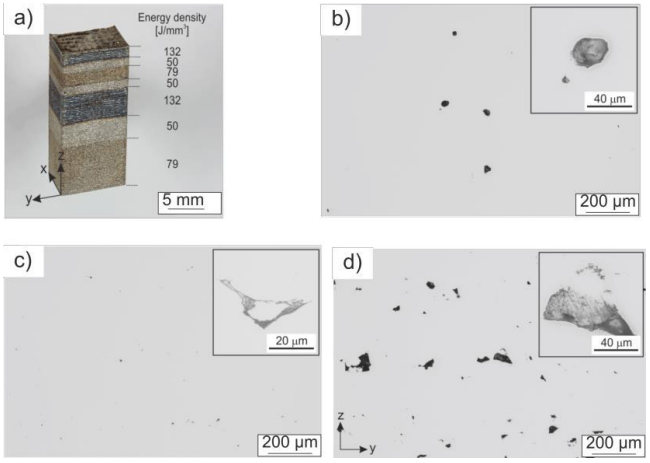

Figure 16: a) SLM test workpiece produced with three energy densities where 50 J/mm^3 are bright regions, J/mm^3 are dark regions and 132 J/mm^3 are blueish regions; b) – d) Typical light microscope cross-section images of the regions produced with a) 132 J/mm^3, b) 79 J/mm^3 and c) 50 J/mm^3. The insets show typical defects observed such as a) tubular, b) small lack-of-fusion and c) large lack-of-fusion defects. The *z*- and *y*-directions correspond to a) (Shevchik et al. 2018).

In the study of Gold et al. (2018), acoustic waves were generted from the weld pool during the fusing step detected by the microphone to generate an acoustic profile (Gold and Spears 2018). The signals are taken from the weld pool's acoustic wave radiation by the sensors and monitoring beam. The signals taken are directed by pulse monitoring laser, which mainly finds out the changes in the index of refraction of shield gas (such as a mixture of nitrogen, argon) above the build surface, also causing variation in the

monitoring beam's path. The photodetector sensed the monitoring beams' variations beam path, and these signals were then analyzed (Redding, Gold, and Spears 2018).

2.5.2.2 AE signal processing methods

Various signal processing techniques have been done by researchers, such as time-domain analysis, frequency-domain analysis, convolutional neural network, and wavelet analysis. The signals are collected with different patterns and with filtering to become more efficient for finding defects. AE features for different signal processing types are peak amplitude, Kurtosis, energy, number of counts, duration, rise time, and peak amplitude frequency (Gaja and Liou 2016). Finding a signal with various AE events such as absolute value, peak value, and RMS value is the preliminary requirement for temporal domain analysis. These AE events can be used for identifying the changes in material and process states due to defects and anomalies. AE events can either be used as individual identifiers or as combined parameters with integrating two or three AE events (Taheri, Delfanian, and Du 2013). Frequency-domain features used for analyzing the data can be identified at different frequency levels. Principle Components Analysis (PCA) (Taheri 2017) and K-means clustering (Taheri et al. 2019) were also used in signal processing to identify defects source mechanism and visualization of data for specific groups (Gaja and Liou 2016).

The dominant frequency component's background noise was identified by Wu et al. (2015) from state 1 (material loading state) and state 2 (normal extruder state) signals. The short-time fast Fourier transform (STFFT) is found that most of the frequency components fall in the range below 333 kHz. The feature was also calculated in the time domain and found a noticeable difference where ABS-energy (absolute energy) can be used as an indicator of different states. It is found that ABS-energy is at a higher level in no material state, as shown in Table 2 and differentiating two states. The AE signals also provided a significant difference between those states, which helps to characterize and identify the data of different states with a high level of accuracy. The results found 100% accurate in the cross-validation process, and there is no overlap between the states. In multistate identification, 60 segments were generated for the experiment, and all state 100 segments were generated (20segments in each state) in 500ms/state duration

(Wu, Wang, and Yu 2016). Shevchik et al. (2018) did AE testing for in-situ monitoring using conventional CNNs (Convolution Neural Network) and Spectral Convolutional Neural Networks (SCNN). Data was collected throughout the whole process, from the manufacturing of a workpiece. During the process, different defects were created intentionally for creating AE signals from those signals that can be accumulated, and the classification of signals can be done. During feature extraction, the frequency band was found using standard wavelength packet transform (WPT) and then filtered. For feature extraction, the Daubechies wavelet provides the best feature extraction with minimum error. Data analysis was done in a running window; it gives a better resolution for a short period, but it is strongly affected by noise. The data analysis of the system was also done by (SCNN) using FFT (Fast Fourier Transformation) (Shevchik et al. 2018).

Table 2: Means and standard deviations of ABS-Energy and RMS for in situ monitoring of FDM machine (Wu, Wang, and Yu 2016)

		With material	Without Material
ABS- Energy	Mean Value (aJ)	4588.08	9270.82
	STD	10560.51	25973.94
RMS	Mean Value (mV)	0.0256	0.0296
	STD	0.0018	0.0034

The signal from 100 to 2000 kHz was filtered with the required bandwidth of the modal acoustic emission sensors, and a cutoff frequency was also utilized to segment low and high frequencies for state segmentation. For the different build conditions, the data was segmented low, high, and centroid position and amplitudes within the bandpass, and the same process was done for centroid locations and amplitudes in high and low-frequency bands (Koester, Taheri, Bigelow, Bond, et al. 2018). Defects created peak events different from other signals, but the certain possible signal that comes from the noise was filtered under a

threshold, where different types of defects can produce a similar waveform. So, it was challenging to find the characteristic of events. Using Fast Fourier transformation or time-domain analysis, the AE signals can be analyzed by different signal features. In the study of Wu et al. (2016), the noise level is significantly smaller than the signal of interest, where noise could be minimized by using frequency filtering between 100 kHz and 1 MHz. In this study, principal components analysis and K-means clustering were used to identify defects source mechanism and visualization of clusters in 2D and 3D plots. PCA was mainly used for dimensionality reduction, and K-means clustering helps for making groups of events into homogeneous subgroups, and a silhouette width was used to find the optimal number of clusters (Gaja and Liou 2016). The study of Gold et al. (2018) collected the signals from the baseline sample, which is "known good," and the defects sample. They found the variation of acoustic signature occurred when there was any defect during the process. The analysis was done both in real-time and at the end of the process (Gold and Spears 2018). The data varied with thickness, defects location, and size, where the data analysis running on one or more processors embodied in different computers used for data analysis, statistical process control, and feedback control. Appropriate computations were used to determine defects, position, and thickness of those defects based on the sensors' acoustic data. (Redding, Gold, and Spears 2018).

2.5.3 Observations of the different previous study

According to different studies of in-situ monitoring for additively manufactured products by acoustic technique, the results seem to be promising for finding defects, while most of the studies were based on qualitative analysis rather than quantitative. The signals found from the defects were varied with the crack characteristics and crack propagation in the AM parts. High amplitude events, such as the high amplitude of frequency or high voltage, are found in the experiment to indicate a possible generation of cracks during the process. A few authors also validated their study with other NDT techniques and found similar results. In the study of Wu et al. (2016) in two-state identification, 100% accuracy was achieved; in multistate identification, 97% accuracy was achieved for data segmentation, and in all states, the overall

accuracy was 95%. The accuracy was increased if the groups were close to each other and if data was taken in a shorter period. It is found that during state transition, time-domain features are more sensitive than the frequency domain in the evaluation of FDM machine extruder working conditions. Further signal processing is required, such as Hilbert-Huang transform, for getting the relationship between frequency features and machine state, but it is difficult to do so when the amount of data is large (Wu, Wang, and Yu 2016). In Gaja and Liou (2016), various defect mechanisms were tested, and the K-Means clustering mechanism was used for analyzing the data. This study identified two types (porosities and cracks) of defects; on one side porosities, it takes shorter decay time and less amplitude, and on the other side, cracks take a short duration and high amplitude. The clustering mechanism is also validated by an optical microscope, which shows the correlation between the number of events and the number of defects (Gaja and Liou 2016). The result found by Koester et al. (2018) was having good repeatability where the data collected from a sensor attached on the build plate were most sensitive and hoped to improve in data in any future study, which includes calibration of data. The data collected from the transducer connected to the build surface, a high-frequency band in clustering, showed less separation but was the same for the low-frequency data band. Further study needs to be done to characterize the data to classify results (Koester, Taheri, Bigelow, Bond, et al. 2018).

In the analysis of acoustic signatures, high amplitude events in the lower side of the threshold were found in the received signal, indicating defects in the structure. By analyzing each layer's signals, it may be possible to identify all the defects in every layer of the build component. After getting the whole complete idea about defects, a build process can be rejected, and it also can be redirected. It is claimed that by using a setup of US patent “US9989495” and “US10073060,” defects identification, controlling of a process whether the process is stopped or redirected of the weld pool can be made (Gold and Spears 2018), (Redding, Gold, and Spears 2018). The inspection done by Redding et al. (2018), it is found that during the fusing of each layer or immediately after each layer or after several layers, the detection system gives the assurance if defects are present or not (Redding, Gold, and Spears 2018).

In the study done by Shevchik et al. (2018) the results were found feasible for the AE technique. The airborne was detected, and the energy of narrow frequency band was taken as signals with that SCNN used to find out defects by classifying features, and the accuracy found almost 83, 85, 89% for high, medium, and poor quality, respectively, where for the high-quality product the features are overlapped. The feature can be different for other manufacturing types and need to be investigated (Shevchik et al. 2018).

2.5.4 Summary of previous studies

The researchers identify in-situ monitoring using the AE system as an efficient methodology compared to other monitoring techniques because of its capability to detect more complex features. Furthermore, AE can be used to assess structural integrity and detect internal defects from the elastic waves. More work is needed for making acoustic-based monitoring an established methodology in the field of AM. The development of different sensors, noise filtering, and data acquisition modules for implementing the AE technique for in-situ monitoring is the primary area that must be precisely done to implement AE for in-situ AM process monitoring effectively. However, the acoustic techniques have shown promising results for in-situ monitoring for additive manufacturing; several parts need to be further investigated. The potential acoustic reflection happening in the broader range of frequencies, the influence of the different connected devices and parts between the transducers and the primary source of the acoustic signal, and correlation study between the AE results and the defect characteristics and identifying the influence on the mechanical properties of the parts are among the major topics for future investigations.

CHAPTER 3

METHODOLOGY

3.1 Experiment Data Description

Experimental data used in this study were obtained from a former project obtained by Quad-City Manufacturing laboratory and Iowa State University using a DED AM machine in 2018. The acoustic emission data was taken by setting up the AE transducers into the additive manufacturing machine during the fabrication process. Five transducers were used to collect the data, where four had placed in the bottom of the base plate, and one was used in the upper section of the base plate. The building process was mainly divided into five different states such as machine at inactive status, powder spray situation only, optimum process, low laser power, low powder feed, and these are recognized as BL (baseline), C0, C1, C2, and C3 as shown in Table 3. A detailed description of the experimental setup and procedure can be found in the study of Taheri et. all 2019 (Taheri et al. 2019).

Table 3: The data has been collected for the following manufacturing process conditions

Name	Abbreviation	Description
Baseline	BL	Machine at inactive status
Control	C0	Powder spray situation only
Condition 1	C1	Optimum process
Condition 2	C2	Low laser power
Condition 3	C3	Low powder feed

3.1.1 AE signals

The data collected during the building process of five different samples mentioned in this section has taken in 820 µs time frames. For the BL, C0, C1, C2, and C3 conditions, a total of 2235 signals, 2240 signals, 4074 signals, 3632 signals, 4123 signals were collected respectively for each signal condition. Several major features are considered for the analysis of the AE signals to identify the process conditions presented in Table 4. The time indicated here the total period taken signals during the data acquisition, peak amplitude is the maximum amplitude of the signals on the full-time interval, and the centroid amplitude is the average value of one full signal for all positions of the time. The FFT value of the signals has frequency and amplitude, the peak value of the FFT amplitude is the highest in one complete signal, and the centroid amplitude of FFT is the average values of the FFT amplitude. Table 4 below depicts the name and symbols used for this paper. The overall data condition for centroid amplitude and peak amplitude of the data plot is shown that all data stay in two basic regions; one is in the low-frequency region, and another is in the high-frequency region. The graph in Figure 17 shows that all conditions are mainly divided into two frequency regions where most of the low-frequency data is up to a 0.25 region and high-frequency data fall in the region of 0.9 to 1.5. There are few data which occupies other regions.

Table 4: Different feature of AE signals

Name	Symbols
Time	t
Frequency	f
Peak Amplitude	PA
Centroid amplitude	CA
Peak amplitude of FFT	PFA
Centroid amplitude of FFT	CFA

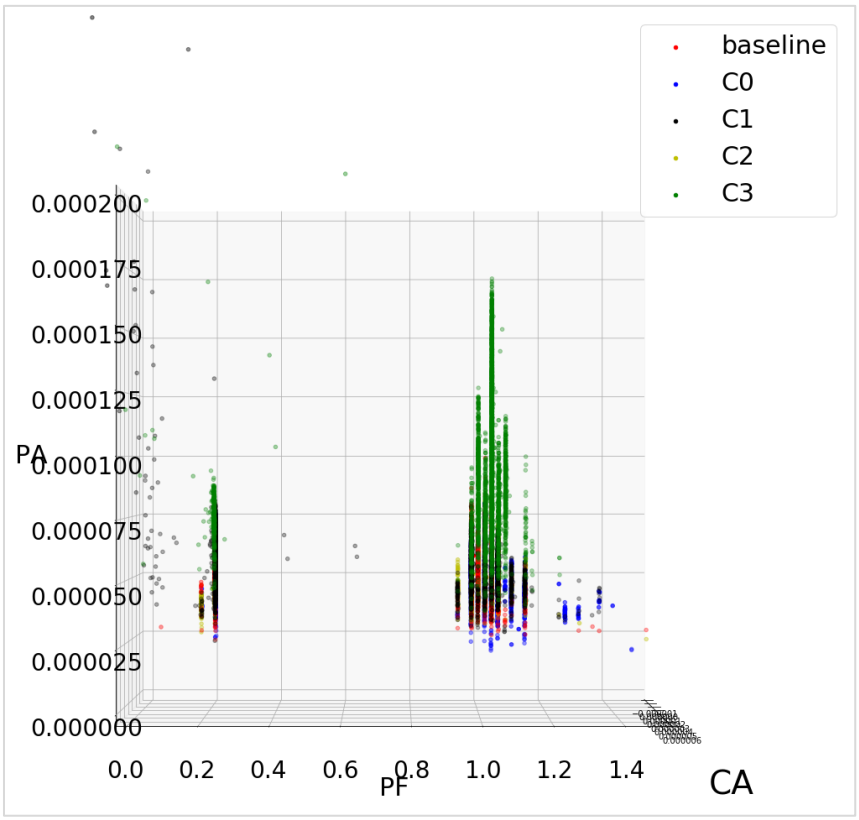

Figure 17: PA vs. PF plot to demonstrate the data fall into the high frequency and low-frequency region

3.1.2 SEM, EDS, Nanoindentation and Microscopic data

Powder of metal alloys is frequently used for powder-based additive manufacturing systems, where Titanium also becomes one of the most popular alloys (Santos et al. 2006)(Taheri 2018). Due to their high tensile strength, lightweight, and capability to withstand extreme temperatures, Ti-based alloys are commonly used in different applications such as aerospace and medical implants (Pegues et al. 2020). The characteristics of the powder, such as morphology, surface chemistry, size, internal porosity, and any incoming defects or foreign materials, have a significant effect on the consistency of the substance as deposited, the transmission of prior defects, the formation of new defects and the mechanical properties involved (Taheri 2018). The mechanical properties of the final component are influenced by and related to the properties of the feedstock materials, the particular method of manufacture used, as well as specific

process parameters. The powder used for creating the samples in this study is made of titanium alloy (Titanium 6Al-4V), deposited on a steel substrate under three different process conditions, as shown in Table 5. Optimum process conditions were created by putting powder, laser power, and other parameters in the ideal condition. On the other hand, low laser power and low powder feed condition were prepared by setting laser power lower than ideal condition and setting power feed to a less than optimum condition. The performance in the study done with wavelet and image processing is evaluated by nanoindentation, SEM, EDS, and optical microscopy.

Table 5: List of samples manufactured at different processing conditions

Samples	Name	Abbreviation	Description
C11&C12	Condition 1	C1	Optimum process
C21&C22	Condition 2	C2	Low laser power
C31&C31	Condition 3	C3	Low powder feed

In this study, the SEM, EDS, and optical microscopic data are collected over a region between the boundary of the substrate material and the additive deposited layer (Ti-6Al-4V), and a 2-dimensional image is created that shows spatial variations in these properties. The study also created nanoindentation data for these three different process conditions.

3.2 AE Data processing/Methodologies

3.2.1 Average/mean values

Many features can be obtained from acoustic emission signals to evaluate signal behavior for the different processing conditions. Preliminary evaluation of AE data shows that the overall feature values have considerable variation for all different process conditions. The direct plotting of CA and PA shows that data points for various conditions show that there are overlaps between the different process conditions.

However, plotting the values modified by arithmetic operations, such as adding or multiplying the individual features, improves the data perception. This output of different parameters by various arithmetic operations has enlightened the idea that the data can be classified by other techniques such as wavelet analysis. The Peak Amplitude (PA), Centroid Amplitude (CA), frequency/Peak Frequency (PF), Fast Fourier Transformed (FFT) Peak Amplitude (PFA), and fast Fourier transformed centroid amplitude (CFA) of each signal have been used to study the variation of data at each process condition. Figure 18 showed the PA vs. CA vs. PF in a 3D graph for a high-frequency region, and Figure 19 shows PFA vs. CFA by 2D scatter plot where data has been scaled by "MinMaxScaler" scaler function in python.

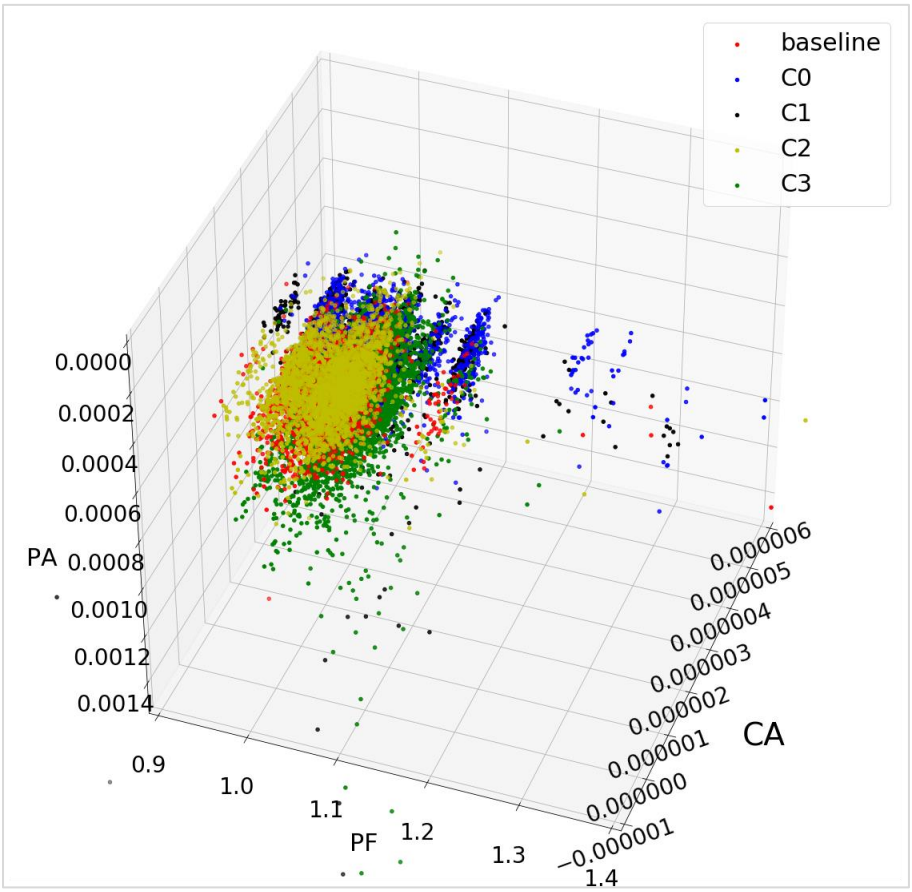

Figure 18: PA vs. CA vs. PF scatter plot for all process condition data

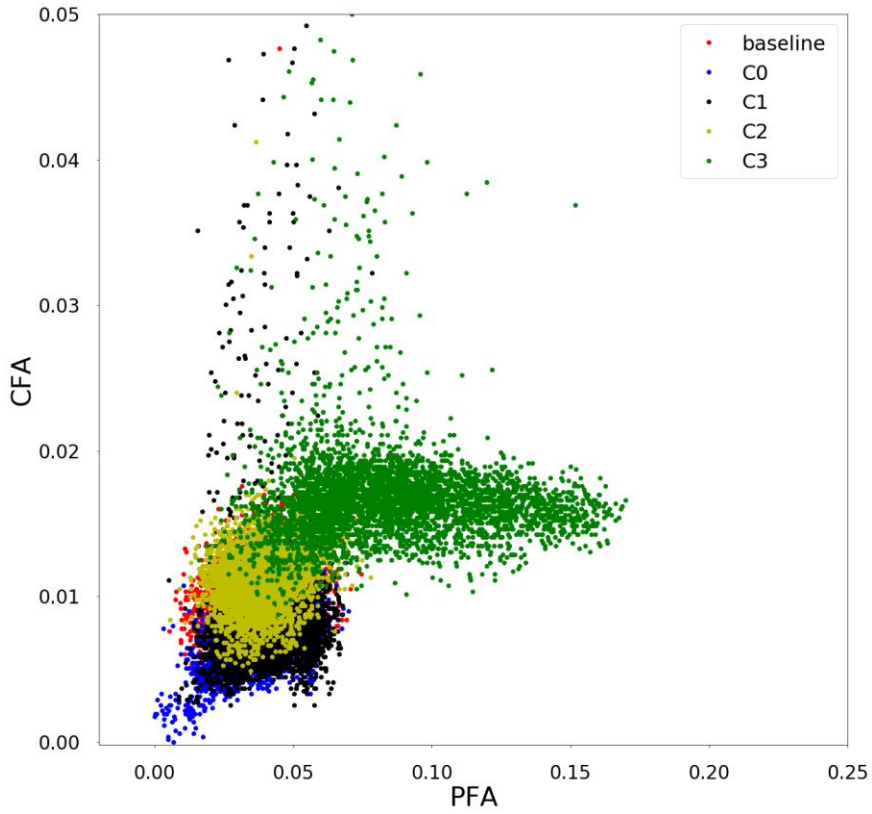

Figure 19: PA vs. CA vs. PF scatter plot for all process condition data

Dividing and multiplying of PA, CA, PFA, and CFA values by the Peak Frequency (PF) have also been done to evaluate the variation of different features for further classification study. The preliminary evaluation of AE signals indicated that the introduced features have considerable variations among different process conditions. For example, the parameter/outcome, **"Baseline_C0_CAvsPA_FD,"** means the value of centroid amplitude and peak amplitude divided by frequency, which presents better performance in the identification of process conditions. The CA and PA plot divided by f in CA/f vs. PA/f plot is shown in Figure 20 below. Finally, the assessment of the average value of all peak amplitude and all centroid amplitude shows that there is a difference between the data at each process condition. This variation helps to understand the feature variations in different process conditions and encourages further analysis.

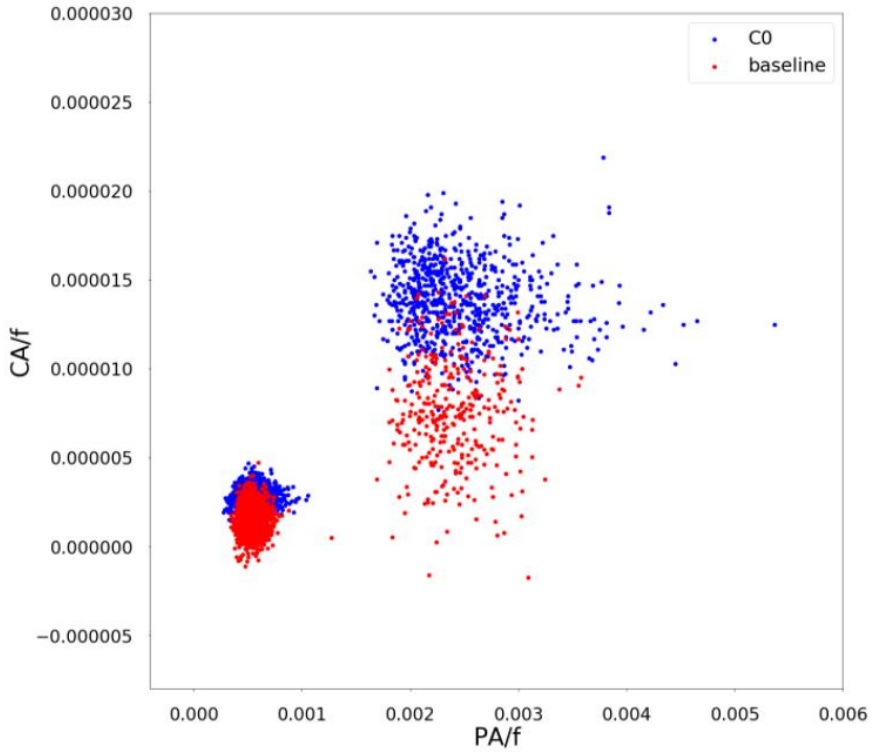

Figure 20: PA/f vs. CA/f with the division by frequency of scatter plot for baseline and C0 condition data

The average data for signals' amplitudes have shown differences where CA (centroid amplitude) vs. PA (peak amplitude) has been plotted in Figure 21. The data structure shows that the average of data in each building condition has given separate signals. These signals individual characteristics also found from the standard deviation and variance of all the process condition mean PA and CA value which is 5.22e-05, and the variance of the different condition of AM is 2.73e-09. Figure 22 shows the clustering of the average value of peak amplitude and centroid amplitude for the process conditions on a scale of 1.

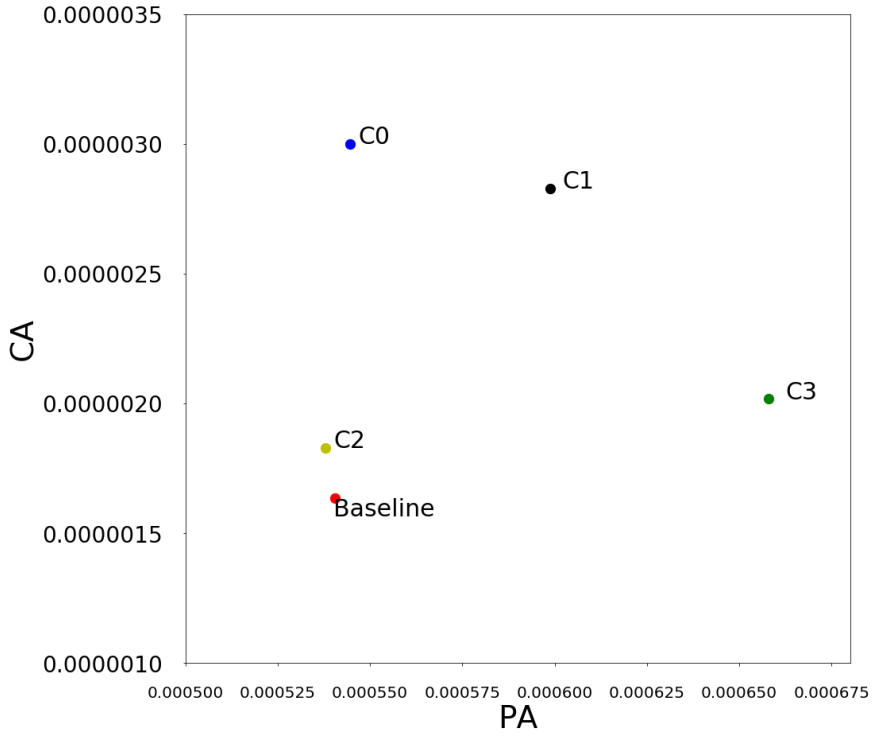

Figure 21: Average value of PA vs. CA for all process condition

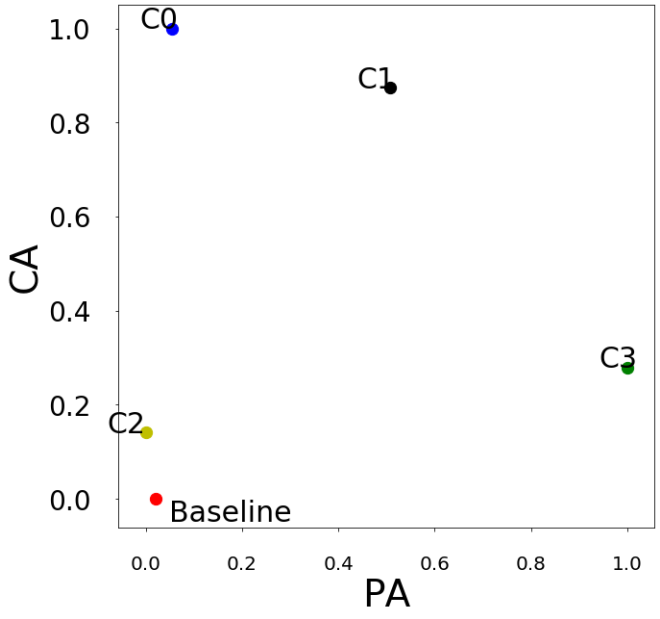

Figure 22: Average value of PA vs. CA for all process condition scaled value

The average data for Amplitude (Found by FFT) has shown differences in different process conditions where CFA (centroid amplitude from FFT conversion) vs. PA (peak amplitude from FFT conversion) has been plotted. This signal also shows that the standard deviation is 3.50e-05, and the variance of the different conditions of AM is 1.23e-09. It is found that the standard deviation and variance are higher for signals (voltage) than the fast Fourier transformed data. Figure 23 shows the clustering of the average value of peak amplitude and centroid amplitude for the process conditions, and Figure 24 shows the same value on a scale of 1.

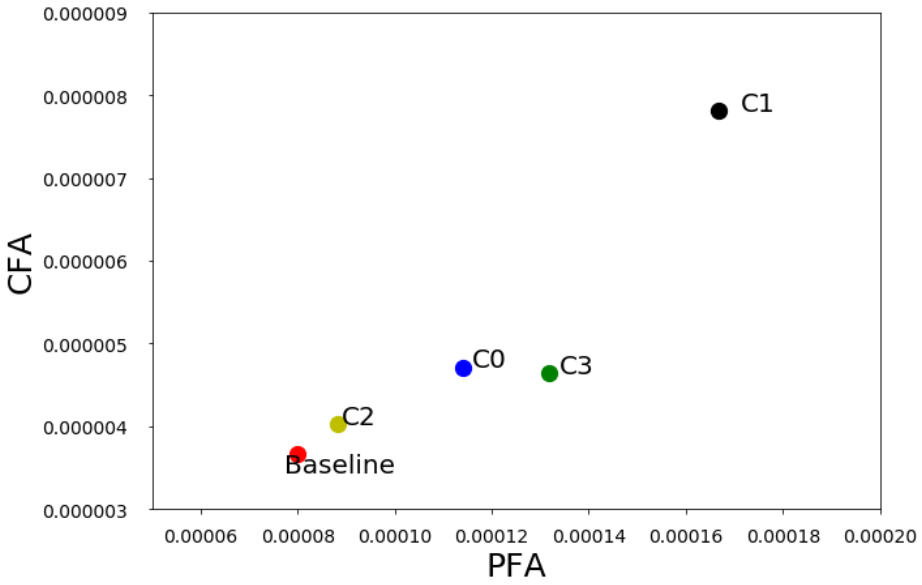

Figure 23: Average value of FFT of PA vs. CA for all process condition

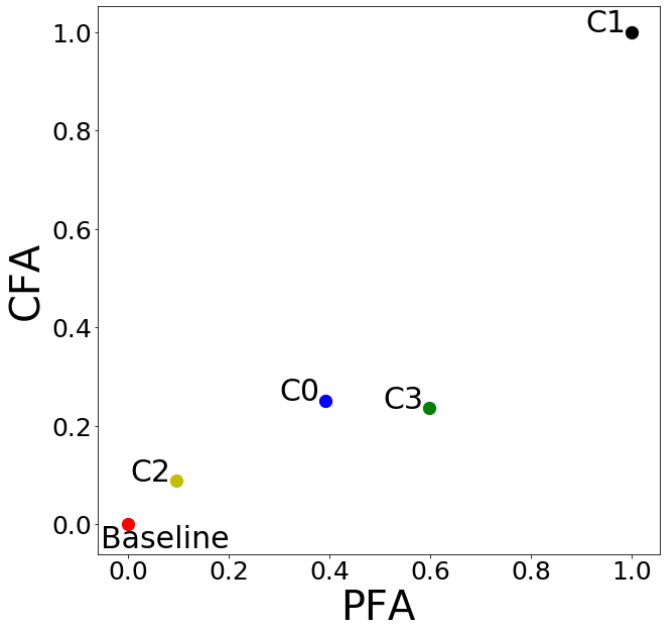

Figure 24: Average value of FFT of PA vs. CA for all process condition scaled value

3.2.2 Wavelet transformation

A wavelet is a "tiny wave" that concentrates its energy in time to provide a method for evaluating intermittent, nonstationary, or time-varying phenomena. It still has the oscillating wavelike function, but with a versatile mathematical base, it also can allow combined time and frequency evaluation. Figure 25 shows a continuous sinusoid and a so-called "continuous" wavelet (a Daubechies 20 wavelet is depicted in this figure). Sinusoids are smooth and consistent and are excellent at representing (stationary) signals of constant frequency. Wavelets are irregular and sometimes non-symmetrical, with short length. Inside the signal, they are better at distinguishing disturbances, bursts, and other occurrences that begin and stop (Burrus, Gopinath, and Guo 1998)(Fugal 2009). While analyzing the signal of AE and Fast Fourier Transform (FFT) of AE signals for different process conditions, the signal amplitude has variation at the different process conditions, as well as there are similarities with respect to time in each process condition. So, the process is identifiable for the different classes when it is possible to transfer the signals with a

specific wavelet filter with a fixed scale with respect to time. The study has been done further and discussed in the following sections to find out suitable wavelet filter and suitable scale for further analysis.

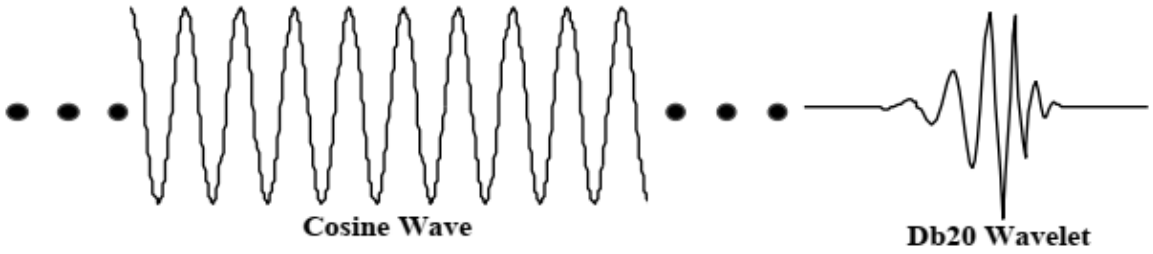

Figure 25: A portion of an infinitely long sinusoid (a cosine wave is shown here) and a finite length wavelet. Notice the sinusoid has an easily discernible frequency while the wavelet has a pseudo frequency in that the frequency varies slightly over the length of the wavelet (Fugal 2009)

There are several types of wavelet which can be used in signal processing. Some wavelets are described and illustrated as continuous and infinite by a mathematical expression, which is called crude wavelets. However, they must first be converted to wavelet filters with a finite number of discrete points to be used with digital signals. In other words, to construct the filter values at those times, we assess the simple wavelet equation at the desired points in time (usually equalized). An explicit mathematical equation produces "crude" wavelets. The pattern of the signal has been identified and shown in Figure 26, where the time is on the x-axis, and signal amplitude is on the y-axis, and the time increment having 0.2 μs for each collection of signals. Among the various wavelet systems, the Morlet wavelet signal is selected for the analysis, which is stretched crude filter. It is derived from a mathematical equation, similar to the Mexican Hat crude wavelet (mexh) as presented by the equation (Eq. 1):

$$morl(t) = e^{(-t^2/2)} \times \cos 5t \tag{1}$$

Figure 27 shows the "continuous" wavelet produced by this equation. Moreover, this equation is simply a cosine modulated by an exponential (Fugal 2009). In this analysis, wavelet transformation has been done with 50 scales and 10 scales, where a scale with 50 shows the better output concerning this

acoustic emission signal received. The scale 50 shows detailed information for the different process conditions, and this is why further analysis, which is image processing of the wavelet analysis figures based on CNN, has been done for classification of the data with the outcome of 50 scale images.

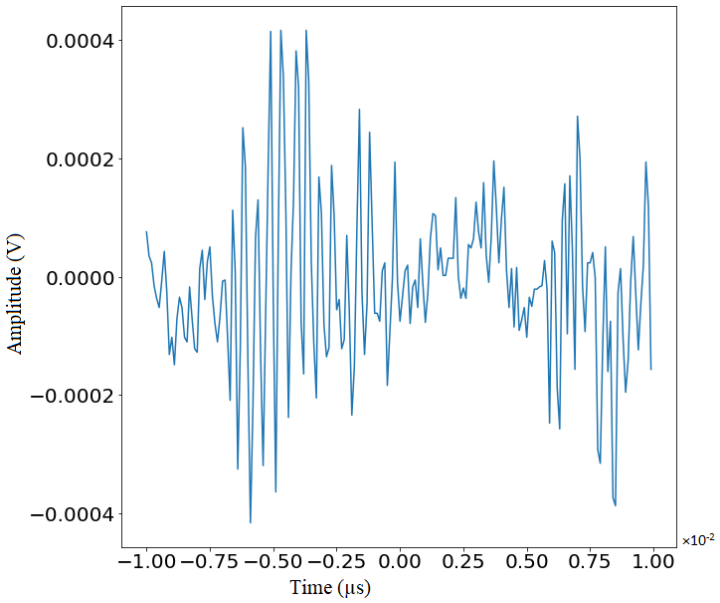

Figure 26 : baseline signal (y-axis) vs. time plot (x-asix)

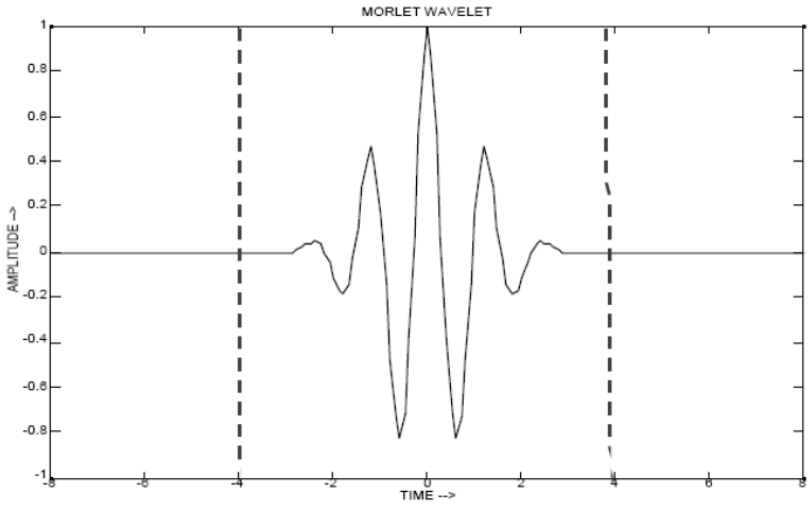

Figure 27: Representation of the Morlet Wavelet. Note that because of the exponential term attenuating the cosine term that values outside the range -4 to +4 are essentially zero (adequate support = -4 to +4) (Fugal 2009).

3.2.3 Convolutional Neural Network (CNN)

Neural network models are algorithms for cognitive tasks, such as learning and optimization, which are loosely based on concepts derived from research into the human brain's nature. Historically, there are two origins to the interest in neural networks: (1) the wish to know the concepts on which the human brain functions, and (2) the urge to build machines capable of performing complex tasks (Müller, Reinhardt, and Strickland 1995). Deep learning is a subset of machine learning which uses various kinds of neural network. A Convolutional Neural Network (CNN) uses a combination of the multilayer perceptron, which requires one or more layers of convolution. These layers may either be completely interconnected or pooled. The convolutional layer uses a convolutional operation on the input before moving the output to the next layer. The ability of a convolutional neural network by which it can go much deeper but with less amount of parameter due to this convolutional operation shows useful results in natural language processing, image and video recognition, and recommender systems. In semantic parsing and paraphrase detection, CNNs also demonstrate outstanding performance, which also can be applied in signal processing and image classification (da Silva et al. 2016) (Goodfellow 2016).

Convolutional Neural Network (CNN) can identify an image similar to the technique the human brain recognizes the different images. A typical layer of a convolutional network consists of three stages. In the first stage, the layer performs several convolutions in parallel to produce a set of linear activations. In the second stage, each linear activation is run through a nonlinear activation function, such as the rectified linear activation function. This stage is sometimes called the detector stage. In the third stage, a pooling function is used to modify further the output of the layers (Goodfellow 2016). All stages of CNN are a necessary combination of convolutional and subsampling layers optionally followed by fully connected layers. The input to a convolutional layer is a $i \times i \times r$ image where i is the height and width of the image, and r is the number of channels (such that an RGB image has r=3). The convolutional layer will have k filters (or kernels) of size $j \times j \times q$ where j is smaller than the dimension of the image, and q can either be

the same as the number of channels r or smaller and may vary for each kernel. The filters' size gives rise to the locally connected structure, which is each convolved with the image to produce k feature maps of size $i - j + 1$. Every map is subsampled typically with mean or max-pooling over $m \times m$ contiguous regions where m ranges between 2 for small images and is usually not more than 5 for larger inputs. For each function map, an additive bias and sigmoidal nonlinearity are added either before or after the subsampling layer. A CNN consisting of convolutional and subsampling sublayers is illustrated as a full layer in Figure 28 below. Units of the same color have weights that are tied. After the convolutional layers, there may be any number of fully connected layers. The fully connected layers are identical to the layers in a standard multilayer neural network (Stanford University n.d.).

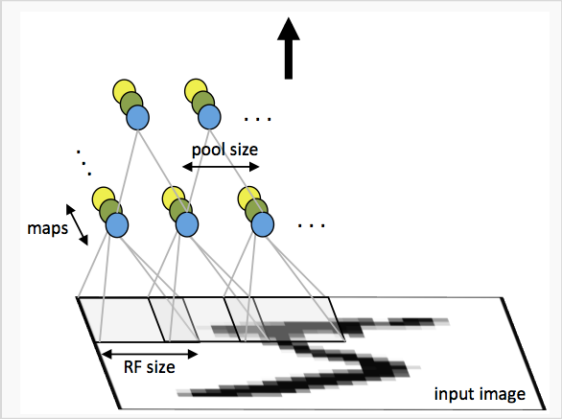

Figure 28: First layer of a convolutional neural network with pooling. Units of the same color have tied weights, and units of different colors represent different filter maps (Stanford University n.d.).

Of those layers, a pooling function is to replace the output of the net at a particular location with a summary statistic of the nearby outputs. Max pooling is used to get maximum value from each pixel, which is a useful operation in object detection (Goodfellow 2016) (Zhou and Chellappa 1988). This study has a convolutional layer, in the beginning, then having a max-pooling layer, then it flattens, and finally, it has densely connected layers. The data processing for validation and training was done in a batch size of three. In CNN, the first convolution layer has 16 filters, the size of the filter is 3x3, and the activation function is "relu," and the input shape is 200x200, then having a max-pooling layer (2x2) which pool max resolution

from the set of data. Then it has another convolutional layer with 32 filters and finally another layer with 64 filters. It can be seen that this program increased the number of filters for later layers to increase the number of channels. Then the convolution layers are flattened out and used two dense layers and activation "softmax" for multiple class classification. The model train is validated with 40 epochs and 5 steps per epoch that have shown high efficiency of the CNN. For further details about deep learning, CNN can be found in those references given in this section.

3.3 Microscopic images

The samples need to be polished for SEM and nanoindentation tests. Initially, the sample was machined by Electrical Discharge Machining (EDM) wire cut. The interested surfaces were then polished by a series of sandpapers with different grades to achieve the desired surface finish. Optical microscopic images for all the samples are shown in Figure 29. It can be seen from the optical microscopic image that for low powder feed condition (Figure 29b), there is a lot of small porosity present because of lack of powder, and it is also found that the layer building layer is thicker than other process condition layers. It can also be seen that there are large gaps in the building layer from the optical microscopic image for the low laser power condition (Figure 29a), which suggests that because of low power, the bonding did not happen appropriately among the layer. It can be seen that for optimum process condition (Figure 29c), the building was smoother than lower laser powder and thicker than low powder feed, even though it can be seen from Figure 29c that there are small porosities in some part of the one sample, which might come from some variation during the process.

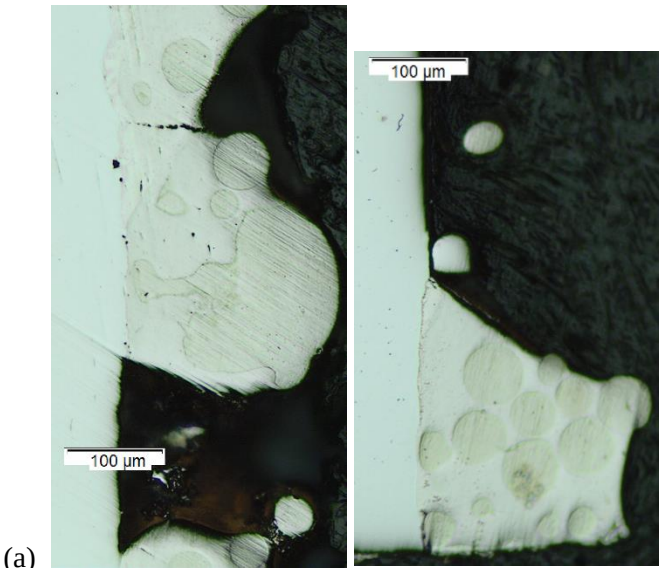

(a)

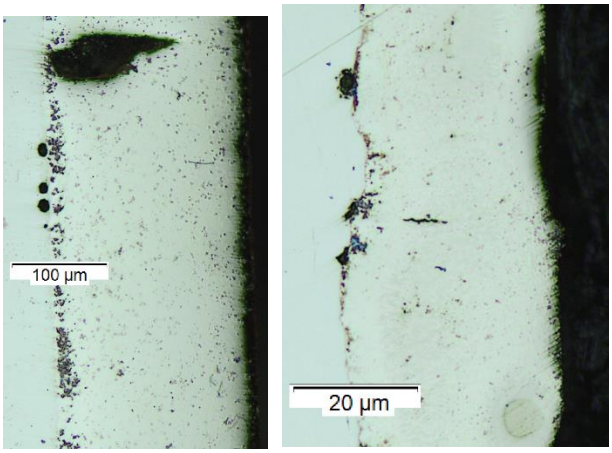

(b)

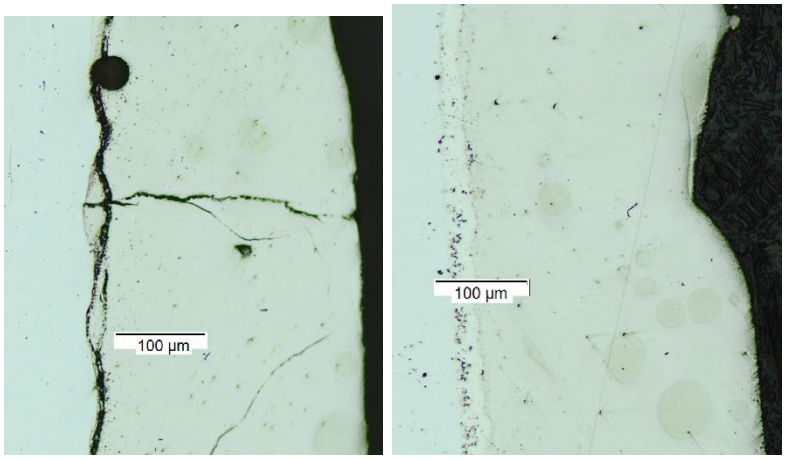

(c)

Figure 29: Optical microscopic image for a) Low laser power, b) Low powder feed, c) Optimum process

The microscopic images show a considerable difference in cross-sectional features between each AM process condition. It is found in microscopic images that the microstructure of the sample for different process conditions of the sample is different, which can be correlated to the AE signal from different process conditions. These distinguishable differences will help to interpret and evaluate the classification through wavelet transformation and image processing.

3.4 SEM and EDS

3.4.1 Sample preparation

The additively manufactured samples were initially cut by EDM to get the surface where both the base material (tool steel) and AM material (Titanium 6Al-4V) can be seen from the same direction (Side view). For making SEM images and generating EDS analysis, the surface was polished to get better results. The polishing has been done in stages to get the fine surface, and finally, drying and cleaning are also done to avoid corrosion. As one of the SEM machine's prime requirements, the sample needed to be dry and free from external particles. So the sample had been kept in a vacuum chamber to make it dry. After taking out the samples from the vacuum, it was put in a bag with zeolite to keep it in dry condition while moving from the vacuum to the machine.

3.4.2 SEM and EDS Experimental Methods

SEM and EDS analysis were performed using the JEOL SEM machine for the sample named as C21, C31, C22, C32, C11, and C12 where C21&C22 are in C2, C31&C32 are in C3, and C11&C12 are in C1 build conditions respectively (Table 5). With the proper alignment of the optical microscope of SEM, an image has been taken. This helps to navigate the sample during the SEM scanning to the required specific place into the samples. Movement of the axis needs to be done for keeping the samples in an appropriate position, especially in z-axis distance, which in our case is 8mm, and reduction of z value from default position 38mm to the needed position 8mm needs to set with few steps to make sure no collision occurs

during the movement. Chamber pressure needs to decrease to 10^{-4} Pa before truing on the electron gun, and during the operation, this pressure needs to be maintained. It takes almost an hour to reach this pressure range. This electron beam hits the sample and creates the required image.

Initially, the machine is set to Low Magnitude (LM) mode and 1kV; for getting a better image, the electron beam voltage is set to 30 kV. The machine was set to current 8A, contrast 1178, and brightness 731 while creating the SEM images, and the optical microscopic image was used to navigate to the specific place where the SEM data needed to take. This setup gives proper images for the samples, and data collection was done on 80X magnification.

For EDS, the same procedure for the machine setup is done, and the IR chamber camera needs to turn off for the operation. The software for EDS (AZtec) needs to start for the operation. The probe current set for this is 10 nA, then the specimen needs to select for the specific area to acquire data, and the elements required to get during the experiment needs to specify to determine the comparison between them in the generated report.

3.5 Nanoindentation

3.5.1 Sample preparation

For preparing the samples for nanoindentation, after the EDM wire cut and polishing of the samples, it needs to be mounted by using a mounting press in a polymer base. The main purpose of mounting the samples is so that material handling becomes convenient regardless of its size and shape, and the mold also supports the samples to stay in a stable and flat position during nanoindentation. The electrohydraulic mounting press was used to mount the samples inside the polymer material mold. After that, the polishing has been done up to a fine surface finish for further work.

3.5.2 Nanoindentation Experimental Methods

A Hysitron TS-75 Triboscope integrated into an AFM (Atomic Force Microscope) (Park System, Model NX-10) was employed to perform the nanoindentation on the mounted samples. A diamond Berkovich tip was employed for all nanoindentation experiments. Samples were mounted on a ferromagnetic base to be secured properly on the XY stage of the nanoindentation setup. Due to the lack of top optical view on the particular nanoindentation setup, a side optical view was obtained by an independent microscope camera to provide an approximate area under the nanoindentation tip during the approaching step. After approaching the surface, several 60×60 μm surface scans with 3μN force have been performed to find the exact point of interest for nanoindentation. Optical Microscopic images were used to compare with the contact mode surface images to identify the point of interest for the nanoindentation experiment. Figure 30 shows an example of an approximate position where data has been taken on sample C21. The position has been selected based on the building condition of the samples. For different samples, the location is in different positions according to the sample. An array of points (3 × 3 points with the minimum distance of 10 μm between them to avoid effects from other indentation points) in the desired area were selected to be examined by nanoindentation. The indentation has been done with the force of 8000 μN and loading rate of 1000 μN/sec, followed by a 2-sec holding time, and finally removing the load at the same rate of 1000 μN/sec. The system monitors the thermal drift to achieve a drift below 0.05nm/sec for 100 sec prior to applying the indentation force. The system has recorded the load and displacement of the tip during the nanoindentation process.

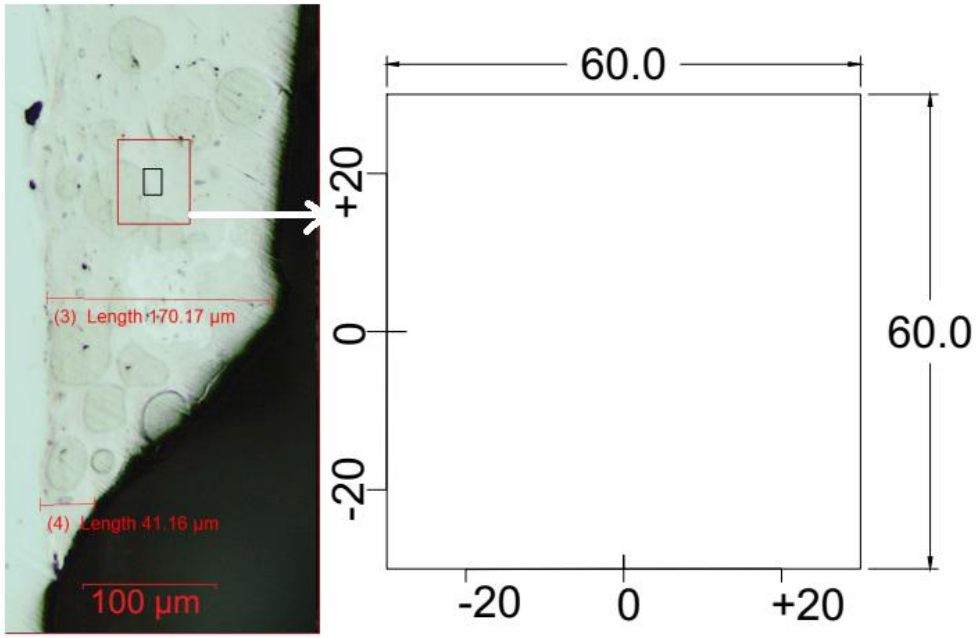

Figure 30: Selecting particular position for nanoindentation

CHAPTER 4

RESULTS AND DISCUSSION

4.1 Wavelet transformation

Sample data has a total of 2235x4096 dimensions, and the total duration for the signal acquisition period forms -117 µs to 700 µs with 0.2 µs interval, so the total number of data taken for one complete signal is 4096. From all that acoustic data, 200 signals for a single wave are between the time of -117 µs to -77.2 µs within 0.2 µs interval. The wavelet used here is a morlet wavelet with scales 10 and 50, where it can be seen that the image in scale 50 shows more details and can be used for further calculation. The image processing is done using CNN on a scale of 50 data for all the process conditions to get the classification. In Figure 31, the image for both scales is seen. All the process conditions AE signals are transformed by wavelet, and the image is saved for further analysis based on the scale of 50. One example for each condition BL, C0, C1, C2, and C3 are shown in Figure 32 below.

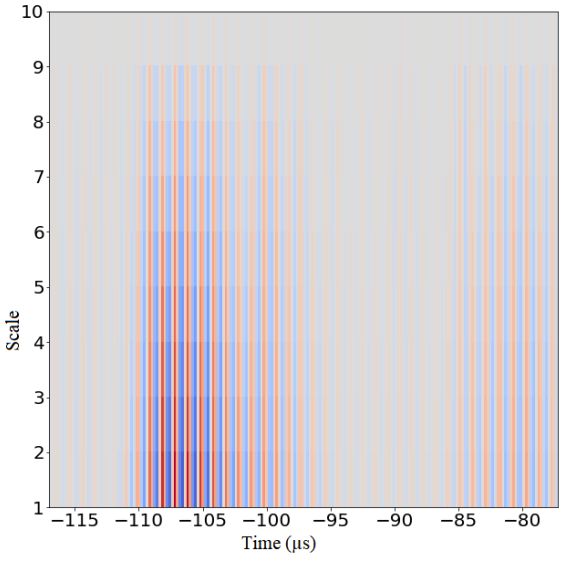

a)

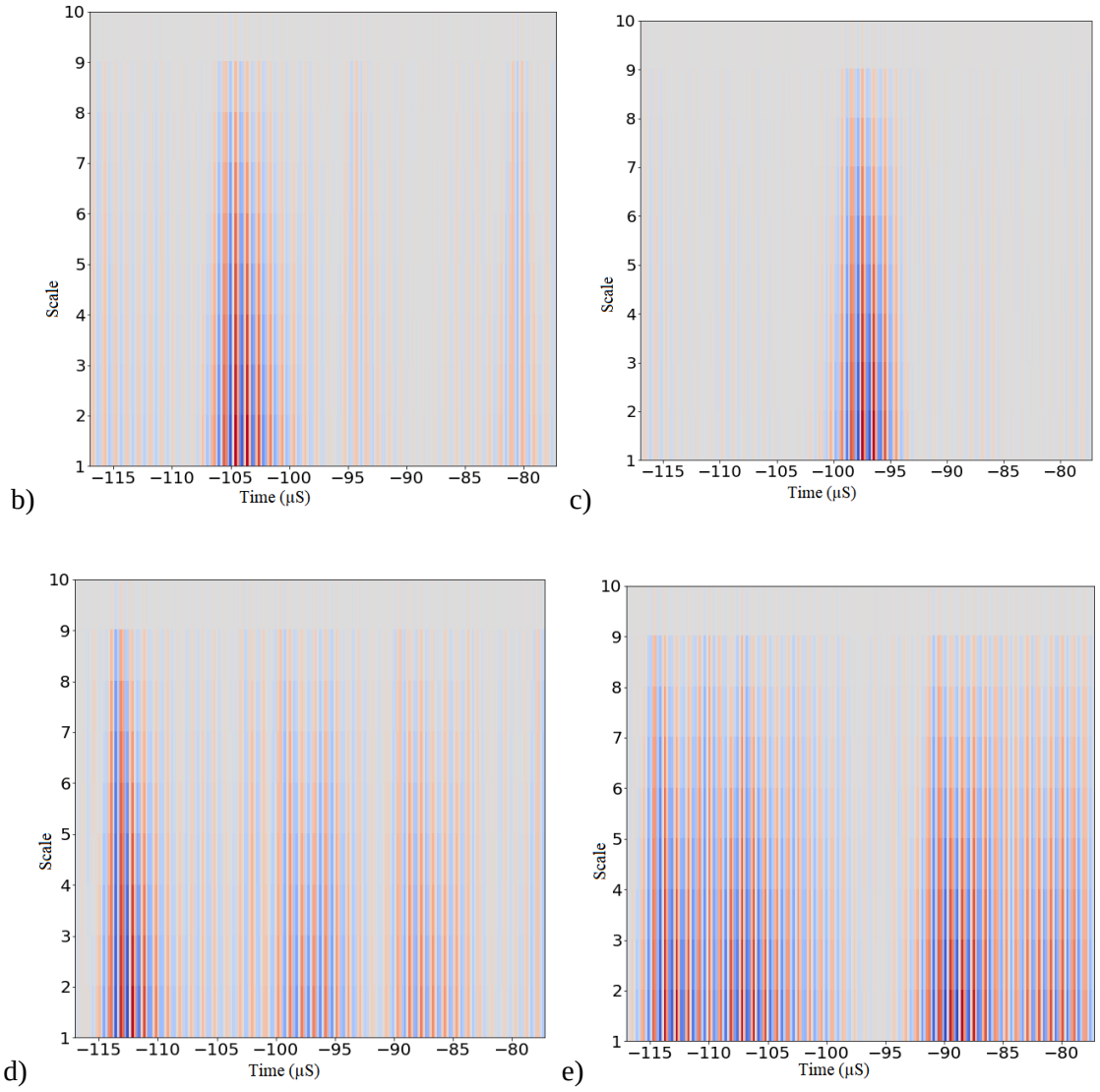

Figure 31: Wavelet transformed image plot for a) BL, b) C0, c) C1, d) C2, and e) C3 condition in scale 10

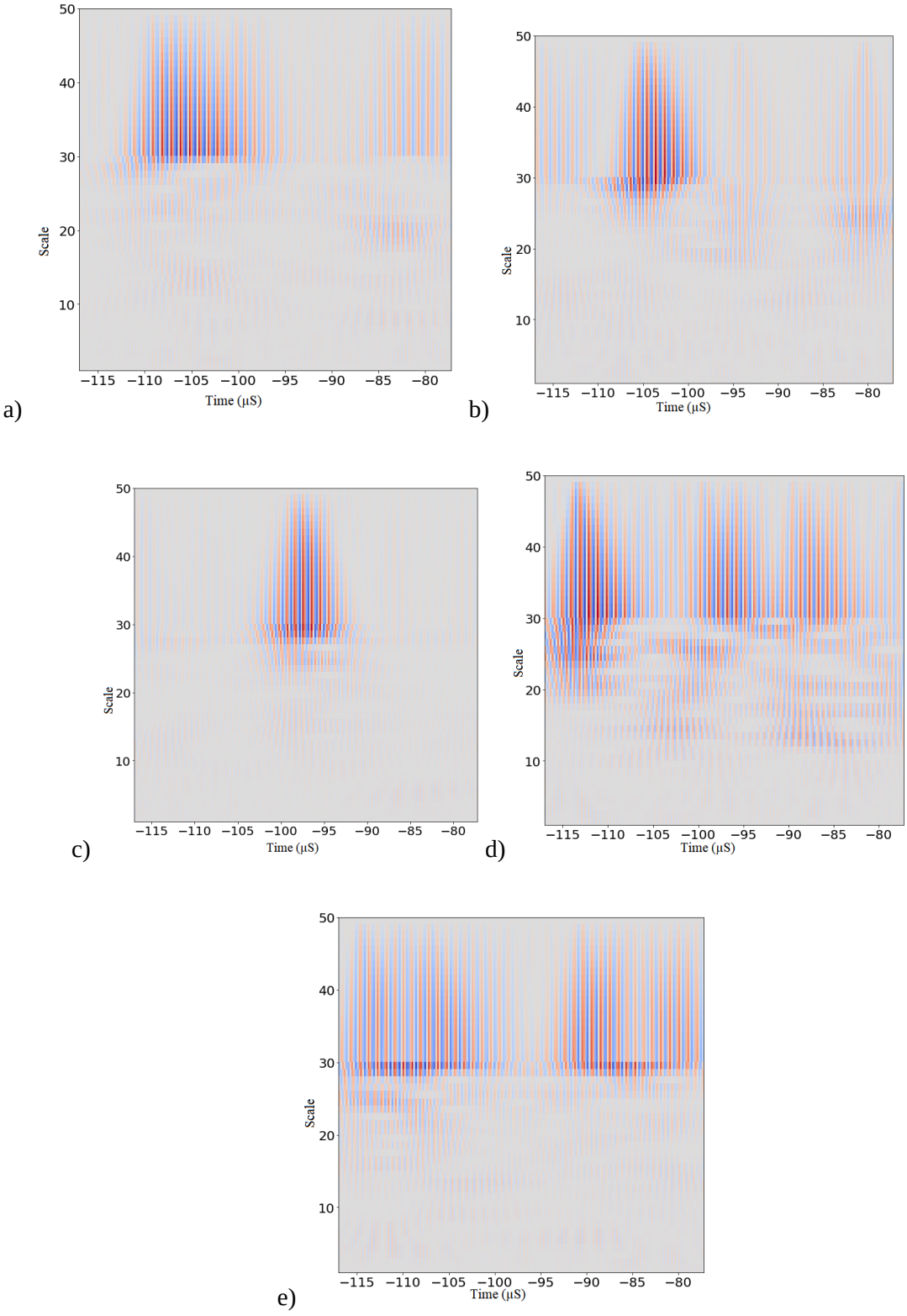

Figure 32: Wavelet transformed image plot for a) BL, b) C0, c) C1, d) C2, and e) C3 condition in scale 50

4.2 Image Processing

The study has been done to identify images by the convolutional neural network. All the output images from the wavelet transformation are saved on a specific folder by splitting them into training, validation, and testing folders. Finally, working on the folders for CNN from the given images with a total of 400 images where 80 images per samples with 75% data for training, 20% data for validation, and the other 5% used for testing by a deep convolutional neural network, which gives following accuracy and loss after completing 50 epoch. The model in Figure 33 shows that validation and training loss become better and closer after 50 epochs, so it is a good fit for the model of classification.

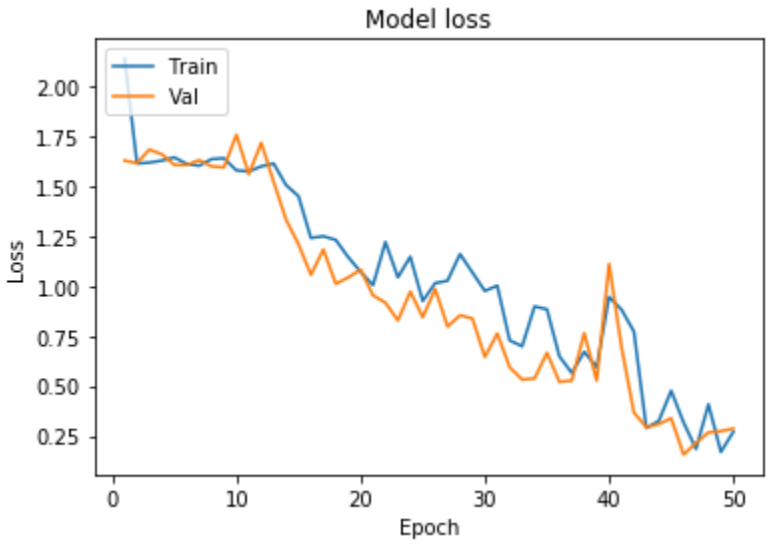

Figure 33: The model loss for validation and training loss against epoch

As CNN's image processing gives high accuracy, all the images in testing images give the proper class. The testing outcome for the different images of various categories/classes is shown in Figure 34 below. The input images for the testing are wavelet_baseline_s50_d200_w, wavelet_C0_s50_d6t8_l1w, wavelet_C1_s50_d14t16_l1w, wavelet_C2_s50_l1w_d200t_2000, and wavelet_C3_s50_l1w_d200t_2200 respectively and the output is shown in the bottom left those are baseline, C0, C1, C2 and C3. It shows that

CNN gives us the proper classification and image recognition for all category and the accuracy is more than 96% validation accuracy 95%.

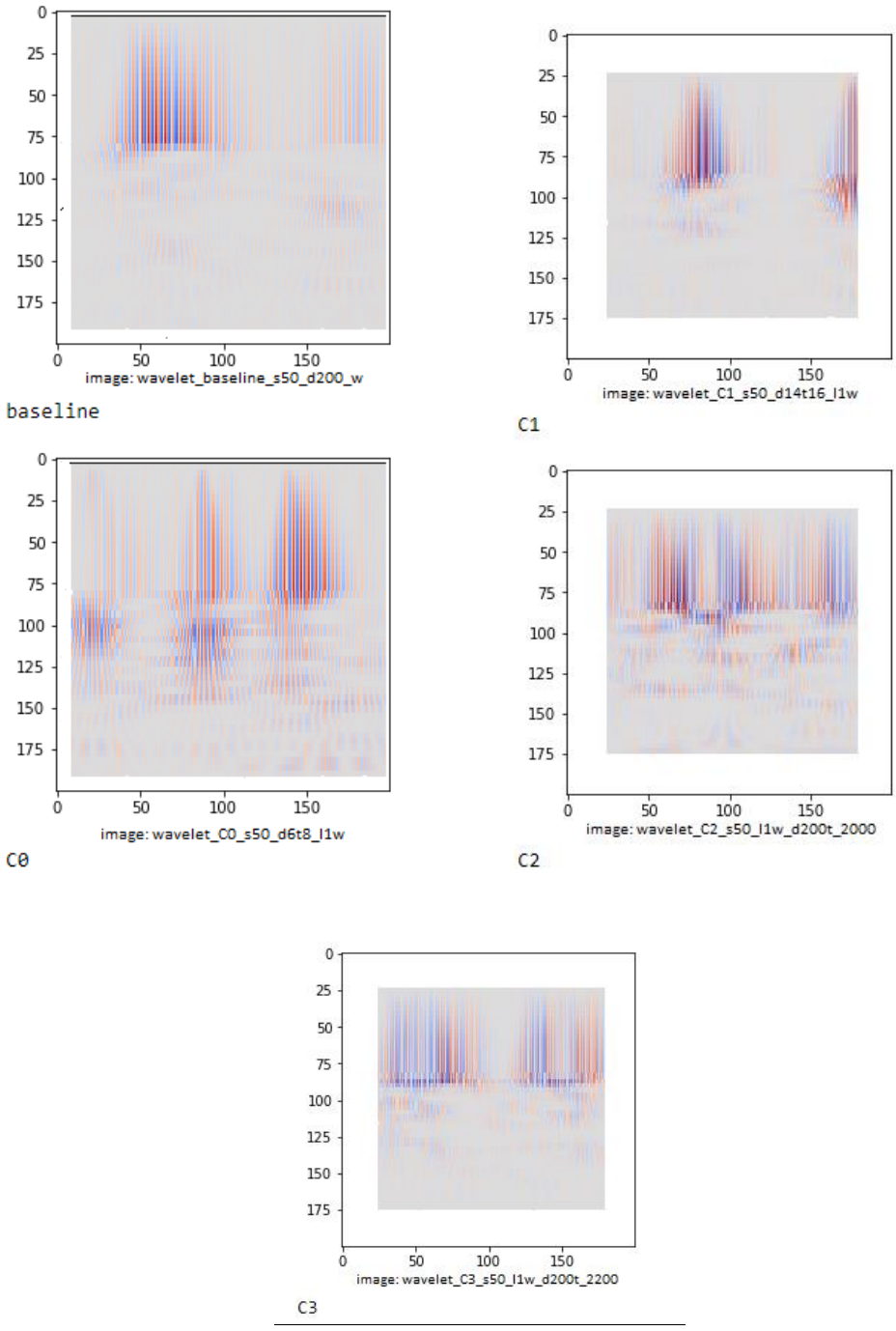

Figure 34: The testing results for the image classification where "image:" shows the actual class of the image and baseline, C0, C1, C2, C3 shows the classification by CNN

4.3 SEM and EDS

4.3.1 SEM

The Scanning Electron Microscopes (SEM) have been used for acquiring SEM images for the different process conditions according to Table 5. Figure 35, Figure 36, and Figure 37 show the side view and top view of sample SEM images for low laser power, low powder feed, and optimum process, respectively. From the images, the variation of images can be seen among different process conditions. From the side view, the overall building is smoother for the optimum process than the other two conditions. A better understanding can be obtained from the top view of the images. For low laser power conditions, the build was not proper. There are significant gaps, which means the big failure (void) of 3D printing due to the laser's low power. It is also seen that the amount of powder is high in some areas, and in another area, there is a low powder or even no powder.

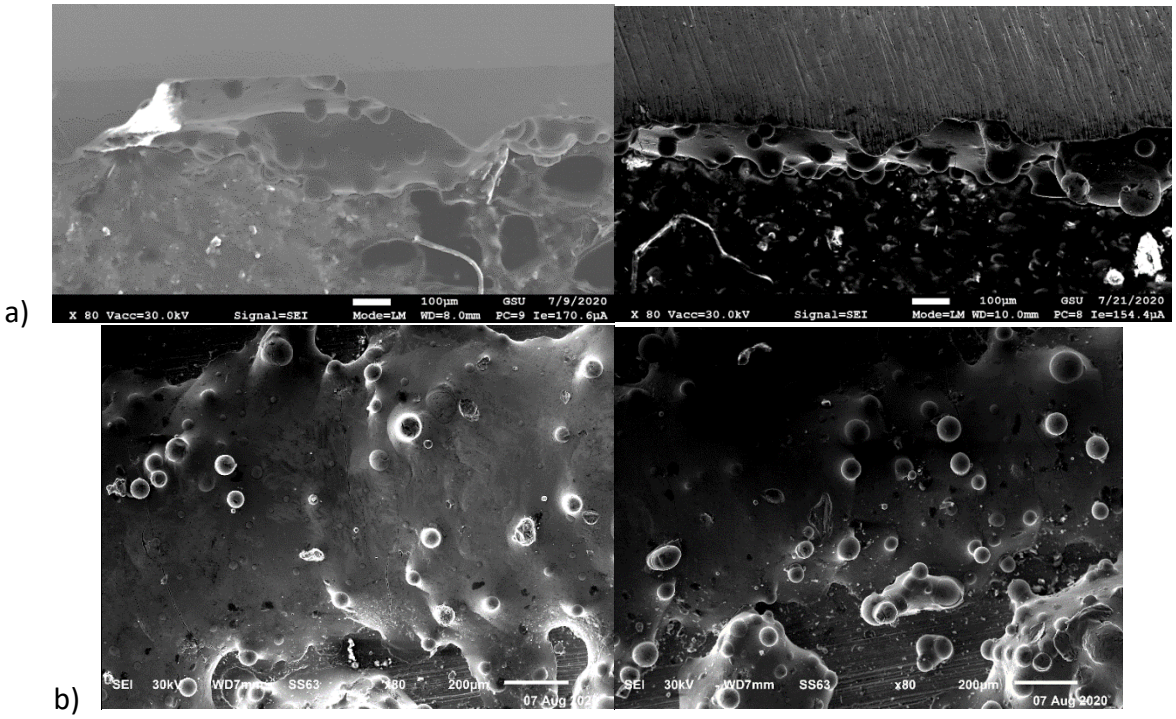

Figure 35: SEM images of sample C21 and C22 (Low laser power); a) Side view b) Top view

For low powder feed conditions, the overall scenario is different where it can be seen that a large number of porosities is presented in the build. Many cracks are also observed, but there is no significant gap or failure of the building in low laser power mode.

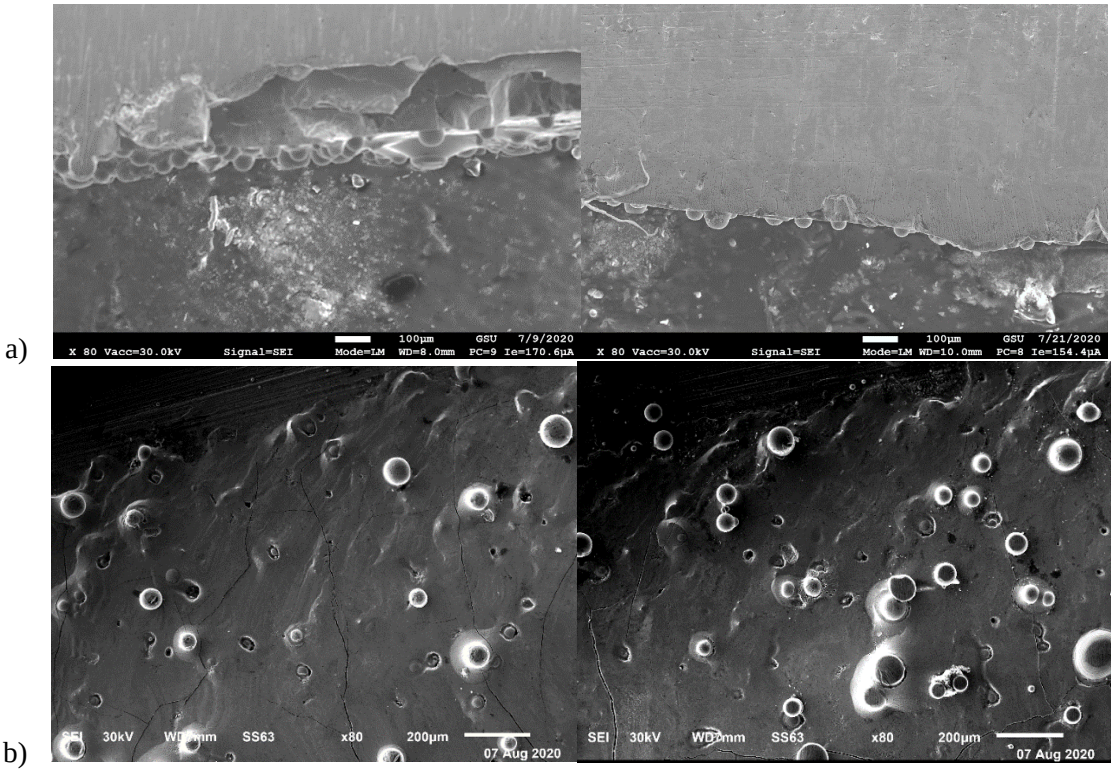

Figure 36: SEM images of sample C31 and C32 (Low powder feed); a) Side view b) Top view

The optimum build condition where the amount of powder feeding and laser power is in its best processing mode. The amount of porosity and crack is significantly lower than in the low power condition. There is also no building gap as it was in low powder feeding mode. So, it can be seen that this process condition might have more strength and other characters also much different than other conditions, which makes classification possible through NDT techniques.

a)

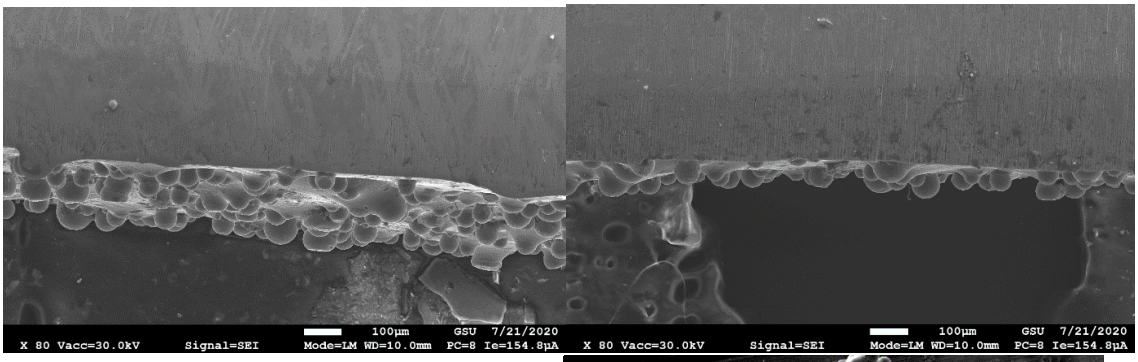

b)

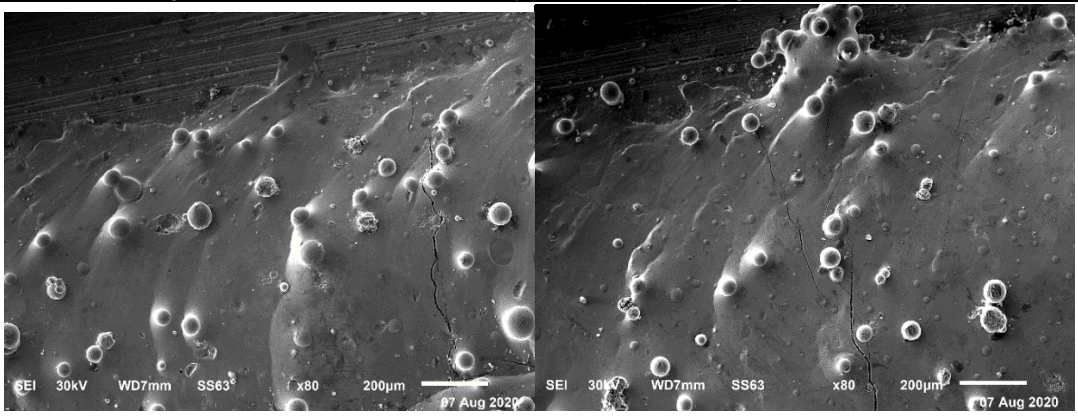

Figure 37: SEM images of sample C11 and C12 (optimum build condition); a) Side view b) Top view

4.3.2 EDS

The samples' EDS signals provide an understanding of various elements present in the samples and the map of their dispersion in the area of interest, while the intensity of the signal provides the weight percentage of each element. It illustrates the SEM images of the zone selected for the analysis, the area of different metals with its place on it, and the map sum spectrum diagram. The EDS analysis for the sample C21 & C22 is presented in Figure 38 and Figure 39. It shows the percentage of different metals in the samples where the Titanium is 60.9% and 56% respectively in these two samples, and the other detected materials are C, O, Fe, Al, Co, and Cr. The electronic image showed the area in which SEM analysis has been done. The other image with different colors shown below depicts molecules density and specific location of each molecule among the selected molecules where Ti and Fe are the main focus. Figure 7 shows the electronic image and the position of different molecules present in that electronic region with

different color options and percentage of each molecule are shown in the chart and same conditional sample, shown in Figure 39 where electronic image, Ti, Fe, and full metal details chart is given.

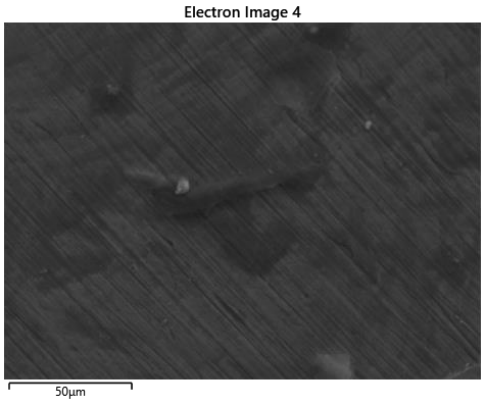

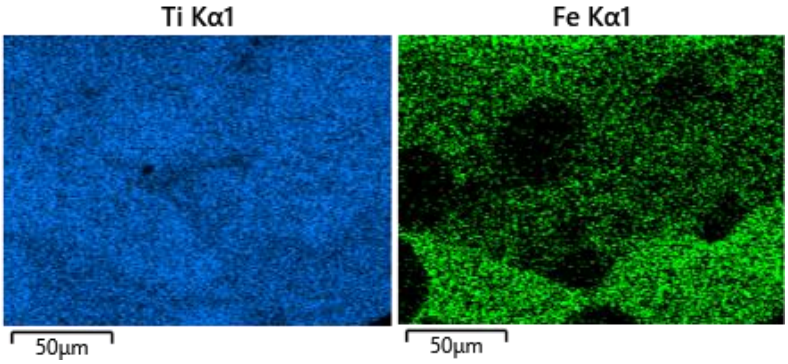

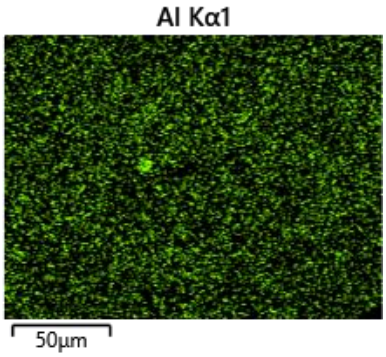

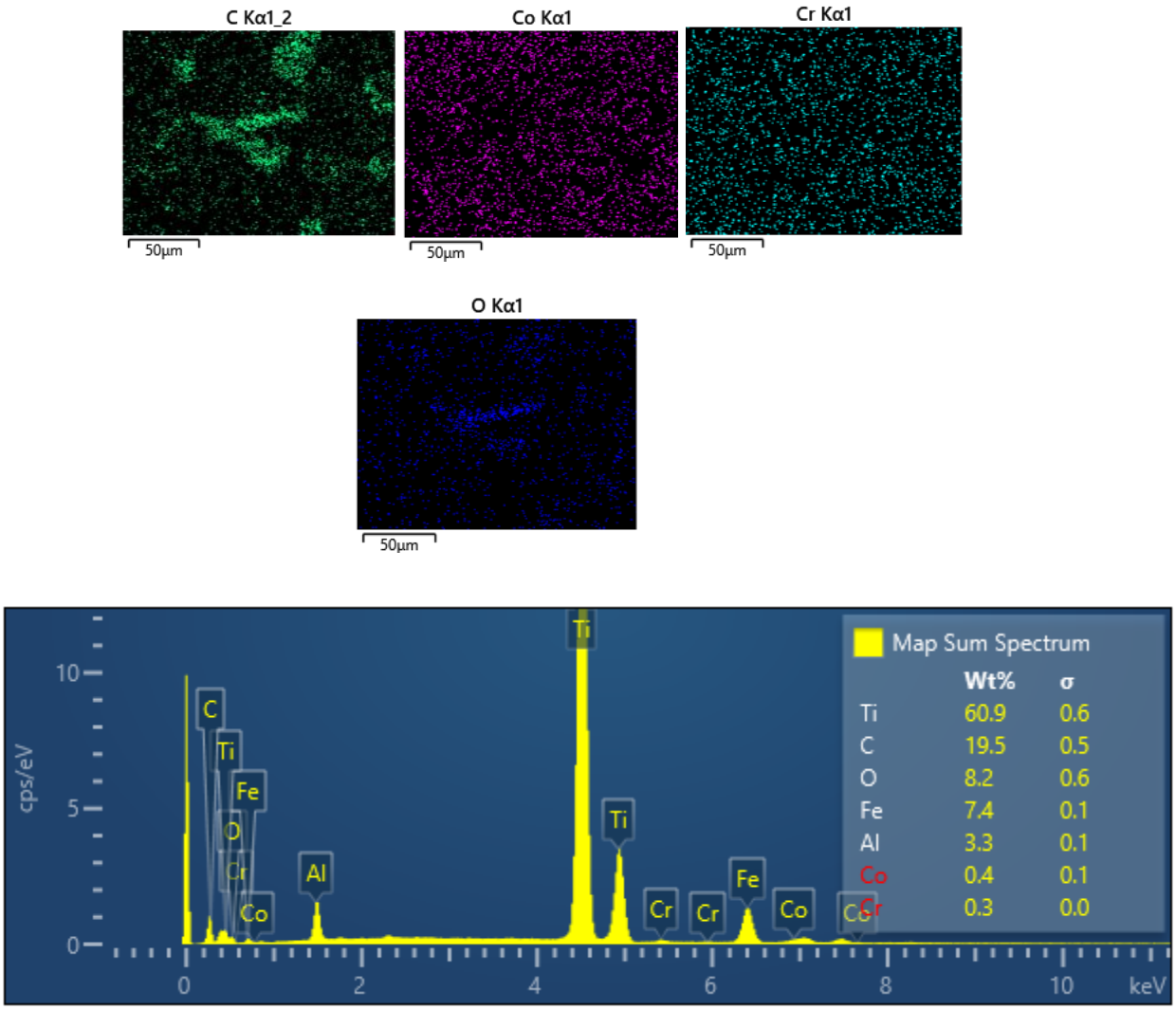

Figure 38: Electronic image, different materials map with different color and percentage of metals for sample C21

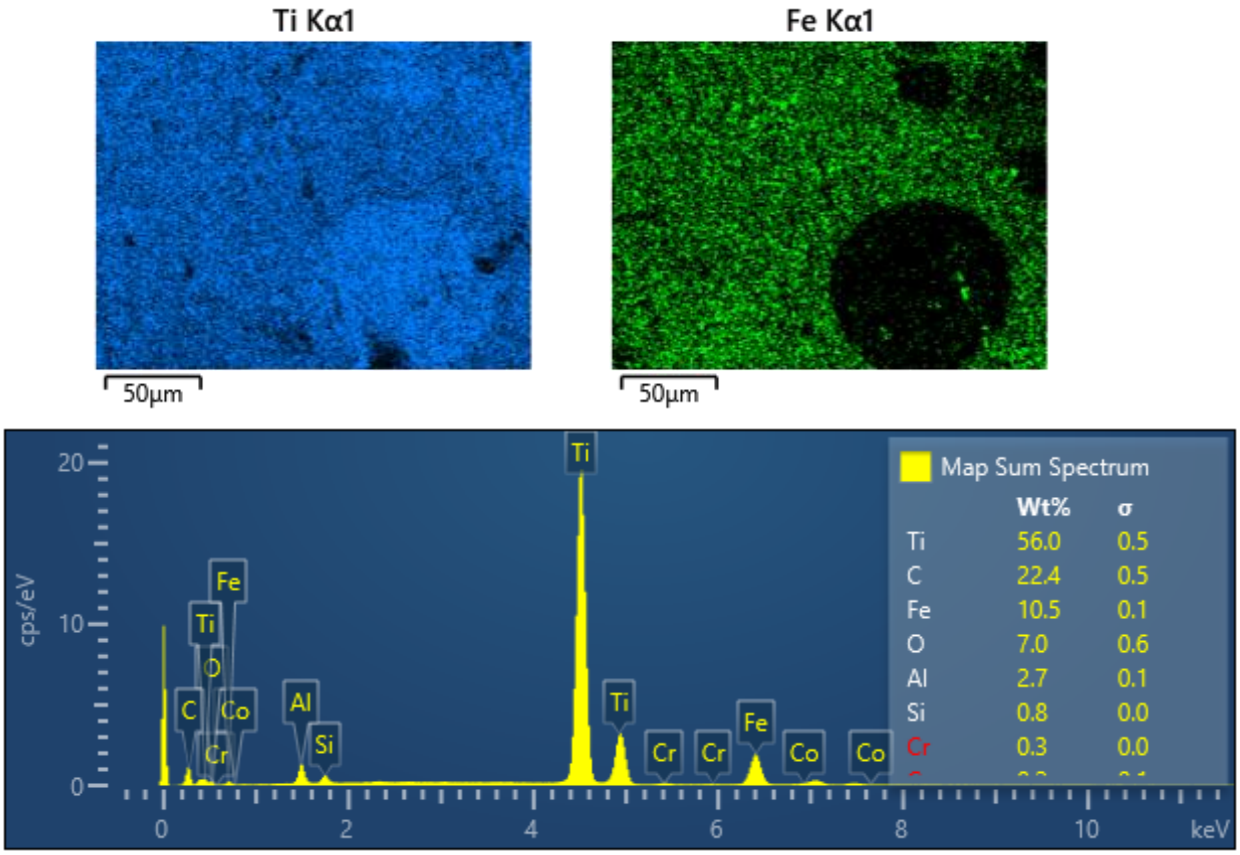

Figure 39: Electronic image, different materials map with different color and percentage of metals for sample C22

The percentage of different molecules for low powder feed condition samples (C31&C32) and optimum process condition samples (C11&C12) are also illustrated in Figure 40. The amount of Ti is higher for the optimum process than the low powder feed condition. Overall, it can be seen that Ti percentage is higher for optimum process and low laser power process (where the powder feeding rate is the same as the optimum process) than low powder feed condition.

a)

Map Sum Spectrum

	Wt%	σ
Fe	44.2	0.3
Ti	30.0	0.2
C	18.8	0.4
O	4.4	0.3
Al	1.8	0.1
Cr	0.5	0.0
Co	0.3	0.1

Map Sum Spectrum

	Wt%	σ
Ti	42.6	0.3
Fe	40.3	0.3
C	9.4	0.4
O	3.2	0.4
Al	2.2	0.1
Si	0.9	0.0
Co	0.9	0.1

b)

Map Sum Spectrum

	Wt%	σ
Ti	64.2	0.4
Fe	20.3	0.2
C	5.9	0.3
O	5.1	0.5
Al	3.2	0.1
Cr	0.5	0.1
Co	0.4	0.1

Map Sum Spectrum

	Wt%	σ
Ti	50.7	0.5
C	22.3	0.5
Fe	16.6	0.2
O	7.4	0.6
Al	1.9	0.1
Co	0.5	0.1
Si	0.4	0.0

Figure 40: Percentage of molecules present for sample a) C31 (left), C32 (right) & b) C11 (left), C12 (right)

All EDS data given below in Figure 41 is taken between the edge of the 3D printing layer and the base substrate area. It can be seen that in the base material, most of the metal is made of Fe, and in the 3D printing layer area, most of the metal is made of Ti. It can also be seen that Ti is not present in the base material area, but some amount of Fe is present in the 3D printing layer area. The amount of Fe is larger for Figure 41c and Figure 41d, which is the low powder feed condition, and for the other two process condition, it is smaller.

a)

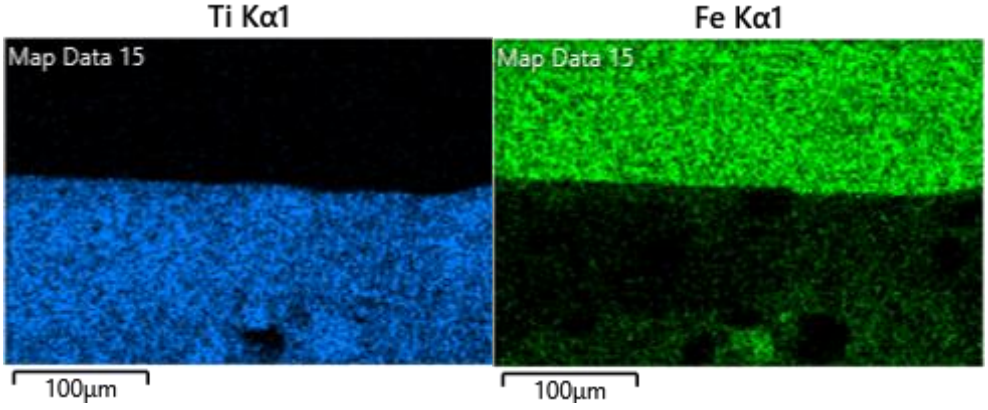

b)

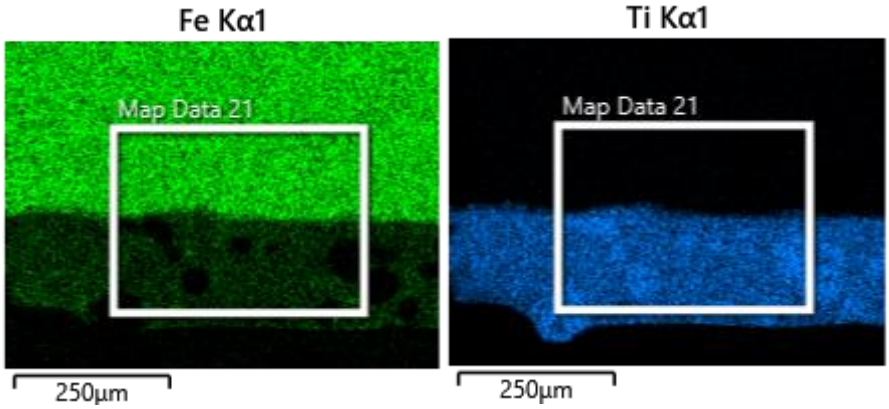
Fe Kα1
Map Data 21
250µm
Ti Kα1
Map Data 21
250µm

c)

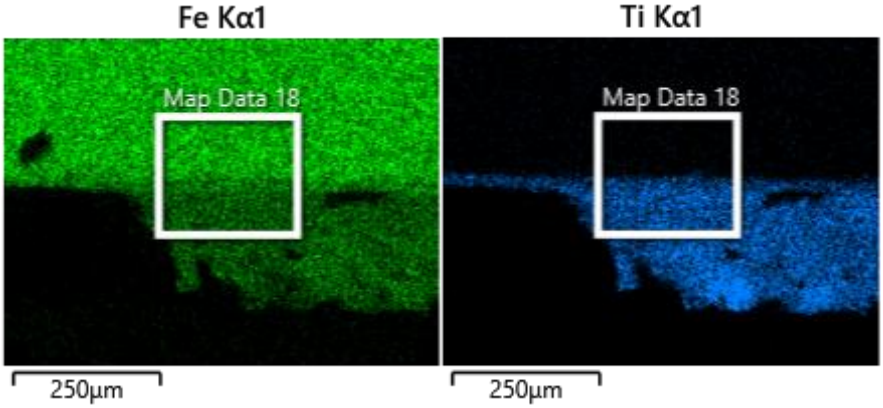
Fe Kα1
Map Data 18
250µm
Ti Kα1
Map Data 18
250µm

d)

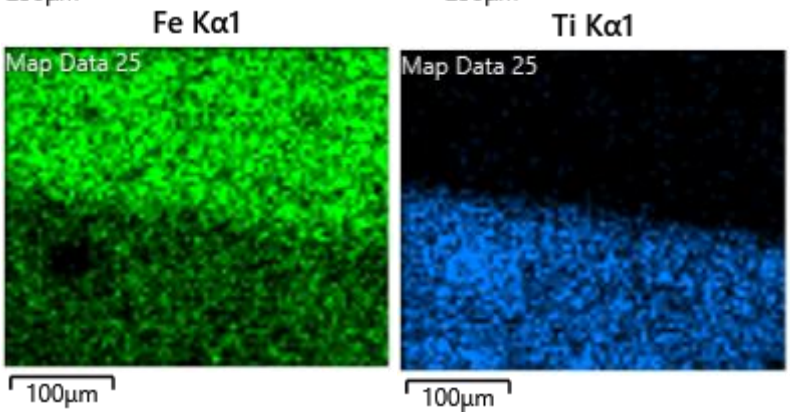
Fe Kα1
Map Data 25
100µm
Ti Kα1
Map Data 25
100µm

e)

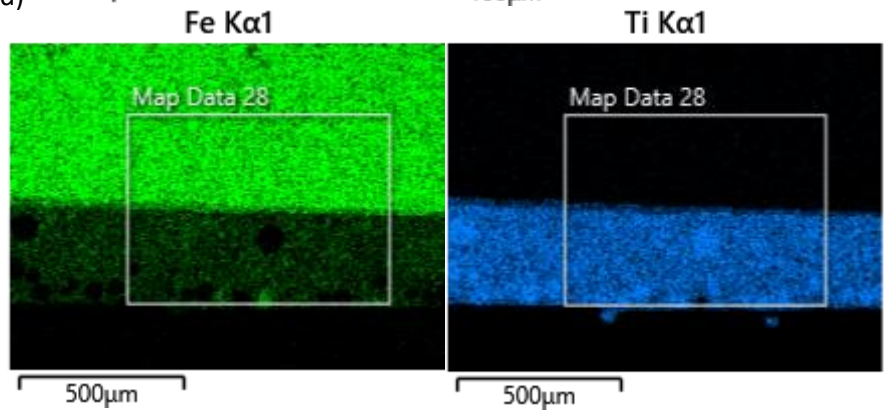
Fe Kα1
Map Data 28
500µm
Ti Kα1
Map Data 28
500µm

f)

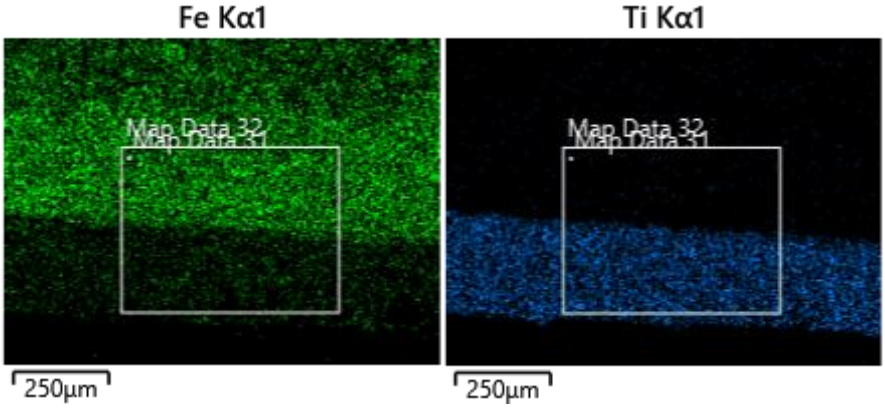

Figure 41: Optical microscopic image for a) sample C21, b) sample C22, c) sample C31, d) sample C32, e) sample C11, f) sample C12

4.3.3 Nanoindentation

The scanning images for all the samples have been collected to do the nanoindentation in specific areas. The scanning image of sample C21 is given in Figure 42, where Figure 42a shows the error plot (which is showing the texture of the scanned surface), Figure 42b shows the Z plot, and Figure 42c shows a 3D view of the Z plot with the µm in X and Y axis and nm scale in Z-axis. More details can be seen in the error plot from the 2D view. From the Z plot 3D view, other details can be seen based on the signal of height and depth of the sample.

a) b)

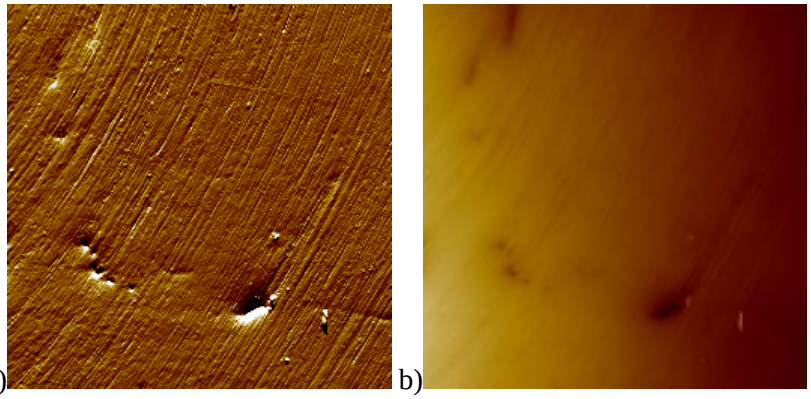

c)

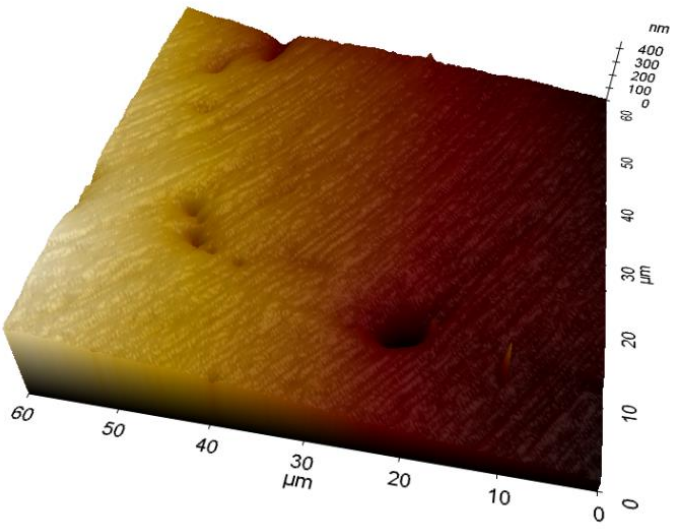

Figure 42: Scanning image for sample C21

Figure 45 shows a representative load-time and displacement-time of the nanoindentation in this study. The resultant force-displacement curves are shown in Figure 44. Using the Oliver-Pharr model in contact mechanics (Oliver and Pharr 1992), reduced modulus and hardness at each point were extracted from force-displacement data. Hardness and reduced modulus versus depth of contact for all examined points of samples C21 are shown in Figure 43.

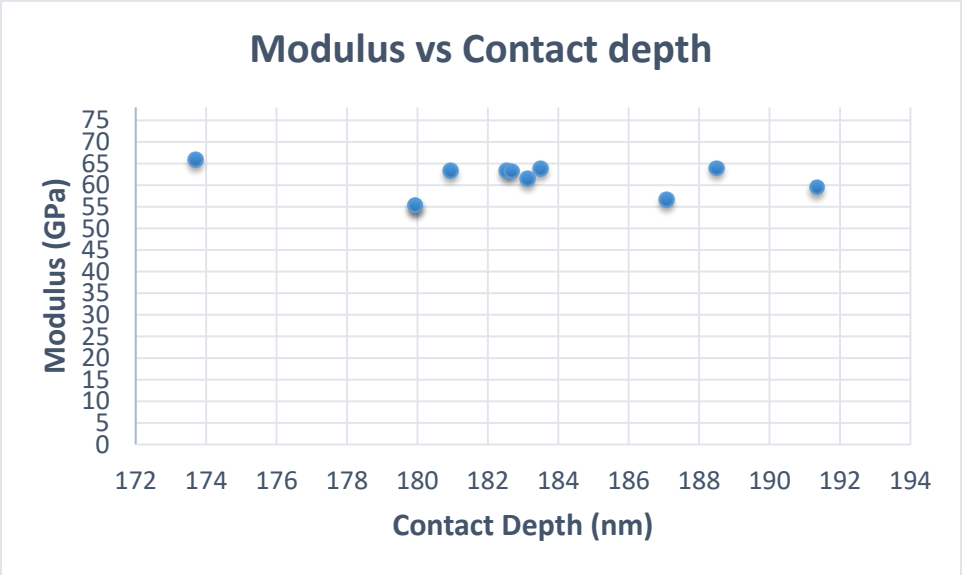

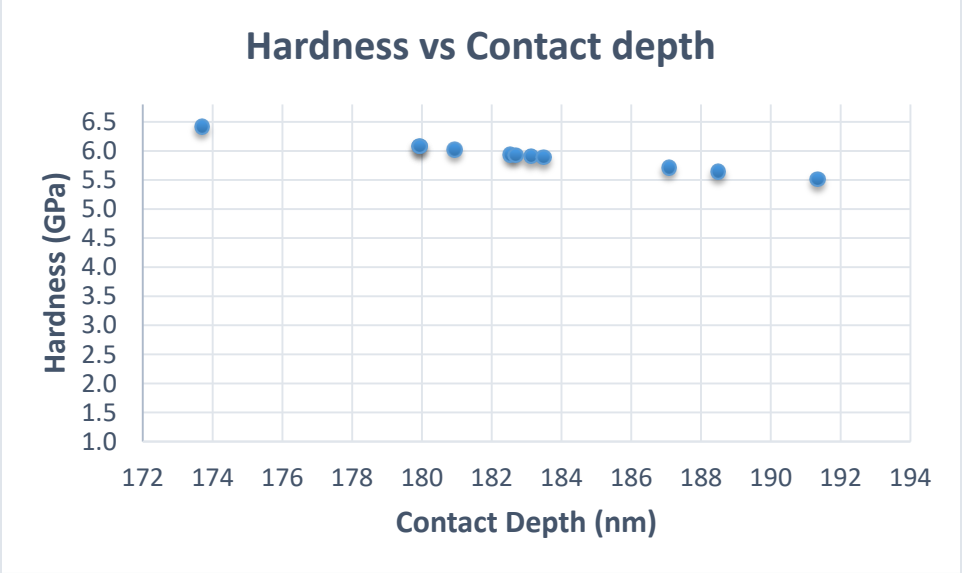

Figure 43: Hardness and Reduced Modulus vs. Contact depth for sample C21

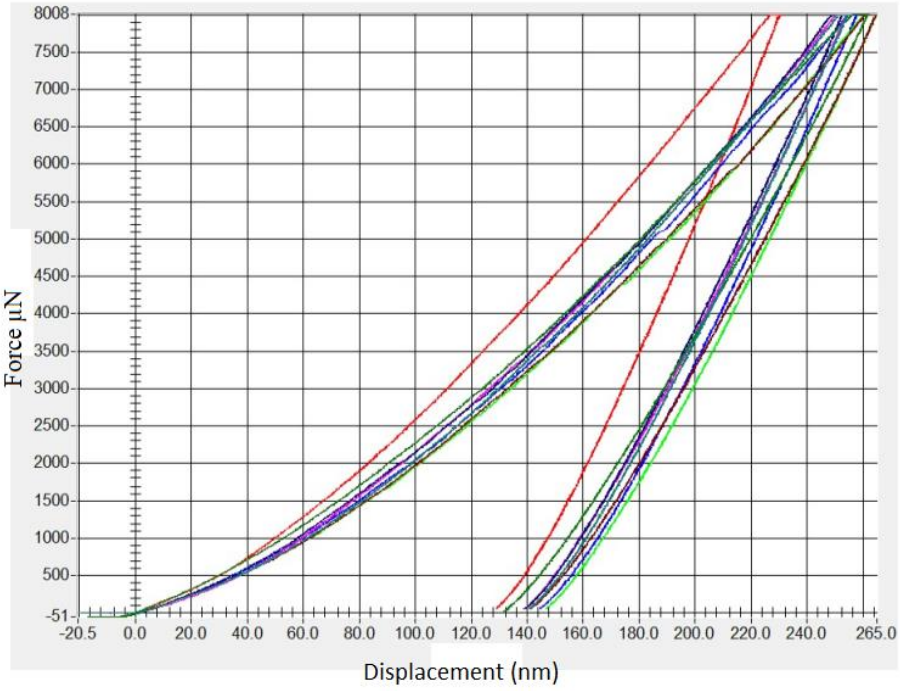

Figure 44: The graph below shows force (µN) vs. displacement (nm) for all points of sample C21

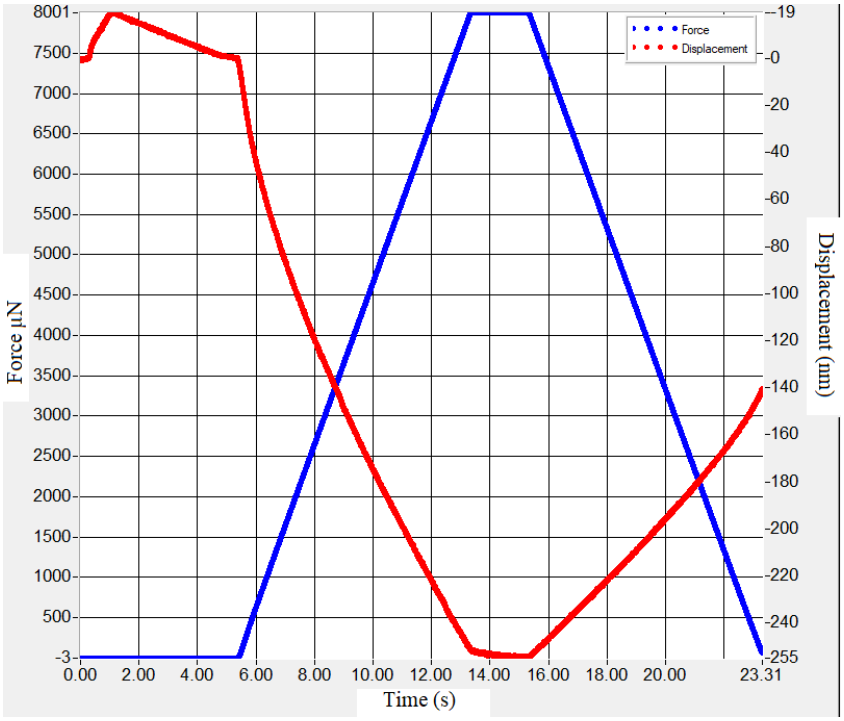

Figure 45: The graph below shows force (µm) vs. displacement (nm) vs. time (s) plot for one standard data point for sample C21

Figure 46 shows the mean value and standard deviation of reduced modulus, contact depth, and hardness for all the samples of building conditions, optimum process conditions, low powder feed, and low laser power. From this three different data sets, it can be seen that the variations in part properties at different process condition is highly distinguishable. From reduced modulus, it is clearly seen that the optimum process condition resulted in higher modulus (86.62 GPa) and higher than the modulus of the samples printed at low powder feed (78.26 GPa) and low laser power (71.42 GPa), which in most cases, a higher modulus is desirable. On the other hand, the mean hardness of the samples printed by optimum process condition is equal to 6.92 GPa and lower than the hardness of the samples printed using low powder feed (9.01 GPa)

To evaluate the variation in measured hardness and modulus of elasticity at different process conditions, a statistical t-test has been done. T-test values for hardness test and modulus of elasticity at different process conditions are summarized in Table 6.

Table 6: Z-test value for Hardness and Modulus for the process conditions

Z-Test / Process Condition	Hardness (GPa)	Modulus (GPa)
Optimum Process vs Low Powder Feed	0.031	0.057
Low Powder feed vs Low laser Powder	2.33E-05	0.354
Optimum Process vs Low laser Powder	1.71E-09	2.90E-13

From this statistical analysis of the results, it can be seen that the hardness values among the three different process conditions are considerably different. On the other hand, the modulus of elasticity for optimum process conditions has a significant difference from the other two process conditions. However, the low laser power and low powder feed process conditions are close to each other in terms of modulus of

elasticity. So, it can be concluded that the three process conditions show variations in hardness and elasticity material properties.

a)

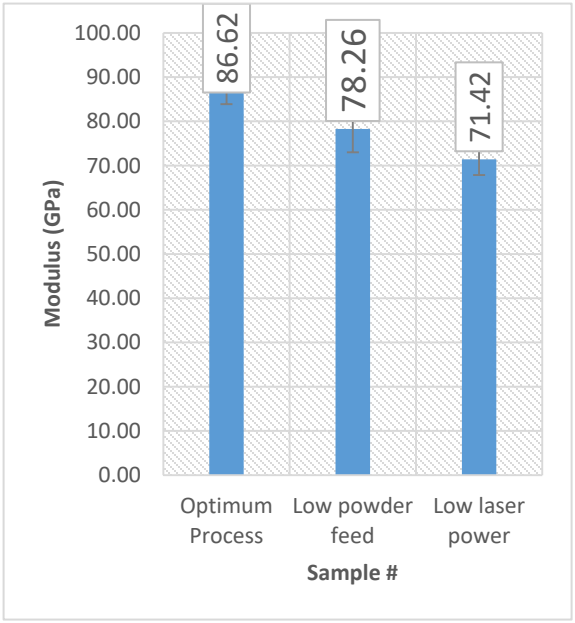

b)

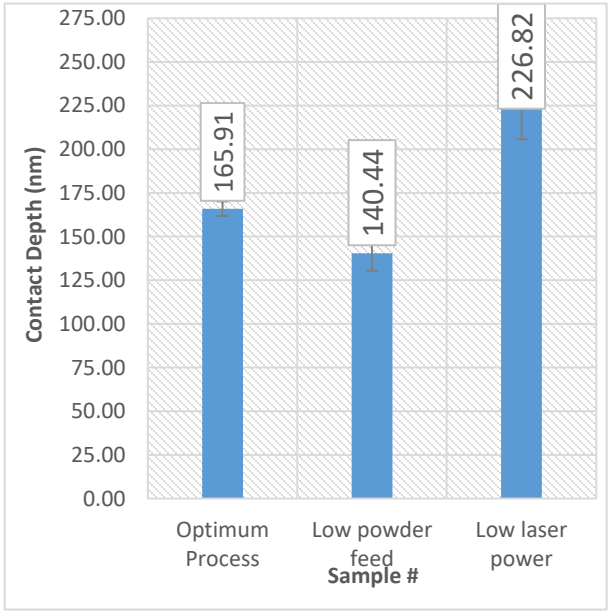

c)

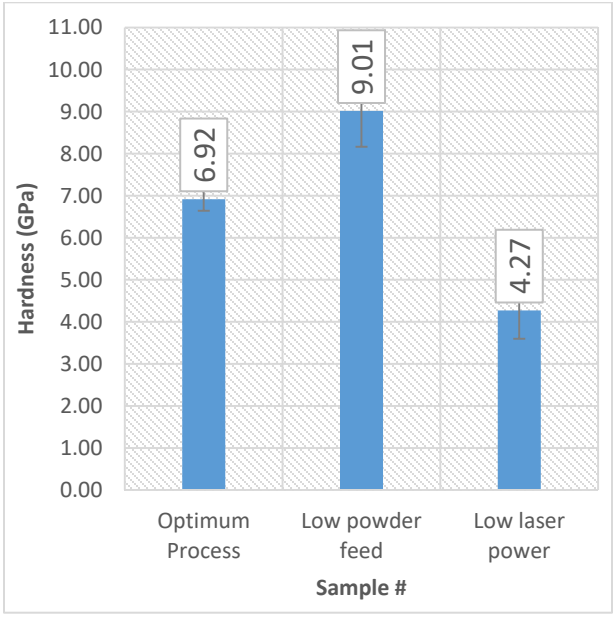

Figure 46: The graph below shows the means and standard deviation of Hardness, Replaced modulus, and Contact depth for all the data points for all samples

The data from the nanoindentation shows variations among different manufacturing process conditions. Each group has data with its characteristics, which confirms that the mechanical properties such as hardness and modulus of elasticity and chemical properties such as the percentage of different components (especially Ti and Fe) present are different.

CHAPTER 5

CONCLUSION AND FUTURE WORK

5.1 Conclusion

5.1.1 Analysis and Clustering of AE data

In this study, while the classification of all five categories of data at different DED manufacturing process conditions, named BL, C0, C1, C2, and C3, the AE data has been analyzed. The first approach of classification with different numerical calculations has given the potential idea where the average of PA and CA at low and high-frequency ranges shows an initial estimation of the classification. Clustering of different build conditions to determine how different the process conditions are from each other (separation of clusters). This is specifically done with the acoustic features of amplitude and time. Clustering has also been done with converted Fast Fourier Transformed (FFT) amplitude and frequency. Clustering shows that despite few overlaps of the feature in recorded data, the center (average values) of the clusters are different for different process conditions (isolation of clusters).

5.1.2 Wavelet Transformation

In this stage, wavelet transformation of the data done by a morlet wavelet filter, which shows the process conditions (data classes) are distinguishable from each other, given an idea for implementing CNN. The wavelet transformation has been done by different scales; among these various scales, it is found that scale 50 of transformation has given significant details that are suitable for analyzing the image. Besides the microscopic image and SEM image, it is found that the wavelet transformed images of the samples are also different from each other.

5.1.3 Image processing

Finally, image processing has been used to do the classification and performance of the classification so that it can be identified how distinguishable each of the process conditions is from each other. Deep CNN has been done to identify the classification with three convolution layers by different filter sizes and shows that accuracy is 96.0%, and the validation accuracy is 95.0%. By that, it can be found that wavelet transformation images with CNN are among the most effective tools for the classification of metal AM process monitoring through AE signals, and this can be used for process monitoring and evaluation of metal additive manufacturing.

5.1.4 Evaluation by other techniques

In this study, different techniques have been used to evaluate the classification of different process conditions done by the Acoustic Emission (AE) method in a former study. The microscopic image, SEM and EDS analysis, and nanoindentation have been done to find the material characteristics that help to find the variation. Firstly, from optical microscopic and SEM images, it can be seen that for low laser power process conditions, the building layer was not proper, and there are big gaps that can be seen, and from nanoindentation the modulus of elasticity is the lowest. Secondly, it is also found that in low power feed conditions, there is a high amount of porosity, and the modulus of elasticity (78.26GPa) is in between optimum process (86.62GPa) and low laser process (71.42GPa) conditions. Finally, it can be seen that for optimum process condition, the building was smooth, and the modulus of elasticity was also the highest. In this study, six different samples for three different process conditions: low laser power, low powder feed, and optimum process conditions have been used to get the data and the discussion. All the data shows that different process conditions can be distinguished by combining the data set collected here.

5.2 Future work

Further study can be done by acquiring more AE data with a different setup of the sensors. This new setup can be done with various parameters setup and show how different parameters affect AE signals, which can finally be used for more analysis. By finding this difference of AE signals with ML or any other technique, the process conditions can be identified more accurately. There is the scope of work by this technique while building multiple AM layers, and the data can be accumulated from each layer to see if there is any change of mechanical changes between layers. This multilayer setup will be able to give more opportunity data acquisition which can be analyzed further for the process condition more significantly. More data analysis from the current data can be used so that if it can be found whether it gives more accuracy for the data classification. There is another scope where temporal analysis can be done: so that by analyzing the travel time delay of the signal to each sensor, the location of the crack can be detected. This temporal analysis will be able to find out if there is any issue during the process condition. This analysis especially gives the opportunity to find out the location of the cracks, and this is more useful for 3D printed biomedical components where the location of the cracks is one of the major concerns.

REFERENCES

Angulo, Ángela, Jialin Tang, Ali Khadimallah, Slim Soua, Cristinel Mares, and Tat Hean Gan. 2019. "Acoustic Emission Monitoring of Fatigue Crack Growth in Mooring Chains." *Applied Sciences (Switzerland)* 9 (11). https://doi.org/10.3390/app9112187.

ASTM E1316-07b. 2007. *Standard Terminology for Nondestructive Examinations*. West Conshohocken, PA: ASTM International. https://doi.org/10.1520/E1316-07B.

Ball, S. 2018. "Location of Cracks Occurring in an Additive Manufacturing Process by Acoustic Emission." *The British Society for Strain Measurement (BSSM)*, 11–12.

Berumen, Sebastian, Florian Bechmann, Stefan Lindner, Jean Pierre Kruth, and Tom Craeghs. 2010. "Quality Control of Laser- and Powder Bed-Based Additive Manufacturing (AM) Technologies." *Physics Procedia* 5 (PART 2): 617–22. https://doi.org/10.1016/j.phpro.2010.08.089.

Bond, Leonard J, Lucas W Koester, and Hossein Taheri. 2019. "NDE In-Process for Metal Parts Fabricated Using Powder Based Additive Manufacturing." In *Proc.SPIE*, 10973:1097302. Denver, CO: SPIE. https://doi.org/10.1117/12.2520611.

Bontha, Srikanth, Nathan W. Klingbeil, Pamela A. Kobryn, and Hamish L. Fraser. 2006. "Thermal Process Maps for Predicting Solidification Microstructure in Laser Fabrication of Thin-Wall Structures." *Journal of Materials Processing Technology* 178 (1–3): 135–42. https://doi.org/10.1016/j.jmatprotec.2006.03.155.

Burrus, C Sidney, Ramesh A Gopinath, and Haitao Guo. 1998. *Introduction to Wavelets and Wavelet Transforms: A Primer*. *Recherche*. http://www.amazon.com/Introduction-Wavelets-Wavelet-Transforms-Primer/dp/0134896009.

Choudhury, A., and N. Tandon. 2000. “Application of Acoustic Emission Technique for the Detection of Defects in Rolling Element Bearings.” *Tribology International* 33 (1): 39–45. https://doi.org/10.1016/S0301-679X(00)00012-8.

Clijsters, S., T. Craeghs, S. Buls, K. Kempen, and J.-P. P. Kruth. 2014. “In Situ Quality Control of the Selective Laser Melting Process Using a High-Speed, Real-Time Melt Pool Monitoring System.” *International Journal of Advanced Manufacturing Technology* 75 (5–8): 1089–1101. https://doi.org/10.1007/s00170-014-6214-8.

Craeghs, Tom, Stijn Clijsters, Jean Pierre Kruth, Florian Bechmann, and Marie Christin Ebert. 2012. “Detection of Process Failures in Layerwise Laser Melting with Optical Process Monitoring.” *Physics Procedia* 39: 753–59. https://doi.org/10.1016/j.phpro.2012.10.097.

D’Accardi, Altenburg, Maierhofer, Palumbo, and Galietti. 2019. “Detection of Typical Metal Additive Manufacturing Defects by the Application of Thermographic Techniques.” *Proceedings* 27 (1): 24. https://doi.org/10.3390/proceedings2019027024.

Doerner, M.F., and W.D. Nix. 1986. “A Method for Interpreting the Data from Depth-Sensing Indentation Instruments.” *Journal of Materials Research* 1 (4): 601–9. https://doi.org/10.1557/JMR.1986.0601.

Dutta, B., and Francis H. Sam Froes. 2015. “The Additive Manufacturing (AM) of Titanium Alloys.” In *Titanium Powder Metallurgy: Science, Technology and Applications*, 447–68. Elsevier Inc. https://doi.org/10.1016/B978-0-12-800054-0.00024-1.

Eschner, N., L. Weiser, B. Häfner, and G. Lanza. 2020. “Development of an Acoustic Process Monitoring System for Selective Laser Melting (SLM).” *Solid Freeform Fabrication 2018: Proceedings of the 29th Annual International Solid Freeform Fabrication Symposium - An Additive Manufacturing Conference, SFF 2018*, no. Reschetnik 2017: 2097–2117.

Everton, Sarah K., Matthias Hirsch, Petros I. Stavroulakis, Richard K. Leach, and Adam T. Clare. 2016.

"Review of In-Situ Process Monitoring and in-Situ Metrology for Metal Additive Manufacturing." *Materials and Design* 95: 431–45. https://doi.org/10.1016/j.matdes.2016.01.099.

Fisher, Karl A., Jim V. Candy, Gabe Guss, and M. J. Mathews. 2016. "Evaluating Acoustic Emission Signals as an in Situ Process Monitoring Technique for Selective Laser Melting (SLM)." https://doi.org/10.2172/1342013.

Frazier, William E. 2014. "Metal Additive Manufacturing: A Review." *Journal of Materials Engineering and Performance* 23 (6): 1917–28. https://doi.org/10.1007/s11665-014-0958-z.

Fugal, D L. 2009. *Conceptual Wavelets in Digital Signal Processing: An In-Depth, Practical Approach for the Non-Mathematician*. Space & Signals Technical Pub. https://books.google.com/books?id=IUFAAQAAIAAJ.

Gaja, Haythem, and Frank Liou. 2016. "Defects Monitoring of Laser Metal Deposition Using Acoustic Emission Sensor." *International Journal of Advanced Manufacturing Technology* 90 (1–4): 561–74. https://doi.org/10.1007/s00170-016-9366-x.

Gaja, Haythem, and Frank Liou. 2018. "Defect Classification of Laser Metal Deposition Using Logistic Regression and Artificial Neural Networks for Pattern Recognition." *The International Journal of Advanced Manufacturing Technology* 94 (1–4): 315–26. https://doi.org/10.1007/s00170-017-0878-9.

Gaynor, Andrew T, Nicholas A Meisel, Christopher B Williams, and James K Guest. 2014. "Topology Optimization for Additive Manufacturing: Considering Maximum Overhang Constraint." In *15th AIAA/ISSMO Multidisciplinary Analysis and Optimization Conference*. AIAA AVIATION Forum. American Institute of Aeronautics and Astronautics. https://doi.org/doi:10.2514/6.2014-2036.

Ge, Zhiqiang, Zhihuan Song, and Furong Gao. 2013. "Review of Recent Research on Data-Based Process Monitoring." *Industrial and Engineering Chemistry Research* 52 (10): 3543–62. https://doi.org/10.1021/ie302069q.

Gold, Scott Alan, and Thomas Graham Spears. 2018. Acoustic Monitoring Method For Additive Manufacturing Processes. US9989495B2, issued 2018. https://patents.google.com/patent/US9989495B2/en?oq=US+9989495+B2.

Goodfellow, Ian. 2016. “Deep Learning.” https://doi.org/https://doi. org/10.4258/hir. 2016.22. 4.351.

Gostautas, Richard S., Guillermo Ramirez, Robert J. Peterman, and Dave Meggers. 2005. “Acoustic Emission Monitoring and Analysis of Glass Fiber-Reinforced Composites Bridge Decks.” *Journal of Bridge Engineering* 10 (6): 713–21. https://doi.org/10.1061/(ASCE)1084-0702(2005)10:6(713).

Grasso, Marco, and Bianca Maria Colosimo. 2017. “Process Defects and in Situ Monitoring Methods in Metal Powder Bed Fusion: A Review.” *Measurement Science and Technology* 28 (4). https://doi.org/10.1088/1361-6501/aa5c4f.

Hay, J.L., and G.M. Pharr. 2000. “Instrumented Indentation Testing.” In *Mechanical Testing and Evaluation,* 8:232–43. ASM International. https://doi.org/10.31399/asm.hb.v08.a0003273.

Hossain, Md Shahjahan, Russell Krenek, Hossein Taheri, and Fadwa Dababneh. 2020. “Ultrasonic Phased Array Technique for Defect Detection and Sizing in Heavy-Walled Cast Components.” In *Proceedings of the ASME 2020 International Mechanical Engineering Congress and Exposition*. American Society of Mechanical Engineers. https://doi.org/10.1115/IMECE2020-23319.

Hossain, Md Shahjahan, and Hossein Taheri. 2020. “In Situ Process Monitoring for Additive Manufacturing Through Acoustic Techniques.” *Journal of Materials Engineering and Performance*, September. https://doi.org/10.1007/s11665-020-05125-w.

Hossain, Md Shahjahan, Hossein Taheri, Niraj Pudasaini, Alexander Reichenbach, and Bishal Silwal. 2020. “Ultrasonic Nondestructive Testing for In-Line Monitoring of Wire-Arc Additive Manufacturing (WAAM).” In *Proceedings of the ASME 2020 International Mechanical Engineering Congress and Exposition*. American Society of Mechanical Engineers. https://doi.org/10.1115/IMECE2020-23317.

James Li, C., and S. Y. Li. 1995. “Acoustic Emission Analysis for Bearing Condition Monitoring.” *Wear* 185 (1–2): 67–74. https://doi.org/10.1016/0043-1648(95)06591-1.

Kano, Manabu, and Yoshiaki Nakagawa. 2008. “Data-Based Process Monitoring, Process Control, and Quality Improvement: Recent Developments and Applications in Steel Industry.” *Computers and Chemical Engineering* 32 (1–2): 12–24. https://doi.org/10.1016/j.compchemeng.2007.07.005.

Koester, Lucas W., Hossein Taheri, Timothy A. Bigelow, Leonard J. Bond, and Eric J. Faierson. 2018. “In-Situ Acoustic Signature Monitoring in Additive Manufacturing Processes.” *AIP Conference Proceedings* 1949 (April). https://doi.org/10.1063/1.5031503.

Koester, Lucas W., Hossein Taheri, Timothy A. Bigelow, Peter C. Collins, and Leonard J. Bond. 2018. “Nondestructive Testing for Metal Parts Fabricated Using Powder-Based Additive Manufacturing.” *Materials Evaluation* 76 (4): 514–24.

Kouprianoff, D., N. Luwes, I. Yadroitsava, and I. Yadroitsev. 2020. “Acoustic Emission Technique for Online Detection of Fusion Defects for Single Tracks during Metal Laser Powder Bed Fusion.” *Solid Freeform Fabrication 2018: Proceedings of the 29th Annual International Solid Freeform Fabrication Symposium - An Additive Manufacturing Conference, SFF 2018*, 2087–96.

Krauss, Harald, Thomas Zeugner, and Michael F. Zaeh. 2015. “Thermographic Process Monitoring in Powderbed Based Additive Manufacturing.” *AIP Conference Proceedings* 1650: 177–83. https://doi.org/10.1063/1.4914608.

Kruth, P.d.i.J.P., B. Vandenbroucke, I.J. Vaerenbergh van, and I. Naert. 2005. “Rapid Manufacturing of Dental Prostheses by Means of Selective Laser Sintering/Melting, in Proceedings of the AFPR,S4,” no. 2.

Leung, Chu Lun Alex, Sebastian Marussi, Robert C. Atwood, Michael Towrie, Philip J. Withers, and Peter D. Lee. 2018. “In Situ X-Ray Imaging of Defect and Molten Pool Dynamics in Laser Additive

Manufacturing." *Nature Communications* 9 (1): 1–9. https://doi.org/10.1038/s41467-018-03734-7.

Li, Feng, Zhonghua Yu, Zhensheng Yang, and Xuanwei Shen. 2019. "Real-Time Distortion Monitoring during Fused Deposition Modeling via Acoustic Emission." *Structural Health Monitoring* 19 (2): 412–23. https://doi.org/10.1177/1475921719849700.

Li, Lin. 2002. "A Comparative Study of Ultrasound Emission Characteristics in Laser Processing." *Applied Surface Science* 186 (1–4): 604–10. https://doi.org/10.1016/S0169-4332(01)00695-X.

Li, X. 2002. "A Brief Review: Acoustic Emission Method for Tool Wear Monitoring during Turning." *International Journal of Machine Tools and Manufacture* 42 (2): 157–65. https://doi.org/10.1016/S0890-6955(01)00108-0.

Liang, S. Y., and D. A. Dornfeld. 1989. "Tool Wear Detection Using Time Series Analysis of Acoustic Emission." *Journal of Manufacturing Science and Engineering, Transactions of the ASME* 111 (3): 199–205. https://doi.org/10.1115/1.3188750.

Lopez, Ana, Ricardo Bacelar, Inês Pires, Telmo G. Santos, José Pedro Sousa, and Luísa Quintino. 2018. "Non-Destructive Testing Application of Radiography and Ultrasound for Wire and Arc Additive Manufacturing." *Additive Manufacturing* 21 (January): 298–306. https://doi.org/10.1016/j.addma.2018.03.020.

Lu, Q. Y., and C. H. Wong. 2017. "Additive Manufacturing Process Monitoring and Control by Non-Destructive Testing Techniques: Challenges and in-Process Monitoring." *Virtual and Physical Prototyping* 13 (2): 39–48. https://doi.org/10.1080/17452759.2017.1351201.

Ludwig, Samuel. 2020. "Instrumented Build Plate for In-Situ Stress Monitoring and Crack Detection during the Laser Powder Bed Fusion Additive Manufacturing Process." The University of North Carolina at Charlotte. https://doi.org/27993613.

Milo, Michael W., Michael Roan, and Bradley Harris. 2015. "A New Statistical Approach to Automated

Quality Control in Manufacturing Processes." *Journal of Manufacturing Systems* 36: 159–67. https://doi.org/10.1016/j.jmsy.2015.06.001.

Mireles, Jorge, Shakerur Ridwan, Philip A. Morton, Alejandro Hinojos, and Ryan B. Wicker. 2015. "Analysis and Correction of Defects within Parts Fabricated Using Powder Bed Fusion Technology." *Surface Topography: Metrology and Properties* 3 (3). https://doi.org/10.1088/2051-672X/3/3/034002.

Müller, Berndt, Joachim Reinhardt, and Michael T. Strickland. 1995. *Neural Networks*. Physics of Neural Networks. Berlin, Heidelberg: Springer Berlin Heidelberg. https://doi.org/10.1007/978-3-642-57760-4.

Nair, Archana, and C. S. Cai. 2010. "Acoustic Emission Monitoring of Bridges: Review and Case Studies." *Engineering Structures* 32 (6): 1704–14. https://doi.org/10.1016/j.engstruct.2010.02.020.

Nasrazadani, Seifollah, and Shokrollah Hassani. 2016. "Chapter 2 - Modern Analytical Techniques in Failure Analysis of Aerospace, Chemical, and Oil and Gas Industries." In , edited by Abdel Salam Hamdy Makhlouf and Mahmood B T - Handbook of Materials Failure Analysis with Case Studies from the Oil and Gas Industry Aliofkhazraei, 39–54. Butterworth-Heinemann. https://doi.org/https://doi.org/10.1016/B978-0-08-100117-2.00010-8.

Newey, D, M A Wilkins, and H M Pollock. 1982. "An Ultra-Low-Load Penetration Hardness Tester." *Journal of Physics E: Scientific Instruments* 15 (1): 119–22. https://doi.org/10.1088/0022-3735/15/1/023.

Oliver, W C, and G M Pharr. 1992. "An Improved Technique for Determining Hardness and Elastic Modulus Using Load and Displacement Sensing Indentation Experiments." *Journal of Materials Research* 7 (6): 1564–83. https://doi.org/DOI: 10.1557/JMR.1992.1564.

Pegues, J W, S Shao, N Shamsaei, N Sanaei, A Fatemi, D H Warner, P Li, and N Phan. 2020. "Fatigue of

Additive Manufactured Ti-6Al-4V, Part I: The Effects of Powder Feedstock, Manufacturing, and Post-Process Conditions on the Resulting Microstructure and Defects." *International Journal of Fatigue* 132: 105358. https://doi.org/https://doi.org/10.1016/j.ijfatigue.2019.105358.

Plessis, Anton Du, Stephan G. Le Roux, Johan Els, Gerrie Booysen, and Deborah C. Blaine. 2015. "Application of MicroCT to the Non-Destructive Testing of an Additive Manufactured Titanium Component." *Case Studies in Nondestructive Testing and Evaluation* 4: 1–7. https://doi.org/10.1016/j.csndt.2015.09.001.

Plotnikov, Yuri, Dan Henkel, Jeffrey Burdick, Arthur French, John Sions, and Keith Bourne. 2019. "Infrared-Assisted Acoustic Emission Process Monitoring for Additive Manufacturing." In *AIP Conference Proceedings*. Vol. 2102. https://doi.org/10.1063/1.5099710.

Purtonen, Tuomas, Anne Kalliosaari, and Antti Salminen. 2014. "Monitoring and Adaptive Control of Laser Processes." *Physics Procedia* 56 (C): 1218–31. https://doi.org/10.1016/j.phpro.2014.08.038.

Qin, S. Joe. 2012. "Survey on Data-Driven Industrial Process Monitoring and Diagnosis." *Annual Reviews in Control* 36 (2): 220–34. https://doi.org/10.1016/j.arcontrol.2012.09.004.

Rahman, Md Hafizur. 2020. "Catalytic Co-Pyrolysis of Pinewood and Waste Plastics for Improving the Selectivity of Hydrocarbons and the Quality of Pyrolysis Oil." *Electronic Theses and Dissertations*. https://digitalcommons.georgiasouthern.edu/etd/2108.

Rahman, Md Hafizur, and Prakashbhai R. Bhoi. 2021. "An Overview of Non-Biodegradable Bioplastics." *Journal of Cleaner Production* 294 (April): 126218. https://doi.org/10.1016/j.jclepro.2021.126218.

Rahman, Md Hafizur, Prakashbhai R. Bhoi, Arpita Saha, Vivek Patil, and Sushil Adhikari. 2021. "Thermo-Catalytic Co-Pyrolysis of Biomass and High-Density Polyethylene for Improving the Yield and Quality of Pyrolysis Liquid." *Energy*, March, 120231. https://doi.org/10.1016/j.energy.2021.120231.

Redding, MacKenzie Ryan, Scott Alan Gold, and Thomas Graham Spears. 2018. Non-Contact Acoustic

Inspection Method For Additive Manufacturing Processes. US010073060B2, issued 2018.

Rens, Kevin L., Terry J. Wipf, and F. Wayne Klaiber. 1997. “Review of Nondestructive Evaluation Techniques of Civil Infrastructure.” *Journal of Performance of Constructed Facilities* 11 (4): 152–60. https://doi.org/10.1061/(ASCE)0887-3828(1997)11:4(152).

Santos, Edson Costa, Masanari Shiomi, Kozo Osakada, and Tahar Laoui. 2006. “Rapid Manufacturing of Metal Components by Laser Forming.” *International Journal of Machine Tools and Manufacture* 46 (12): 1459–68. https://doi.org/https://doi.org/10.1016/j.ijmachtools.2005.09.005.

Scruby, C. B., C. Jones, J. M. Titchmarsh, and H. N. G. Wadley. 1981. “Relationship between Microstructure and Acoustic Emission in Mn-Mo-Ni A533B Steel.” *Metal Science* 44 (6): 241–61.

Scruby, C., and L. Drain. 1990. *Laser Ultrasonic Testing and Applications*. *CRC Press*.

Shao, J., and Y. Yan. 2005. “Review of Techniques for On-Line Monitoring and Inspection of Laser Welding.” *Journal of Physics: Conference Series* 15 (1): 101–7. https://doi.org/10.1088/1742-6596/15/1/017.

Shevchik, S.A., C. Kenel, C. Leinenbach, and K. Wasmer. 2018. “Acoustic Emission for in Situ Quality Monitoring in Additive Manufacturing Using Spectral Convolutional Neural Networks.” *Additive Manufacturing* 21 (May): 598–604. https://doi.org/10.1016/j.addma.2017.11.012.

Silva, Ivan Nunes da, Danilo Hernane Spatti, Rogerio Andrade Flauzino, Luisa Helena Bartocci Liboni, and Silas Franco dos Reis Alves. 2016. *Artificial Neural Networks: A Practical Course*. *Artificial Neural Networks: A Practical Course*. Springer International Publishing. https://doi.org/10.1007/978-3-319-43162-8.

Stanford University. n.d. “Unsupervised Feature Learning and Deep Learning Tutorial.” Accessed March 30, 2021. http://ufldl.stanford.edu/tutorial/supervised/ConvolutionalNeuralNetwork/.

Strantza, Maria, Dimitrios G. Aggelis, Dieter de Baere, Patrick Guillaume, and Danny van Hemelrijck. 2015. “Evaluation of SHM System Produced by Additive Manufacturing via Acoustic Emission and Other NDT Methods.” *Sensors (Switzerland)* 15 (10): 26709–25. https://doi.org/10.3390/s151026709.

Swapp, Susan. n.d. “Scanning Electron Microscopy (SEM).” Accessed December 1, 2020. http://web.archive.org/web/20210302232116/https://serc.carleton.edu/research_education/geochemsheets/techniques/SEM.html.

Taheri, Hossein. 2017. “Classification of Nondestructive Inspection Techniques with Principal Component Analysis (PCA) for Aerospace Application.” In *26th ASNT Research Symposium*.

Taheri, Hossein. 2018. “Nondestructive Evaluation and In-Situ Monitoring for Metal Additive Manufacturing.” *Graduate Theses and Dissertations*. https://lib.dr.iastate.edu/etd/16675.

Taheri, Hossein, Fereidoon Delfanian, and Jikai Du. 2013. “Acoustic Emission and Ultrasound Phased Array Technique for Composite Material Evaluation.” https://doi.org/10.1115/IMECE2013-62447.

Taheri, Hossein, Lucas W. Koester, Timothy A. Bigelow, Eric J. Faierson, and Leonard J. Bond. 2019. “In Situ Additive Manufacturing Process Monitoring with an Acoustic Technique: Clustering Performance Evaluation Using K-Means Algorithm.” *Journal of Manufacturing Science and Engineering, Transactions of the ASME* 141 (4). https://doi.org/10.1115/1.4042786.

Taheri, Hossein, Lucas W Koester, Timothy A Bigelow, and Leonard J Bond. 2017. “Thermoelastic Finite Element Modeling of Laser Generated Ultrasound in Additive Manufacturing Materials.” *2017 ASNT Annual Conference*, no. October: 188–98.

Taheri, Hossein, Mohammad R.M. Rashid Bin Mohammad Shoaib, Lucas W. L.W. Koester, T.A. Timothy A. Bigelow, Peter C. Collins, and Leonard J. Bond. 2017. “Powder-Based Additive Manufacturing - a Review of Types of Defects, Generation Mechanisms, Detection, Property Evaluation and Metrology.” *International Journal of Additive and Subtractive Materials Manufacturing* 1 (2): 172.

https://doi.org/10.1504/ijasmm.2017.10009247.

Tapia, Gustavo, and Alaa Elwany. 2014. “A Review on Process Monitoring and Control in Metal-Based Additive Manufacturing.” *Journal of Manufacturing Science and Engineering, Transactions of the ASME* 136 (6). https://doi.org/10.1115/1.4028540.

Usamentiaga, Rubén, Pablo Venegas, Jon Guerediaga, Laura Vega, Julio Molleda, and Francisco G. Bulnes. 2014. “Infrared Thermography for Temperature Measurement and Non-Destructive Testing.” *Sensors (Switzerland)* 14 (7): 12305–48. https://doi.org/10.3390/s140712305.

Waller, Jess M, Bradford H Parker, Kenneth L Hodges, Eric R Burke, and James L Walker. 2014. “Nondestructive Evaluation of Additive Manufacturing State-of-the-Discipline Report.” *Nasa/Tm-2014-218560*, no. November: 1–36. https://doi.org/10.13140/RG.2.1.1227.9844.

Wevers, M., and M. Surgeon. 2000. “Acoustic Emission and Composites.” In *Comprehensive Composite Materials*, 129:345–57. Elsevier. https://doi.org/10.1016/B0-08-042993-9/00079-6.

Whiting, Justin, Adam Springer, and Federico Sciammarella. 2018. “Real-Time Acoustic Emission Monitoring of Powder Mass Flow Rate for Directed Energy Deposition.” *Additive Manufacturing* 23. https://doi.org/10.1016/j.addma.2018.08.015.

Wolff, Sarah J., Hao Wu, Niranjan Parab, Cang Zhao, Kornel F. Ehmann, Tao Sun, and Jian Cao. 2019. “In-Situ High-Speed X-Ray Imaging of Piezo-Driven Directed Energy Deposition Additive Manufacturing.” *Scientific Reports* 9 (1): 1–14. https://doi.org/10.1038/s41598-018-36678-5.

Wu, Haixi, Yan Wang, and Zhonghua Yu. 2016. “In Situ Monitoring of FDM Machine Condition via Acoustic Emission.” *International Journal of Advanced Manufacturing Technology* 84 (5–8): 1483–95. https://doi.org/10.1007/s00170-015-7809-4.

Wu, Haixi, Zhonghua Yu, and Yan Wang. 2016. “A New Approach for Online Monitoring of Additive Manufacturing Based on Acoustic Emission.” In *Proceedings of the ASME 2016 International*

Manufacturing Science and Engineering Conference. Blacksburg, Virginia, USA: ASME.

Yadavar Nikravesh, Seyed, Hossein Rezaie, Margaret Kilpatrik, and Hossein Taheri. 2019. "Intelligent Fault Diagnosis of Bearings Based on Energy Levels in Frequency Bands Using Wavelet and Support Vector Machines (SVM)." *Journal of Manufacturing and Materials Processing* 3 (1): 11. https://doi.org/10.3390/jmmp3010011.

Yang, Zhensheng, Li Jin, Youruiling Yan, and Yiming Mei. 2018. "Filament Breakage Monitoring in Fused Deposition Modeling Using Acoustic Emission Technique." *Sensors (Switzerland)* 18 (3): 1–16. https://doi.org/10.3390/s18030749.

Yin, Shen, Steven X. Ding, Xiaochen Xie, and Hao Luo. 2014. "A Review on Basic Data-Driven Approaches for Industrial Process Monitoring." *IEEE Transactions on Industrial Electronics* 61 (11): 6414–28. https://doi.org/10.1109/TIE.2014.2301773.

Zhang, Baicheng, Guijun Bi, Youxiang Chew, Pei Wang, Guangyi Ma, Yongfeng Liu, and Seung Ki Moon. 2019. "Comparison of Carbon-Based Reinforcement on Laser Aided Additive Manufacturing Inconel 625 Composites." *Applied Surface Science* 490 (October): 522–34. https://doi.org/10.1016/j.apsusc.2019.06.008.

Zhao, Cang, Kamel Fezzaa, Ross W. Cunningham, Haidan Wen, Francesco De Carlo, Lianyi Chen, Anthony D. Rollett, and Tao Sun. 2017. "Real-Time Monitoring of Laser Powder Bed Fusion Process Using High-Speed X-Ray Imaging and Diffraction." *Scientific Reports* 7 (1): 1–11. https://doi.org/10.1038/s41598-017-03761-2.

Zhou, Yi-Tong, and Rama Chellappa. 1988. "Computation of Optical Flow Using a Neural Network." In *ICNN*, 71–78.

Ziehl, Paul, and Anthony Lamana. 2003. "Monitoring of the Bonnet Carré Spillway Bridge During Extreme OverloadOverload 6. Performing Organization Code," no. 3.

https://www.ltrc.lsu.edu/pdf/report_378.pdf.